HAL
archives-ouvertes.fr

Scalable system level evaluations for LTE using PHY abstraction

Imran Latif

To cite this version:

Imran Latif. Scalable system level evaluations for LTE using PHY abstraction. Networking and Internet Architecture [cs.NI]. Télécom ParisTech, 2013. English. <NNT : 2013ENST0044>. <tel-01180207>

HAL Id: tel-01180207

https://pastel.archives-ouvertes.fr/tel-01180207

Submitted on 24 Jul 2015

HAL is a multi-disciplinary open access archive for the deposit and dissemination of scientific research documents, whether they are published or not. The documents may come from teaching and research institutions in France or abroad, or from public or private research centers.

L'archive ouverte pluridisciplinaire **HAL**, est destinée au dépôt et à la diffusion de documents scientifiques de niveau recherche, publiés ou non, émanant des établissements d'enseignement et de recherche français ou étrangers, des laboratoires publics ou privés.

ParisTech
INSTITUT DES SCIENCES ET TECHNOLOGIES
PARIS INSTITUTE OF TECHNOLOGY

TELECOM ParisTech

2013-ENST-0044

EDITE - ED 130

Doctorat ParisTech

T H È S E

pour obtenir le grade de docteur délivré par

TELECOM ParisTech

Spécialité « Communication et Electronique »

présentée et soutenue publiquement par

Imran LATIF

le 28 Août 2013

Méthodologies pour l'evaluation de performance systéme à grande échelle avec applications au systéme LTE

Directeur de thèse : **Prof. Raymond Knopp, EURECOM**
Co-encadrement de la thèse : **Asst. Prof. Florian Kaltenberger, EURECOM**

Jury

M. Markus Rupp, Professor, Vienna University of Technology	Head of Department
M. Raphael Visoz, PhD, HDR, Orange Labs	Senior Researcher
M. Joan Olmos, Professor, PolyTechnical University of Catalunya	Professor
M. Luc Deneire, Professor, Ecole Polytechnique Universitaire	Professor

TELECOM ParisTech
école de l'Institut Télécom - membre de ParisTech

T H È S E

DISSERTATION

In Partial Fulfillment of the Requirements
for the Degree of Doctor of Philosophy
from TELECOM ParisTech

Specialization: Communications and Electronics

Imran Latif

Scalable System Level Evaluations for LTE Using PHY Abstraction

Defense scheduled on the 28th of August 2013 before a committee
composed of:

Reviewers	Prof. Markus Rupp, Vienna University of Technology
	Raphael Visoz, PhD, HDR, Orange Labs
Examiner	Prof. Joan Olmos, PolyTechnical University of Catalunya
	Prof. Luc Deneire, University of Nice, Sophia Antipolis
Thesis Supervisor	Prof. Raymond Knopp, EURECOM
	Asst. Prof. Florian Kaltenberger, EURECOM

THESE

présentée pour obtenir le grade de

Docteur de TELECOM ParisTech

Spécialité: Electronique et Communications

Imran Latif

Méthodologies pour l'evaluation de performance systéme à grande échelle avec applications au systéme LTE

Soutenance de thèse prévue le 28 Août 2013 devant le jury composé de :

Reviewers	Prof. Markus Rupp, Vienna University of Technology
	Raphael Visoz, PhD, HDR, Orange Labs
Examinateur	Prof. Joan Olmos, PolyTechnical University of Catalunya
	Prof. Luc Deneire, Ecole Polytechnique Universitaire
Directeur de thèse	Prof. Raymond Knopp, EURECOM
	Asst. Prof. Florian Kaltenberger, EURECOM

Acknowledgements

First of all I shall like to thank Almighty God for His greatness and everything I have in life. Then I would like to extend sincere thanks to my advisor Florian Kaltenberger who gave me a chance to pursue my doctorate at Eurecom. The interest and eagerness exhibited by him in my research work has acted like a fuel for me to continue my research. This work would not have been possible without his patient, consistent and professional guidance. Then I shall like to thank Prof. Raymond Knopp as well for his valuable ideas and support during the three years of my doctorate.

I would like to thank all of my friends at EURECOM, all my former colleagues and current PhD students. I will always cherish my good memories earned at EURECOM. I am particularly indebted to some fellow PhD students at EURECOM. I was extremely lucky to have the best persons as my office mates. Among all of them Ayse and Tania were the most consistent ones and they had to suffer through most of my jokes for which I am specially thankful to them. Then I shall like to extend my gratitude towards Ankit, Duy, Sebastian, Arun, Riadh and Wael.Among other friends I shall like to thank Sabir, Rizwan, Najam, Usman and Umer for being always there.

I would like to thank my wife, Summan, for her true and unconditional love and support since the time we are together. I shall also like to thank her for giving me the best gift in life, my son, Ahad. He is the delight of my life and the reason for my happiness.

Finally, I would like to thank my late-parents who stood by me unconditionally through all thick and thin. I am sure if they were alive today they would be the happiest persons on this accomplishment of mine. As a matter of fact, although it is negligible compared to what they have offered to me, I dedicate my PhD to my parents.

Abstract

The main focus of this thesis is to highlight the importance of PHY abstraction for the system level evaluations in the framework of 3GPP Long Term Evolution (LTE) networks. This thesis presents a pragmatic approach towards the use of PHY abstraction in LTE based system level simulators. PHY abstraction is an extremely valuable low complexity tool for efficient and realistic large scale system evaluations. This thesis shows that apart from the primary purpose of PHY abstraction of providing instantaneous link quality indicator for the purpose of system level evaluations, it can be further used for an improved channel quality indicator (CQI) feedback based on the different antenna configurations and for the performance prediction of LTE networks based on the real life channel measurements.

This thesis is mainly divided into two parts; methodologies and applications. The first part presents the complete design and validation methodology of PHY abstraction schemes for various antenna configurations corresponding to different transmission modes in LTE. The validation is performed using link level simulators and it also highlights the calibration issues necessary for the PHY abstraction to be accurate in predicting the performance of capacity achieving turbo codes.

For the special case of multi-user multiple-input multiple-output (MU MIMO) an improved PHY abstraction model is presented which exploits the knowledge about the fact that multi-user interference (MUI) deviates greatly from its Gaussian assumption and therefore must be exploited while predicting the PHY performance especially in the case of interference aware receivers. The first part also presents a novel semi-analytical PHY abstraction approach towards incorporating the incremental-redundancy hybrid automatic repeat request (IR HARQ) for a wide variety of resource block assignment in LTE and it further reduces the storage requirements for PHY abstraction by bringing down the number of required reference curves to only three from hundreds.

The second part presents the applicable scenarios where the concepts of PHY abstraction can be effectively utilized. The most important and pri-

mary use of PHY abstraction is to reduce the necessary simulation time in system level simulators by predicting the link quality based on the instantaneous channel by a fewer number of operations than are required for the processing of complete PHY procedures. Thus by doing so it was found that the overall simulation time for large scale simulation can be decreased enormously by speeding up the simulation by a factor of at least 30 times. Which means that the simulation which took the run time of a month can now be performed with in a day only. Furthermore, it is shown in this part that the performance predicted by PHY abstraction matches the performance obtained by running the simulations with full PHY procedures.

The second part also presents the complete methodology for the use of PHY abstraction in the CQI feedback calculation necessary for the scheduling purposes. In this part we propose to exploit the knowledge on the antenna configuration for the CQI mapping for an improvement in the link adaptation at the MAC layer. Last but not the least, the second part presents a complete methodology for the PHY abstraction to be used for the validation of different LTE transmission modes based on real channel measurements in rural areas at 800 MHz. We use concepts from PHY abstraction to predict the performance of LTE network by means of the channel measurements which were stored during a measurement campaign. We showed that using PHY abstraction not only the performance of the system being operated in different transmission modes can be predicted but also it can be used for the validation of soft LTE modems. This shows that PHY abstraction models has lots of potential and are an important tool for the research community in both industry and academia.

All of the results presented in this thesis have been obtained using open-source OpenAirInterface platform which is implemented in highly optimized C. It is one of the very few open-source platforms who have the capability of performing simulations with both full PHY or PHY abstraction and are composed of both link level simulator and system level simulator. Further it can be used for simulation, emulation and real life demonstrations using the LTE hardware especially designed for it.

Abstract

L'objectif de cette thèse est de souligner l'importance de l'abstraction de la couche physique (PHY abstraction) dans l'évaluation des systèmes LTE (Long Term Evolution). Cette thèse propose une approche pragmatique pour l'utilisation de PHY abstraction dans les simulateurs des systèmes LTE. PHY abstraction est un outil très important pour l'évaluation des systèmes LTE à grande échelle car il est efficace, pratique et à complexité réduite . Dans cette thèse, nous prouvons que, à part son objectif principal et qui consiste à fournir un indicateur instantané de la qualité de liaison pour l'évaluation du système, le PHY abstraction peut aussi: améliorer le feedback de l'indicateur sur la qualité de canal (CQI) en se basant sur les différentes configurations d'antennes, et la prédiction de la performance des réseaux LTE en se basant sur des mesures de canal réelles.

Cette thèse est principalement divisée en deux parties: méthodologies et applications. La première partie présente la conception complète et la méthodologie de validation des systèmes de captage PHY pour différentes configurations d'antennes correspondant à des différentes modes de transmissions en LTE. La validation est effectuée en utilisant des simulateurs de niveau de liaison. Nous soulignons aussi les astuces de calibrage nécessaires pour que la production PHY soit précise dans la prédiction de la performance de capacité réalisant turbo-codes.

Pour le cas particulier de multi-utilisateur multiple-input multiple-output (MU MIMO) un modèle amélioré de l'abstraction PHY est présenté, il exploite la connaissance du fait que l'interférence multi-utilisateur (MUI) s'écarte considérablement de son hypothèse Gaussienne et doit donc être utilisé pour la prédiction de la performance de PHY notamment dans le cas des récepteurs conscients de brouillage. La première partie présente aussi une nouvelle démarche d'abstraction PHY semi-analytique pour intégrer l'hybride demande de répétition automatique incrémentielle de redondance (IR HARQ) concernant une variété de cession de blocs de ressources dans le LTE. Ca permettra aussi de réduire les besoins de stockage pour PHY abstraction en abaissant le nombre de courbes de référence requis de centaines à seulement trois.

La deuxième partie présente différents scénarios, là où les concepts de PHY abstraction peuvent être utilisés davantage. L'utilisation la plus fondamentale de PHY abstraction est de réduire le temps de simulation nécessaire dans les simulateurs de niveau système en estimant la qualité de la liaison basée sur le canal instantanée par un moins d'opérations que celles qui sont nécessaires pour le traitement des procédures complètes PHY. En faisant ainsi, on a constaté que le temps global de simulation pour la simulation à grande échelle peut être diminué en accélérant la simulation par un facteur d'au moins 30 fois. Ce qui signifie que la simulation qui a eu le temps d'exécution d'un mois peut maintenant être effectuée pendant une seule journée. En outre, c?est clair dans cette partie que la performance estimée par PHY abstraction correspond à la performance obtenue en exécutant des simulations avec des procédures complètes PHY.

La deuxième partie présente également la méthodologie complète pour l'utilisation de l'abstraction PHY dans le calcul de feedback CQI nécessaire aux fins de scheduling. Dans cette partie, nous proposonsd'exploiter les connaissances sur la configuration d'antenne pour la cartographie CQI pour une amélioration de l'adaptation de liaison à la couche MAC. Enfin, la deuxième partie présente une méthodologie complète pour l'abstraction PHY à être utilisé pour la validation des différents modes de transmission LTE basés sur des mesures de canaux réels dans les zones rurales à 800 MHz. Nous utilisons des concepts d'abstraction PHY pour prédire la performance de réseau LTE au moyen des mesures de canal qui ont été stockées au cours d'une campagne de mesure. Nous avons montré qu'en utilisant l'abstraction PHY, non seulement la performance du système étant utilisé dans différents modes de transmission peut être prédite, mais aussi il peut être utilisé pour la validation des modems LTE soft. Cela montre que les modèles d'abstraction PHY ont beaucoup de potentiel et sont un outil important pour la communauté de la recherche à la fois dans l'industrie et le milieu académique.

Tous les résultats présentés dans cette thèse ont été obtenus en utilisant la plateforme open-source OpenAirInterface qui est implémentée en un langage C hautement optimisé. Elle est l'une des rares plates-formes open source qui ont la capacité d'effectuer des simulations soit de la couche PHY complète ou bien d'une abstraction de la PHY et sont constitués à la fois de simulateur de niveau de liaison et un simulateur au niveau du système. En outre, elle peut être utilisée pour la simulation, émulation et pour les tests et démonstrations grandeur réelle de la vie en utilisant le matériel LTE spécialement conçu pour elle.

Table of Contents

Acknowledgements i
Abstract iii
Abstract v
Contents vii
List of Figures xi
Acronyms xvii
Notations xxi

1 Introduction **1**
1.1 Motivation and Scope 1
1.2 Outline and Contributions 6
1.2.1 Fundamentals 7
1.2.2 Part I - Methodologies 7
1.2.3 Part II - Applications 9
1.2.4 Conclusion & Future Work 11

2 Fundamentals **13**
2.1 Brief history of Cellular Standards 13
2.2 Third Generation Partenership Project - Long Term Evolution 14
2.2.1 Evolved Packet Core 15
2.2.2 Protocol Stack and Data Flow 16
2.3 LTE Physical (PHY) Layer 17
2.3.1 Radio Frame 17
2.3.2 PHY Processing 20
2.3.3 HARQ in LTE 22
2.4 Bit Interleaved Coded Modulation (BICM) 22
2.4.1 BICM Capacity for QAM Constellation 23
2.5 OpenAirInterface 25
2.6 PHY Abstraction 26
2.6.1 PHY abstraction for OFDM-based Systems 26

I Methodologies **29**

3 LTE Single-User (SU) SISO & MISO Systems **31**
3.1 Introduction . . . 31
3.1.1 Related Work . . . 32
3.1.2 Contributions . . . 33
3.2 LTE Signal & System Model . . . 34
3.2.1 LTE Transmission Mode 1 . . . 34
3.2.2 LTE Transmission Mode 2 . . . 35
3.2.3 LTE Transmission Mode 6 . . . 36
3.3 PHY Abstraction in LTE . . . 38
3.3.1 Link Quality Metric . . . 38
3.3.2 Link Performance Modeling . . . 38
3.4 Calibration of Adjustment Factors . . . 41
3.4.1 Link Level Simulations . . . 42
3.4.2 Sufficient number of Channel estimates for Trace Files 43
3.4.3 PHY Abstraction without Adjustment Factors . . . 45
3.4.4 PHY Abstraction with Adjustment Factors . . . 48
3.4.5 Results With Adjustment Factors . . . 48
3.4.6 Global Optimality of Adjustment Factors . . . 52
3.5 Summary . . . 54
Appendix 3.A Calibration Factors and MSE . . . 55

4 LTE Multi-User MIMO with Interference Aware Receiver **61**
4.1 Introduction . . . 61
4.1.1 Related Work . . . 62
4.1.2 Contributions . . . 63
4.1.3 Organization . . . 63
4.2 Multi-User MIMO in LTE . . . 64
4.2.1 MU-MIMO in Release 8 . . . 64
4.2.2 MU-MIMO in Release 9 and 10 . . . 65
4.3 System Model . . . 66
4.3.1 Scheduler . . . 67
4.3.2 Interference Aware Receiver . . . 68
4.3.3 Information theoretic View . . . 69
4.4 PHY abstraction for Interference Aware Receiver . . . 70
4.4.1 EESM . . . 71
4.4.2 MIESM . . . 72
4.4.3 Interference-Aware PHY abstraction (IAPA) . . . 73
4.5 Application to Other Interference-Limited Scenarios . . . 75
4.6 Link Level Results . . . 76
4.7 Summary . . . 82

5 LTE Incremental Redundancy HARQ 83
5.1 Introduction . . . 83
5.1.1 Related Work . . . 83
5.1.2 Contributions . . . 84
5.1.3 Organization . . . 84
5.2 System Model . . . 85
5.3 Bit Level Modeling . . . 85
5.4 Symbol Level Modeling . . . 87
5.4.1 Effective Channel Code Rate . . . 87
5.5 Reference Performance Curves . . . 90
5.6 Summary . . . 94
5.7 Results . . . 95
5.8 Conclusion . . . 99
Appendix 5.A Bit Level Approach . . . 100

II Applications 101

6 System Level Simulations 103
6.1 Introduction . . . 103
6.1.1 Related Work . . . 104
6.1.2 Contributions . . . 104
6.2 PHY Abstraction in OpenAirInterface . . . 105
6.2.1 Parametrization . . . 105
6.2.2 Processing . . . 106
6.2.3 Implementation on System Simulator . . . 106
6.3 System level validation for Single User SISO and MISO channels 106
6.3.1 System Model . . . 107
6.3.2 Speed . . . 108
6.3.3 Realims and Accuracy . . . 109
6.3.4 Applicability . . . 110
6.3.5 Scalability . . . 111
6.4 System level validation for Multi-User MIMO . . . 112
6.5 Conclusion . . . 113

7 Comparison of LTE TMs using Channel Measurements at 800 MHz 115
7.1 Introduction . . . 115
7.1.1 Contributions . . . 116
7.1.2 Organization . . . 116
7.2 The OpenAirInterface testbed . . . 116
7.2.1 Hardware . . . 116
7.2.2 Implemented LTE subset . . . 118
7.2.3 Achievable PHY (coded) Throughput . . . 120

7.3 Measurements description 120
7.4 BICM Throughput Calculation using PHY Abstraction 121
7.4.1 Modulation Model 121
7.4.2 Coding Model 124
7.5 LTE Transmission Modes Performance Comparison 125
7.5.1 Feedback calculation 125
7.5.2 Scheduling and sum throughput 126
7.5.3 Link level abstraction 126
7.5.4 Results 127
7.6 Conclusion 129

8 Fast Link Adaptation 131
8.1 Introduction 131
8.1.1 Related Work 132
8.1.2 Contributions 132
8.2 System Model 133
8.3 Proposed Link Adaptation 133
8.3.1 CQI Calculation 133
8.3.2 MCS Selection at eNodeB 139
8.4 Results 140
8.5 Summary 142

9 Conclusion & Future Work 145
9.1 Conclusions 145
9.2 Future Work 148

10 Summary 149
10.1 Motivation 149
10.2 Outline and Contributions 155
10.2.1 Fondamentaux 155
10.2.2 Part I - Méthodologies 157
10.2.3 Part II - Applications 162

Bibliography 168

List of Figures

1.1 Global ICT development 2001-2013 [1] 2
1.2 Increasing Use of Internet in daily lives [1] 3
1.3 Simplified Profiling Diagram for System Level Simulations . . 4
1.4 Comparison of Protocol Stack with and without PHY abstraction 5
1.5 Profiling for System Simulation with 1 eNodeB and 1 UE in the context of LTE, SISO channel, frequency selective Rayleigh channel and constant bit rate traffic. 12

2.1 LTE: From separate circuit-switched and packet-switched cores to an all-IP core [2] 15
2.2 An example of data flow in LTE protocol 16
2.3 Time and Frequency view of LTE Frame Grid 18
2.4 An Example for the Frequency Domain Bandwidth allocation in LTE with 5MHz bandwidth 18
2.5 LTE Frame structure 20
2.6 Channel coding, Rate matching and Modulation Mapping in LTE 20
2.7 Turbo Coding and IR-HARQ in LTE 21
2.8 Baseband BICM-ID transmission model 23
2.9 Mutual Information versus SNR for different QAM constellations 24
2.10 Link performance model 27
2.11 Link-to-System Mapping Procedure 27

3.1 SISO: system model with one singe antenna eNodeB and U single antenna UEs 35
3.2 Transmit Diversity: system model with a dual antenna eNodeB and U single antenna UEs 36
3.3 Transmit Precoding: system model with a dual antenna eNodeB and U single antenna UEs 37
3.4 PHY Abstraction in LTE 38
3.5 Comparison of Normalized Mutual Information functions and EESM function 41

3.6 AWGN Link Performance Curves in LTE with 5 MHz Bandwidth for MCS 0 - 27 42
3.7 Symbol Reference Signals (SRS) with NCP used for the channel estimation in LTE. For antenna port 0,1 on the left side and for antenna port 0, 1, 2 and 3 on the right. 45
3.8 For Transmission Mode 1, 2 and 6 using ideal channel estimation, MSE for different MCS using EESM and MIESM with single and dual adjustment factors 49
3.9 For Transmission Mode 1, 2 and 6 using ideal channel estimation, comparison of single and dual adjustment factors for EESM and MIESM 49
3.10 LTE Transmission Mode 1 - EESM with two calibration factors for MCS 0 - 22 50
3.11 LTE Transmission Mode 2 - EESM with two calibration factors for MCS 0 - 22 50
3.12 LTE Transmission Mode 6 - EESM with two calibration factors for MCS 0 - 22 51
3.13 For Transmission Mode 1, 2 and 6 using real channel estimation, MSE for different MCS using EESM and MIESM with single and dual adjustment factors 51
3.14 For Transmission Mode 1, 2 and 6 using real channel estimation, comparison of single and dual adjustment factors for EESM and MIESM 51
3.15 Performance comparison of MIESM and EESM for transmission mode 1, 2 and 6 using real channel estimation and dual adjustment factors. 52
3.16 Global optimality of the MSE optimization problem 53

4.1 Demodulation Reference Signal structure for the case of two antenna ports 65
4.2 Demodulation Reference Signal structure for more than two antenna ports 66
4.3 PHY abstraction model for MU MIMO using Interference Aware receivers in LTE 71
4.4 Mutual Information of MU MIMO in LTE for Interference Aware Receiver when the desired user and interfering user transmit using QPSK constellation 74
4.5 AWGN Link Performance Curves in LTE with 5 MHz Bandwidth with ideal channel estimation 77
4.6 MSE for Rayleigh channel model using different PHY abstraction models for MU MIMO in LTE 79
4.7 MSE for SCM-C channel model using different PHY abstraction models for MU MIMO in LTE 80

4.8 Adjustment factor for Rayleigh channel model using different PHY abstraction models for MU MIMO in LTE 80
4.9 Adjustment factor for SCM-C channel model using different PHY abstraction models for MU MIMO in LTE 81
4.10 Result for Rayleigh8 channel model: IA-PHY abstraction of different MCS for MU MIMO in LTE 81
4.11 Result for SCM-C channel model: IA-PHY abstraction of different MCS for MU MIMO in LTE 82

5.1 Overlapping of bits in consucetive rounds 89
5.2 $\xi(MCS, t)$ in the second, third and fourth HARQ round for MCS 0 and 9 for different PRB Assignment - It is clear that for different bandwidth assignment the value of $\xi(MCS, t)$ does not changes significantly. 89
5.3 Normalized BICM Mutual Information and calculation of Shift with respect to the mother code rate 93
5.4 Calculation of bandwidth dependent performance offset . . . 94
5.5 Reference AWGN curves for LTE Systems using QPSK, 16QAM and 64QAM Modulations 95
5.6 LTE MIESM IR HARQ MCS 9 (QPSK) For All Four Retransmissions 96
5.7 LTE MIESM IR HARQ MCS 10 (16 QAM) For All Four Retransmissions 96
5.8 LTE MIESM IR HARQ MCS 16 (16 QAM) For All Four Transmissions 97
5.9 LTE MIESM IR HARQ MCS 17 (64 QAM) For All Four Retransmissions 97
5.10 LTE MIESM IR HARQ MCS 25 (64 QAM) For All Four Retransmissions 98
5.11 Mean Squared Error (MSE) at 10% BLER points of Rayleigh channel model with respect to the shifted AWGN curves for different MCS in LTE after 4 HARQ rounds 98

6.1 PHY Abstraction in System Performance Evaluation in OpenAirInterface 105
6.2 System model with 4 randomly placed UEs 107
6.3 Comparison of simulation times for the transmission mode 1, 2 and 6 using PHY abstraction and full PHY 108
6.4 Comparison of accumulated average system throughput over given number of frames for full PHY and PHY abstraction with transmission mode 1, 2 and 6 110
6.5 For 2 UEs, Comparison of accumulated average system throughput over given number of frames for full PHY and PHY abstraction with transmission mode 1, 2 and 6 111

6.6 For 4 UEs, accumulated average system throughput over given number of frames with PHY abstraction for transmission mode 1 . . . 112
6.7 Average System Throughput for the Given MU MIMO Scenarion in LTE . . . 113
6.8 Instantaneous Throughput for the first UE in the Given MU MIMO Scenario in LTE . . . 114
6.9 Instantaneous Throughput for the second UE in the Given MU MIMO Scenario in LTE . . . 114

7.1 Base Station Control Room . . . 117
7.2 Antennas with PAs on mast . . . 118
7.3 UE with its antenna and GPS receiver . . . 118
7.4 Traces used for the multi-user MIMO comparison . . . 121
7.5 PHY abstraction model for BICM Throughput Calculation . 122
7.6 Throughput based in mutual information (MI) as well as on simulation results for different SNR values in an AWGN channel. The difference between the MI and the simulated results is called the implementation loss. . . . 125
7.7 CDF comparison of sum throughput of the system with 2 single antenna UEs and an eNodeB equipped with two antennas for different LTE transmission modes using 4QAM . . . 127
7.8 CDF comparison of sum throughput of the system with 2 single antenna UEs and an eNodeB equipped with two antennas for different LTE transmission modes using 16-QAM. . . . 128
7.9 CDF comparison of the best selected user throughput of a system with 2 single antenna UEs and an eNodeB equipped with two antennas for different LTE transmission modes when using 64QAM. . . . 128
7.10 CDF comparison of the different interference levels for transmission mode 5 of a system with 2 single antenna UEs and an eNodeB equipped with two antennas. . . . 129

8.1 Reference AWGN curves for SISO with probability of error below 10% . . . 135
8.2 Reference AWGN curves for transmission mode 2 with probability of error below 10% . . . 136
8.3 Reference AWGN curves for transmission mode 5 with probability of error below 10% . . . 136
8.4 Reference AWGN curves for transmission mode 6 with probability of error below 10% . . . 137
8.5 Required SNR Vs Code rate for having probability of error below 10% . . . 138

8.6 Accumulated average throughput of the system with and without proposed link adaptation for transmission mode 6 and tapped delay line Rice channel model having 8 taps 141
8.7 Accumulated average throughput of the system with and without proposed link adaptation for transmission mode 6 and tapped delay line Rice channel model having 1 taps 141
8.8 Accumulated average throughput of the system with and without proposed link adaptation for transmission mode 6 and EVA channel model 142

10.1 Global ICT development 2001-2013 [1] 150
10.2 Utilisation croissante d'Internet dans la vie quotidienne [1] . . 151
10.3 Schéma simplifié de profilage au niveau système de simulations 153
10.4 Comparaison de la pile de protocole avec et sans PHY abstraction 154
10.5 Profiling for System Simulation with 1 eNodeB and 1 UE in the context of LTE, SISO channel, frequency selective Rayleigh channel and constant bit rate traffic. 167

Acronyms

Here are the main acronyms used in this document. The meaning of an acronym is usually indicated once, when it first appears in the text.

2G	Second Generation
3G	Third Generation
3GPP	Third Generation Partnership Project
AcVI	Actual Value Interface
AMC	Adaptive Modulation and Coding
AMPS	Advanced Mobile Phone Service
AVI	Average Value Interface
AWGN	Additive White Gaussian Noise
BICM	Bit Interleaved Coded Modulation
BICM-ID	Bit Interleaved Coded Modulation Iterative Decoding
BLER	Block Error Rate
BS	Base Station
CDMA	Code Division Multiple Access
CB	Circular Buffer
CC	Chase Combining
CP	Cyclic Prefix
CQI	Channel Quality Indicator
CRC	Cyclic Redundancy Check
CRS	Cell-specific Reference Symbols
CSI	Channel State Information
CSIR	Channel State Information at the Receiver
CSIT	Channel State Information at the Transmitter
DL	Downlink
DMRS	De-Modulation Reference Symbols
DOF	Degrees of Freedom
DPC	Dirty Paper Coding
EDGE	Enhanced Data rates for GSM Evolution
EESM	Exponential Effective SINR Mapping
eNodeB	Enhanced NodeB
EPC	Evolved Packet Core

ESM	Effective SINR Mapping
EVA	Extended Vehicular A Channel
FDD	Frequency-Division Duplex
FLA	Fast Link Adaptation
GPRS	General Packet Radio Service
GSM	Global System for Mobile
HARQ	Hybrid Automatic Repeat Request
HSPA	High Speed Packet Access
IA	Interference Aware
IAPA	Interference Aware PHY Abstraction
ICT	Information Communication Technology
iid	Independent and Identically Distributed
IR	Incremental Redundancy
ISI	Intersymbol Interference
ISR	Interference to Signal Ratio
ITU	International Telecommunication Union
L2S	Link-to-System
LDPC	Low-Density Parity-Check
LLR	Log-likelihood Ratio
LQM	link Quality Metric
LTE	Long Term Evolution
LUT	Look Up Table
MAC	Multiple Access Channel
MCS	Modulation and Coding Scheme
MF	Matched Filter
MIESM	Mutual Information Effective SINR Mapping
MIMO	Multiple Input Multiple Output
MISO	Multiple Input Single Output
ML	Maximum Likelihood
MMSE	Minimum Mean Square Error
MRC	Maximum Ratio Combining
MS	Mobile Station
MSE	Mean Square Error
MU	Multiuser
MUI	Multiuser Interference
NACK	Not-ACKnowledged
PDCP	Packet Data Convergence Protocol
PDCCH	Physical Downlink Control Channel
PDSCH	Physical Downlink Shared Channel
PHY	Physical Layer
PRB	Physical Resource Block
QAM	Quadrature Amplitude Modulation
OAI	OpenAirInterface
OCC	Orthogonal Cover Codes

OFDM	Orthogonal Frequency Division Multiplexing
OFDMA	Orthogonal Frequency Division Multiplexing Access
QoS	Quality of Service
QPSK	Quadrature Phase-Shift Keying
RE	Resource Element
RLC	Radio Link Control
RRM	Radio Resource Management
RV	Redundancy Version
SCM	Spatial Channel Model
SDU	Service Data Unit
SIC	Successive Interference Cancellation
SIMO	Single Input Multiple Output
SINR	Signal to Interference and Noise Ratio
SISO	Single Input Single Output
SNR	Signal to Noise Ratio
STBC	Space Time Block Coding
SU	Single-user
TBS	Transport Block Size
TDD	Time Division Duplex
THP	Tomlinson-Harashima precoding
TM	Transmission Mode
TTI	Transmission Time Interval
UE	User Equipment
UMTS	Universal Mobile Telephone Service
WCDMA	Wideband CDMA
w.r.t.	with respect to
ZF	Zero Forcing
ZMCSCG	Zero Mean Circularly Symmetric Complex Gaussian

Notations

Here is a list of main operators and symbols used in this document. We have tried to keep the notation consistent throughout the thesis, but rarely symbols have different definitions in different chapters and in that case they are defined very explicitly to avoid any confusion.

x or X	Scalar
$\mathbf{x}$	Vector
$\mathbf{X}$	Matrix
$h, \mathbf{h}, \mathbf{H}$	Channel (scalar, vector, matrix)
$z, \mathbf{z}, \mathbf{Z}$	Noise (scalar, vector, matrix)
$y, \mathbf{y}, \mathbf{Y}$	Received signal (scalar, vector, matrix)
$(.)^*$	Conjugate operation
$(.)^T$	Transpose operation
$(.)^\dagger$	Hermitian operation
$\Re(.)$	Real part of a complex number
$\Im(.)$	Imaginary part of a complex number
$\lvert x \rvert$	Absolute value of scalar
$\lVert \mathbf{x} \rVert$	Euclidean norm of vector
$\mathcal{E}(.)$	Mathematical expectation
y'	Matched filter output of the received signal y
$\mathcal{CN}$	Complex Normal Distribution
$\mathcal{C}$	Complex space
$\mathbb{C}^M$	M-dimensional complex space
$\mathcal{H}(.)$	$= -\mathcal{E} \log p(.)$ Entropy of the argument
log	All logarithms are to the base 2
$I(.;.)$	Mutual information between the two arguments
n_t	Number of transmit antennas
n_r	Number of receive antennas
P_T	Transmit power constraint
χ	Constellation
$x \in \chi_b^i$	Subset of the signal set $x \in \chi$ whose labels have the value $b \in \{0, 1\}$ in the position i
M	$\lvert \chi \rvert$ i.e. cardinality of the constellation χ

Chapter 1

Introduction

1.1 Motivation and Scope

Mobile communication has truly revolutionized the way world communicates. It has provided a complete paradigm shift in the field of telecommunication from wired to wireless and has reached to even those remote areas where the deployment of wired infrastructure was once a question mark. As per the estimates of International Telecommunication Union (ITU) for 2013, the mobile subscriptions around the world have reached a number of 6.8 billion which is almost 96% of today's world population [1]. The evolution in the mobile subscription as compared to other subscriptions is shown in Figure 10.1 which clearly demonstrates the strong desire of the people around the world to communicate with each other all the time while on the move. Another important technology which undoubtedly transformed the world into a global village is the *internet*. With the latest concept of cloud computing, it has become an indispensable global network which is now being used in almost all aspects of daily life i.e., medical, defense, business and not to forget the social media. It can be observed from Figure 10.2 that today almost 80% of homes in the developed world and 43% of homes in the over all world are equipped with broadband internet access. Similar trend can be observed for the individuals using the internet across the globe. The rise in the mobile subscriptions and in the usage of internet shows an ever increasing trend for the demand of internet based data services and mobile connectivity.

Over the last 10 years the mobile communication has evolved from complete circuit switched network to all IP network. Due to this evolution it has become possible to provide such higher data rates on mobile devices which were

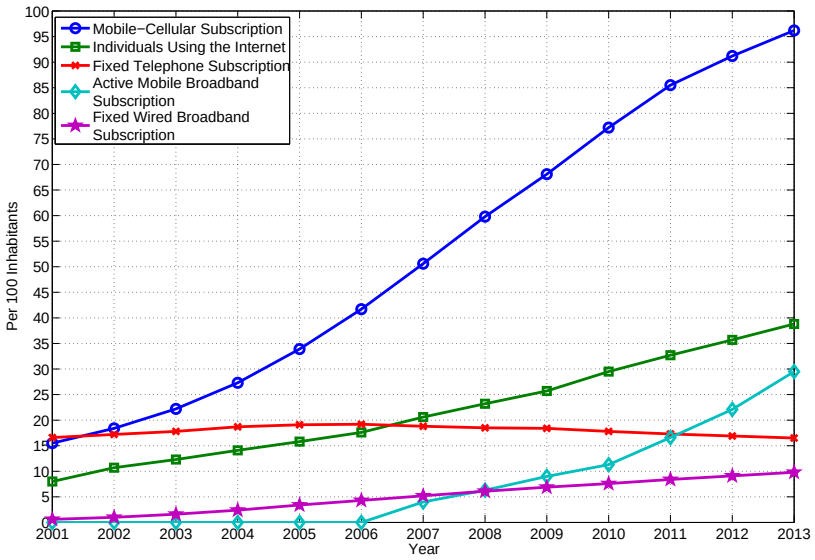

Figure 1.1: Global ICT development 2001-2013 [1]

only possible on fixed broadband networks only a decade ago. Today, the third generation partnership project (3GPP) Long Term Evolution (LTE) [3] for cellular networks has already been deployed in some regions of the world and it is providing almost 100Mbps on the downlink and 50Mbps on the uplink. As per ITU statistics, not only the number of mobile subscribers are increasing but the mobile broadband subscriptions are also on the increase. This can be observed from Figure 10.1 which presents the global Information Communication Technology (ICT) trends and it can be seen that before 2006 the mobile broadband subscriptions were zero and since then it has reached the level of 30% of world's population. This is a clear indication that there will be a significant increase in the demand of higher data rates for mobile data services in the future.

However, to meet the increasing demand of higher data rates, it is required to investigate more efficient and innovative techniques which can not only provide the required data rate by being more spectral efficient but are also environment friendly in terms of energy consumption. One example of such efforts is the standardization of the 3GPP LTE system. It deploys not only the large scale networks where multiple antennas are used at mobile and base station, but also small scale networks which make use of the base stations transmitting at a very low power, i.e., femtocell networks, to increase the spectral efficiency. Also it supports the co-operative communication where the base stations of neighboring cells can share data and control signals in

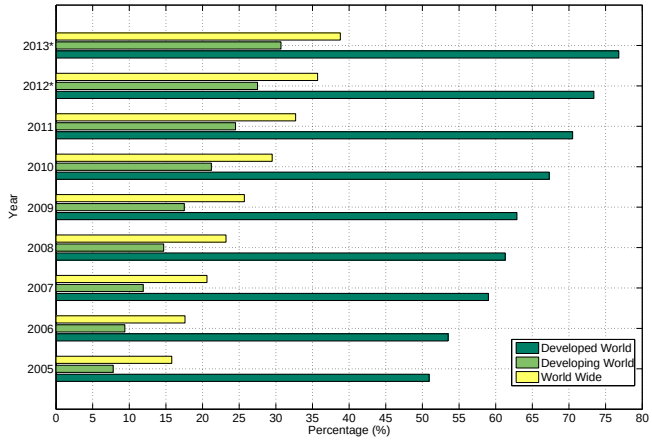

(a) Evolution in use of Internet by individuals in daily life

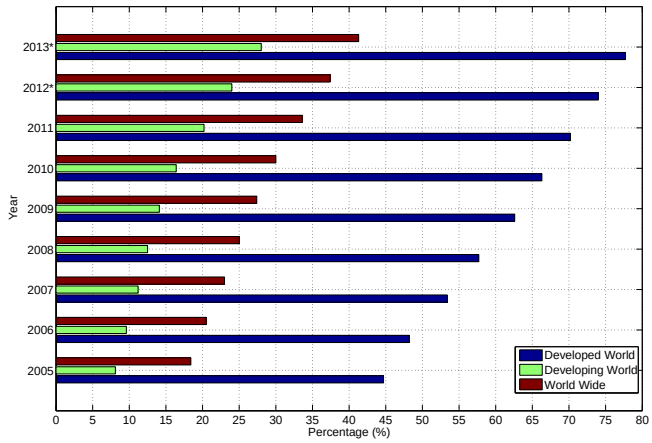

(b) Households with Internet access at home

Figure 1.2: Increasing Use of Internet in daily lives [1]

order to avoid interference and increase the signal strength at the desired mobile user. It also supports advanced concepts like virtual multiple-input multiple output (MIMO) and relaying.

The gains offered by these techniques on the single communication link do not necessarily represent the same gains when deployed in a huge system. Therefore, the system level simulations are an absolute necessasity for the performance evaluations before the deployment of such schemes. And this is where one realizes the importance of system level simulators. In system level simulations the true performance of the proposed techniques is evalu-

ated with full scale system implementation and the compatibility of these schemes with already existing ones is also validated.

System level simulations normally require heavy computations for extremely long duration of time because of the characterization of the radio links between each user and base station. The link level simulations of all such links is the bottle neck in these simulations. To find about the impact of the link level computations we performed a small simulation with one eNodeB (LTE acronym for base station - enhanced NodeB) and one UE (LTE acronym for mobile station - user equipment) using Eurecom's OpenAirInterface (OAI) system level simulator which has an integrated link level simulator as well.

To find out about the resources spent on the physical layer we performed profiling on different blocks of the simulator. During the simulation we calculated the time which has been spent on each block in the simulator and also the frequency of calling a certain block was calculated. This is shown in Figure 10.5 where the boxes in green corresponds to the main tasks related to the downlink link level simulator[1]. It can be seen that most of the simulation time and resources are spent on the blocks which correspond to the link level simulator.

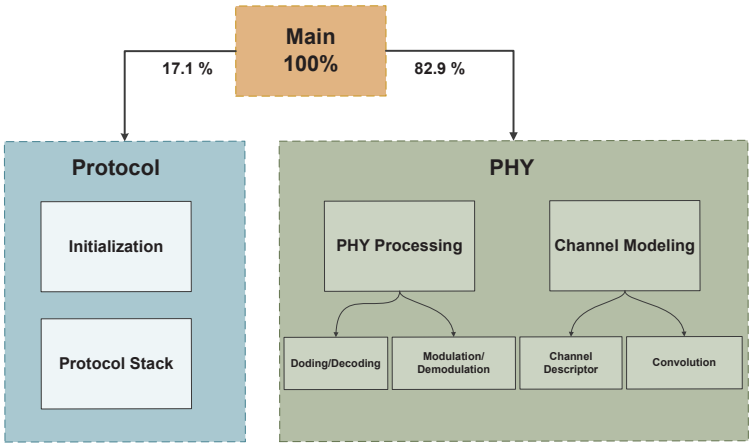

Figure 1.3: Simplified Profiling Diagram for System Level Simulations

[1]Please note that profiling was performed using *gprof* under Linux operating system and gprof has the limited capability of profiling and can not profile for the hardware specific instructions. In OAI simulator Turbo decoder is implemented with high precision and extremely low complexity using Intel instruction set and the calls to Turbo decoder are not visible in the profiling figure.

A rather simplified version of profiling is shown in Figure 10.3 where the percentage of the time duration spent for the link level simulations and rest of the system level related tasks is shown. Although it was an extremely trivial system but still more than 82% of the simulation time was spent on the link level simulation whereas only a small fraction of time was spent on the protocol stack and other system related tasks.

Therefore, to reduce the complexity and duration of system level simulations it is absolutely necessary to have an accurate physical layer (PHY) abstraction model which replaces the actual link level computations and provides the higher layers with necessary and accurate link quality metric, i.e., block error rate (BLER) or packet error rate (PER). A link abstraction model is used to determine the required system level quality indicator using ideal link adaptation without actually having to simulate any PHY processing , i.e., coding, modulation, convolution of channel with signal, demodulation and decoding. This is depicted in Figure 10.4 where it can be seen that PHY abstraction provides upper layers with necessary decision on the decodability of the packet under instantaneous channel conditions whereas in full PHY processing this decision is only obtained from the decoder itself. In this form it is an extremely valuable low complexity tool for efficient large scale system simulations. Moreover it can also be used for fast resource scheduling, fast link adaptation using adaptive power control and adaptive modulation and coding.

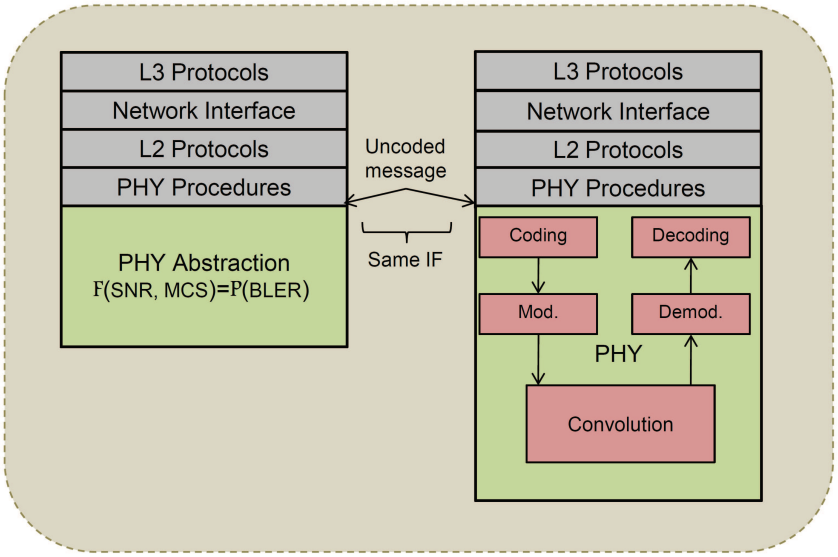

Figure 1.4: Comparison of Protocol Stack with and without PHY abstraction

The main motivation of this thesis, therefore, was to investigate and propose new PHY abstraction models for different antenna configurations in LTE and provide a pragmatic approach so that these abstraction models have higher level of applicability, accuracy and realism. This shall not only provide the fundamental basis in the improvement for the system level simulators, with which it shall be possible to test different higher layer protocols and scheduling schemes, but also these PHY abstraction schemes can be used in the real time evaluations of the base stations.

Moreover, this thesis provides fundamental parameters for the PHY abstraction of different transmission modes of LTE and provides an in-depth analysis on the various aspects of PHY abstraction. The problem of having an analytical solution for the inclusion of incremental redundancy hybrid automatic repeat request (IR-HARQ) is also handled in this thesis and two semi-analytical approaches has been proposed to map the benefits of IR-HARQ with high level of precision and efficiency.

Another objective of this thesis is to show that PHY abstraction techniques have actually lot of potential and can be used in more than one scenario and for more than one purpose. We show that the PHY abstraction implemented in system level simulator provides at least 30 times the speed up of the simulation as compared to the system with full PHY processing. We also showed by providing an aggregated throughput over the given number of frames to show that PHY abstraction provides exactly same kind of performance as a system with full PHY processing. This provides an extremely encouraging and positive result for the use of PHY abstraction in system simulations. Also we showed that it can improve the channel quality indicator (CQI) feedback for the selection of appropriate modulation and coding scheme (MCS) on the downlink and with a slight modification it can also be used for real channel estimates to prove fundamental communication concepts in various environments.

1.2 Outline and Contributions

This thesis is mainly divided in two parts, methodologies and applications. Some basic concepts related to LTE and the topics covered in this thesis are presented as background knowledge in Chapter 2. Part-I describes the PHY abstraction schemes for different transmission modes of LTE and their validation through link level simulators. At first this part provides a global view on the methodology of PHY abstraction and answers some very important questions about the validation of these schemes with the help of link level simulators. Then it extends the abstraction schemes for the case of multi-user (MU) MIMO communication where the interference is non-Gaussian

and its structure is exploited during the decoding therefore the PHY abstraction should also be able to exploit the knowledge about interference for accurate modeling. The inclusion of IR-HARQ for LTE is then discussed in detail and two novel semi-analytical procedures are proposed which make use of only three reference additive white Gaussian noise (AWGN) curves and provide simple solution for variable bandwidth assignment.

Part-II presents some of the possible applications of PHY abstraction starting with its implementation for system level simulations and then comparing different aspects of PHY abstraction where it is beneficial. It can also be used for the fast link adaptation in LTE where an efficient CQI can be calculated using PHY abstraction and an appropriate modulation and coding scheme (MCS) can be selected for the downlink. Another very important application of PHY abstraction is the validation of different communication aspects with the help of measured channel estimates. A brief overview of each chapter is presented below.

1.2.1 Fundamentals

This chapter covers the basic concepts related to the LTE standard in general and specifically about the physical layer. It is intended to provide a quick reference to different concepts about LTE system which shall be frequently used in the rest of the thesis. It starts with a very brief history on the evolution of cellular standards and discusses the LTE protocol, LTE frame structure and downlink processing, e.g., channel coding, modulation etc, and forward error correction in LTE using IR-HARQ. Then it provides a short introduction to an important concept of bit interleaved coded modulation (BICM) and presents the BICM capacity for the quadrature amplitude modulation (QAM) alphabets. Finally this chapter concludes with a formal introduction of PHY abstraction for orthogonal frequency division multiplexing (OFDM)-based systems.

1.2.2 Part I - Methodologies

Chapter 3

This chapter presents PHY abstraction methodologies for single-user (SU) communication in LTE. It provides the detailed training and validation of PHY abstraction schemes with the help of link level simulator for different transmission modes of LTE. It answers the various fundamental questions about the design and validation of PHY abstraction schemes with the help of detailed results. It provides the AWGN reference performance curves used for the link quality indication and shows that the calibration of adjustment factors in popular PHY abstraction schemes is a necessary step especially for the case of mutual information based PHY abstraction and multi-antenna

configurations. The methodology is presented for single-input single-output (SISO) channel and for multiple-input single-output (MISO) channels, employing space time block codes (STBC), i.e., Alamouti codes and transmit precoding. Some of the results from this chapter are published in,

- Imran Latif, Florian Kaltenberger Navid Nikaein and Raymond Knopp, "**Large scale system evaluations using PHY abstraction for LTE with OpenAirInterface**", EMUTOOLS 2013, *1st Workshop on Emulation Tools, Methodology and Techniques, March 5, 2013*, Cannes, France in conjunction with SIMUTools 2013, *6th International ICST Conference on Simulation Tools and Techniques, March 5-7, 2013*, Cannes, France.

and will be presented as one part of the invited paper in,

- Imran Latif, Florian Kaltenberger and Raymond Knopp, "**On Scalability, Robustness and Accuracy of physical layer abstraction for large-scale system level evaluations of LTE networks**", ASILOMAR 2013, *47th Annual Conference on Signals, Systems, and Computers, November 3-6*, 2013, Pacific Grove, CA, USA.

Chapter 4

This chapter presents a novel PHY abstraction model for incorporating the knowledge of interference along with the desired signal strength to predict the link performance for the MU MIMO systems. The important aspect of this method is that it can be used for not only MU MIMO systems but for other interference limited MIMO systems as well where the interference is non-Gaussian. A particular example of such scenario is the transmission based on the spatial multiplexing in LTE with two independent data streams. For this case the interference received on both streams is not Gaussian and belongs to a finite QAM alphabet whose structure can be exploited during the decoding. The proposed PHY abstraction is able to exploit this information for the PHY abstraction. This chapter shows the results for the validation of proposed scheme with the two state-of-the-art methods and its superiority is proved using link level simulator. Some of the results are published in,

- Imran Latif, Florian Kaltenberger and Raymond Knopp, "**Link abstraction for multi-user MIMO in LTE using interference-aware receiver**", WCNC 2012, *IEEE Wireless Communications and Networking Conference, April 1-4*, 2012, Paris, France.

and will be submitted as one part of journal paper,

- Imran Latif, Florian Kaltenberger and Raymond Knopp, "**Link Performance Prediction for Single and Multi-User MIMO in LTE with Interference Aware Receivers**", under preparation.

Chapter 5

This chapter presents two novel semi-analytical PHY abstraction models which predict the link performance of LTE systems with IR-HARQ for variable bandwidth assignment. These proposed models make use of an intelligent design of rate matching in LTE for making the modeling of IR-HARQ independent of the size of transport block size (TBS) and reduces the storage requirements for the PHY abstraction by utilizing reference performance curves corresponding to the mother code rate. The two proposed approaches are *symbol level modeling* and *bit level modeling*. As it is clear from the names that former is based on symbol level modeling and is thus easier to implement whereas the latter is based on bit level modeling and is more accurate. The results for different rounds of IR-HARQ are shown in this chapter and it is observed that the proposed models provides very accurate validation results from the link level simulator. The results from the symbol level modeling are published in,

- Imran Latif, Florian Kaltenberger, Raymond Knopp and Joan Olmos, "**Link abstraction for variable bandwidth with incremental redundancy HARQ in LTE**",WiNMEE 2013, *9th International Workshop on Wireless Network Measurements*, in conjunction with *11th Intl. Symposium on Modeling and Optimization in Mobile, Ad Hoc, and Wireless Networks (WiOpt 2013), May 13-17*, 2013, Tsukuba Science City, Japan.

and the results for the bit level modeling are published in,

- Joan Olmos, Albert Serra, Silvia Ruiz, Imran Latif, "**On the use of mutual information at bit level for accurate link abstraction in LTE with incremental redundancy H-ARQ**", COST IC 1004, *5th MC and Scientific Meeting, Technical Research Report IC1004 TD(12)05046, 24-26 September 2012*, Bristol, UK.

These results are also being planned to be published in journal paper.

1.2.3 Part II - Applications

Chapter 6

This chapter presents a complete methodology for implementing the PHY abstraction in a system level simulator with the help of Eurecom's OAI system level simulator. It shows that how the PHY abstraction should be transparent to the upper layers of the LTE protocol stack to benchmark the performance of PHY abstraction and full PHY processing. It provides a detailed comparison of different transmission modes of LTE for the simulations with and without PHY abstraction. It shows that PHY abstraction is a valuable tool for large scale system simulations by providing very similar

results as a system with full PHY processing would provide. It also shows that using PHY abstraction can provide a huge amount of speed up in the simulation and thus can be used for an efficient real time performance evaluations without the loss of real transceiver performance. The results from this chapter are published in the paper presented at EMUTOOLS and shall also be published in the invited paper at ASILOMAR 2013.

Chapter 7

This chapter provides another important application of PHY abstraction. It provides the performance comparison of different LTE transmission modes in rural areas at 800 MHz band with the help of real channel estimates and mutual information based PHY abstraction scheme. It provides a detailed methodology for the use of PHY abstraction for such experiments. It can not only validate some of the well understood concepts of communications but can also be used for extensive analysis by extrapolating the results to various other scenarios. In this chapter the results for MU MIMO are extrapolated from the channel estimates of another transmission mode and it is shown that it is advantageous to do opportunistic MU MIMO whenever it is possible as it provides overall better throughput even when we restrict our results to only lower modulation. The results from this chapter are published in,

- Imran Latif, Florian Kaltenberger, Rizwan Ghaffar, Raymond Knopp, Dominique Nussbaum, Hervé Callewaert, and Gaël Scot. "**Performance of LTE in Rurual Areas - Benefits of Opportunistic Multi-User MIMO**", PIMRC 2011, *22nd Annual IEEE International Symposium on Personal, Indoor, and Mobile Radio Communications, September 11-14*, 2011, Toronto, Canada.

- Andrea F. Cattoni, Hung T. Nguyen, Jonathan Duplicy, Deepaknath Tandur, Bilijana Badic, Rajarajan Balraj, Florian Kaltenberger, Imran Latif, Ankit Bhamri,Guillaume Vivier, Istvan Z. Kovacsk, Peter Horvat, "**Multi-user MIMO and carrier aggregation in 4G systems: the SAMURAI approach**", WCNC 2012, *IEEE Wireless Communications and Networking Conference, April 1-4*, 2012, Paris, France.

Chapter 8

This chapter presents the problem of fast link adaptation (FLA) in LTE and shows that using the knowledge of antenna configuration from the control channel information, an improved CQI can be calculated with the help of mutual information based PHY abstraction. Then using this improved CQI the scheduler at the eNodeB can select more appropriate MCS which can increase the overall system throughput. We show that when a UE is being

scheduled in transmission mode 6 then this improved link adaptation can provide gain in the throughput of the system by selecting a more feasible MCS on the downlink. The results from this chapter shall be published in,

- Imran Latif, Florian Kaltenberger and Raymond Knopp, "**Improved Link Adaptation and Scheduling for Transmit Beamforming in LTE using OpenAirInterface**", under preparation.

1.2.4 Conclusion & Future Work

Finally this chapter concludes the thesis by giving a quick summary of the achievements of the thesis and also provides the guidelines for the future directions in which this work can be further extended.

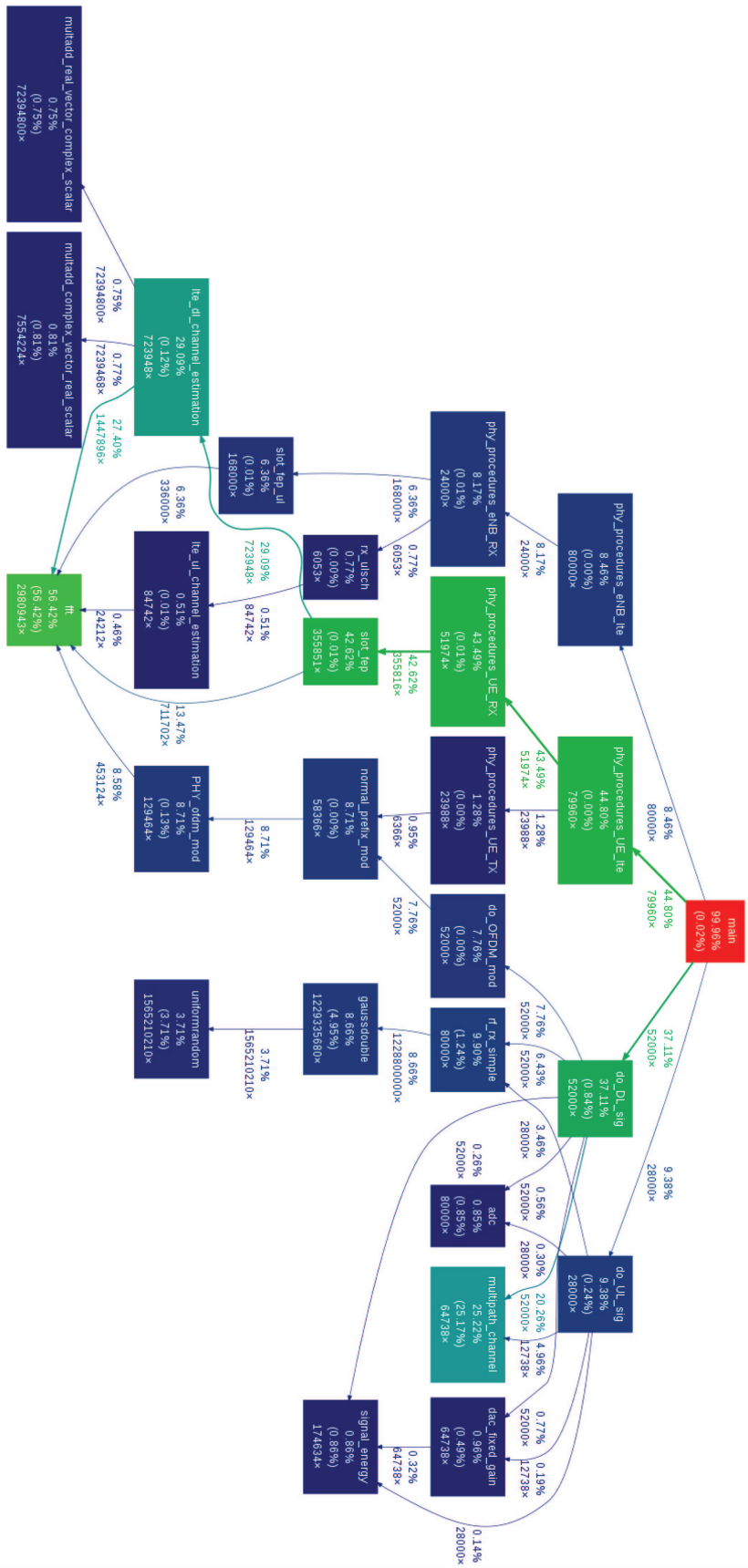

Figure 1.5: Profiling for System Simulation with 1 eNodeB and 1 UE in the context of LTE, SISO channel, frequency selective Rayleigh channel and constant bit rate traffic.

Chapter 2

Fundamentals

2.1 Brief history of Cellular Standards

The first popular cellular system Advanced Mobile Phone Service (AMPS) was deployed in 1983 in USA and was purely based on analog communication. Later it was deployed in several countries in South America, Asia and North America. With the installation of the first global system for mobile (GSM) in 1991 came the era of second generation (2G) mobile communications. It was a major break through in terms of quality, latency and privacy of mobile communications. GSM was the first complete digital mobile phone system which was immediately welcomed by the major countries of the world and still holds the majority of global market share. The second generation was initially designed to be circuit switched system for an improved voice communication but later with the demand of data services an additional plane for the packet-based services was included in this standard. This data plane was known as general packet radio service (GPRS) which evolved into enhanced data rates for GSM evolution (EDGE). EDGE could provide peak data rates up to 384kbps and the average data rate of 80-120kbps. But soon the desire for higher data rates moved the standardization bodies to develop standards which can provide higher data rates with low latency and multimedia support which lead to the design of third generation (3G) systems.

The third generation systems were a significant improvement over 2G systems with comparatively higher data rates, improved voice capacity as well as advanced data services and applications. These systems were wideband communication systems and were based on code division multiple access (CDMA). The first 3G standard was named as universal mobile telephone

Table 2.1: Summary Comparison of GSM (2G), WCDMA (3G) and LTE

	GSM	WCDMA	LTE
Standard	GSM	3GPP release 99	3GPP Release 8
Frequency Bands	850/900MHz, 1.8/1.9GHz	850/900MHz, 1.8/1.9/2.1GHz	700MHz, 1.7/2.1GHz, 2.6GHz, 1.5GHz & more
Channel Bandwidth	200KHz	5MHz	1.3, 3, 5, 10, 15, 20MHz
Multiple Access	TDMA,FDMA	CDMA	OFDMA (DL) & SC-FDMA (UL)
Duplexing	FDD	FDD	FDD & TDD
Peak Data Rate	GPRS 107kbps; Edge 384kbps	2048kbps	150Mbps (DL) & 75Mbps (UL)
User Plane Latency	600-700ms	100-200ms	5-15ms

service (UMTS) Release 99 by the 3GPP and was published in 1999. It became very popular and soon it was deployed in most of the countries. UMTS Release 99 was further enhanced by introducing high speed packet access (HSPA) and HSPA + whose evolution is still ongoing. But all these systems were still not able to meet the data requirement of today's market and thus in parallel to these standards, 3GPP started from scratch to develop a new standard known as Long Term Evolution (LTE) which can provide high amount of data rates and low latency [4]. A detailed comparison of LTE with legacy mobile standards in terms of latency, peak data rate on DL and UL, spectral efficiency, etc. is given in Table 2.1.

2.2 Third Generation Partenership Project - Long Term Evolution

3GPP finalized the standardization of its first LTE release in 2008 and as a result it was named Release 8. LTE was designed primarily with a goal in mind to effectively provide the performance comparable with the wired broadband services. It was designed to provide 100Mbps at the downlink (DL) and 50Mbps on the uplink (UL). Almost a decade ago, these data rates were only possible on broadband wired networks but today LTE Release 8 has even surpassed its minimum requirements by providing even higher data rates on both UL and DL. the LTE standard uses OFDM as the underlying modulation scheme with OFDMA on the downlink and single-carrier (SC)-FDMA on the uplink. OFDM has number of benefits when compared to its predecessor WCDMA, especially the ease of frequency domain equalization and the inclusion of cyclic prefix to fight inter-symbol-interference (ISI). Furthermore, OFDM converts a frequency selective broadband channel into

several narrowband flat fading channels because of which it becomes ideal candidate for the MIMO techniques. Moreover, the use of OFDM allows frequency domain resource allocation in LTE which increases the spectral efficiency of the system.

Among other improvements in LTE are the support of multi-layer transmission using multiple antennas at the transmitter and receiver, inclusion of capacity achieving Turbo codes, bit interleaved coded modulation (BICM), efficient rate matching, HARQ at the physical layer and adaptive modulation and coding (AMC) at the MAC layer. Although it is not absolutely necessary in the scope of this thesis to highlight the core network components of LTE, a few details of the evolved packet core (EPC) nevertheless be mentioned. LTE has in fact revolutionized the cellular communications by providing a complete paradigm shift to all IP network core from the architecture of having a separate circuit switched and packet switched cores. It is shown in Figure 2.1 that all the components which were necessary in 2G and 3G networks are replaced by rather simple and efficient all IP-based EPC.

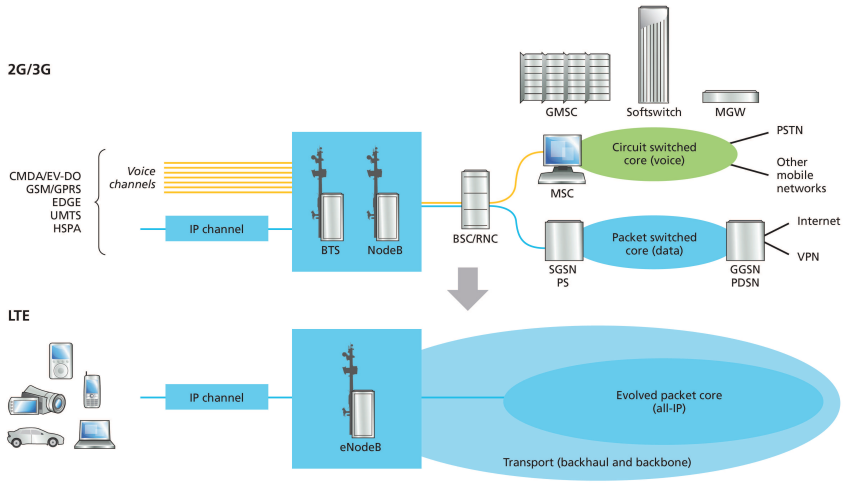

Figure 2.1: LTE: From separate circuit-switched and packet-switched cores to an all-IP core [2]

2.2.1 Evolved Packet Core

EPC is designed in Release 8 to provide high capacity, all IP, reduced latency, flat architecture that dramatically reduces cost. It also supports advanced, real time and media rich services with an enhanced quality of experience. Its intelligent design includes backward compatibility to legacy 2G GSM-EDGE

Radio Access Networks (GERAN) and 3G Universal Terrestrial Radio Access Networks (UTRAN) connected via Serving GPRS support nodes (SGSN). EPC takes care of access control, packet routing and transfer, mobility management, security, radio resource management (RRM) and network management. More details about the LTE network architecture and EPC can be found in [2].

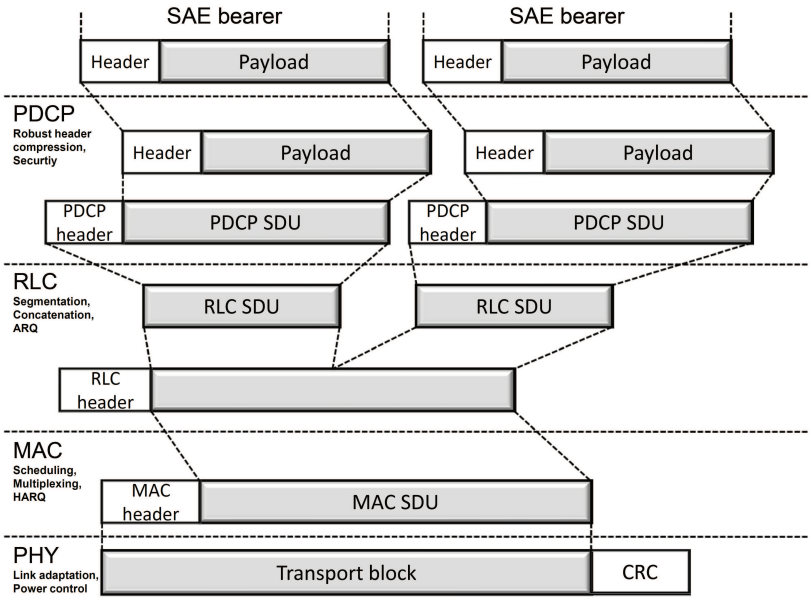

Figure 2.2: An example of data flow in LTE protocol

2.2.2 Protocol Stack and Data Flow

In LTE protocol stack is structured into four main layers and each layer is responsible for different tasks. An example of data flow between these layers is shown in Figure 2.2 where the data from or to higher layers is known as service data unit (SDU). The brief introduction of four layers is given below as,

- Packet Data Convergence Protocol (PDCP) [5] is responsible for the robust header compression of the incoming IP packet and performs ciphering to provide security.
- Radio Link Control (RLC) [6] is responsible for segmentation/concatenation and in order transmission of the RLC SDU. It also perform RLC retransmission employing automatic repeat request (ARQ).

- Medium Access Control (MAC) [7] is responsible for scheduling, multiplexing of users and Hybrid-ARQ (HARQ) retransmissions for the packets which were received in error and could not be decoded at the receiver.
- Physical Layer (PHY) [8] is responsible for the actual transmission and contains processes like channel coding, modulation, multi-antenna processing, resource mapping etc.

In the rest of this chapter we shall give more details about the structure of the physical layer and the processing performed on this layer in the LTE standard.

2.3 LTE Physical (PHY) Layer

In LTE the physical layer is responsible for the final transmission and reception of the data. The communication is organized in the form of radio frames. Generally one radio frame spans some duration in time and bandwidth in the frequency domain.

2.3.1 Radio Frame

In LTE the smallest resource for which the data can be allocated is the resource element (RE). A resource element consists of one OFDM symbol plus cyclic prefix (CP) in time domain and 15kHz of bandwidth in the frequency domain. In this sense the RE is a two dimensional quantity which can be allocated for data transmission. Twelve of such consecutive resource elements in the frequency domain combined with 6 or 7 (depending on the length of the CP) OFDM symbols in the time domain form a physical resource block (PRB). A PRB is a RE grid with a duration of 0.5ms and has a bandwidth of 180kHz. This is shown in Figure 2.3.

In LTE the whole bandwidth is divided into several PRBs and the users are allocated certain number of PRBs. The possible number of PRBs and REs for variety of available bandwidths in LTE are given in the Table 2.2. Furthermore, the PRB allocation for a specific bandwidth of 5 MHz is shown in Figure 2.4. It can be seen in Figure 2.4 that there exists some percentage of the total bandwidth which acts as a guard bandwidth and a user can be assigned a specific number of PRBs as its allocated bandwidth.

In the time domain 6 or 7 OFDM symbols make one slot of duration 0.5ms and a cyclic prefix is added to the beginning of each slot. This can be seen in Figure 2.5. In LTE standard there exist two types of cyclic prefixes,

- Normal Cyclic Prefix (NCP)

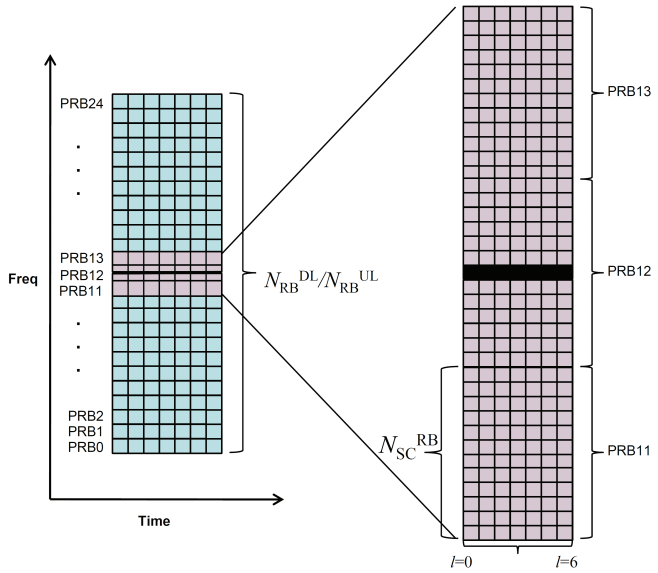

Figure 2.3: Time and Frequency view of LTE Frame Grid

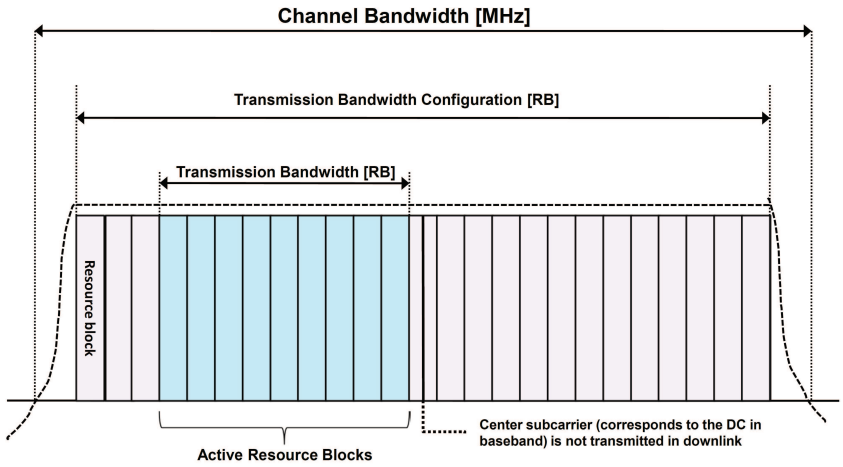

Figure 2.4: An Example for the Frequency Domain Bandwidth allocation in LTE with 5MHz bandwidth

- Extended Cyclic Prefix (ECP)

For an ECP there are six OFDM symbols in each slot whereas for NCP there are 7 OFDM symbols in one slot. A detailed information about the length of a normal and extended cyclic prefix is shown Figure 2.5. ECP provides more protection against ISI by having longer duration of CP and is thus used

Table 2.2: Available Bandwidths in LTE and Corresponding REs and PRBs

Channel Bandwidth [MHz]	1.4	3	5	10	15	20
Useful Bandwidth [MHz]	1.08	2.7	4.5	9.0	13.5	18
Bandwidth Expansion (%)	23	10	10	10	10	10
Sampling Frequency [MHz]	1.92	3.84	7.68	15.36	23.04	30.72
Number of PRBs	6	15	25	50	75	100
Number of REs	72	180	300	600	900	1200

for scenarios where the multiple copies of the signal can arrive with a larger delay.

It can be seen in Figure 2.5 that two slots are combined together to make a subframe of duration 1ms. This duration is also called transmission time interval (TTI) and each TTI duration a new scheduling and AMC decision can be taken in LTE. Ten of such subframes combined together make an LTE *radio frame* of duration 10ms, which is the main unit for transmission on the LTE PHY layer. The discussion until this point is more relevant to the time division duplexing (TDD) frame configurations. For the case of frequency division duplexing (FDD) the only difference is that there exists no special subframe and all of the subframes are allocated either for the DL or the UL, whereas in the TDD there exists many different configurations with a special subframe for the choice of DL and UL communication which are shown in the Table 2.3.

Table 2.3: LTE TDD Frame Configurations

TDD DL/UL Configuration	Subframe Number									
	0	1	2	3	4	5	6	7	8	9
0	D	S	U	U	U	D	S	U	U	U
1	D	S	U	U	D	D	S	U	U	D
2	D	S	U	D	D	D	S	U	D	D
3	D	S	U	U	U	D	D	D	D	D
4	D	S	U	U	D	D	D	D	D	D
5	D	S	U	D	D	D	D	D	D	D
6	D	S	U	U	U	D	S	U	U	D

In this thesis, however, all the results are based on the TDD configuration 3 only where there are 6 DL subframes, 3 UL subframes and one special subframe. Also throughout this thesis normal cyclic prefix is used for all of the discussions and for generating the results.

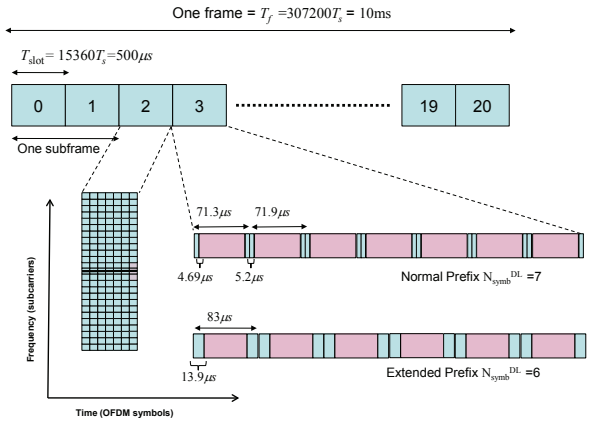

Figure 2.5: LTE Frame structure

2.3.2 PHY Processing

For the LTE downlink the physical layer processing mainly consists of channel coding, modulation and layer mapping as shown in Figure 2.6. Channel coding takes the input from the MAC layer as transport blocks and performs coding on them to obtain codewords whereas the modulation generates complex valued OFDM basedband signals for each antenna port which are then upconverted to the carrier frequency.

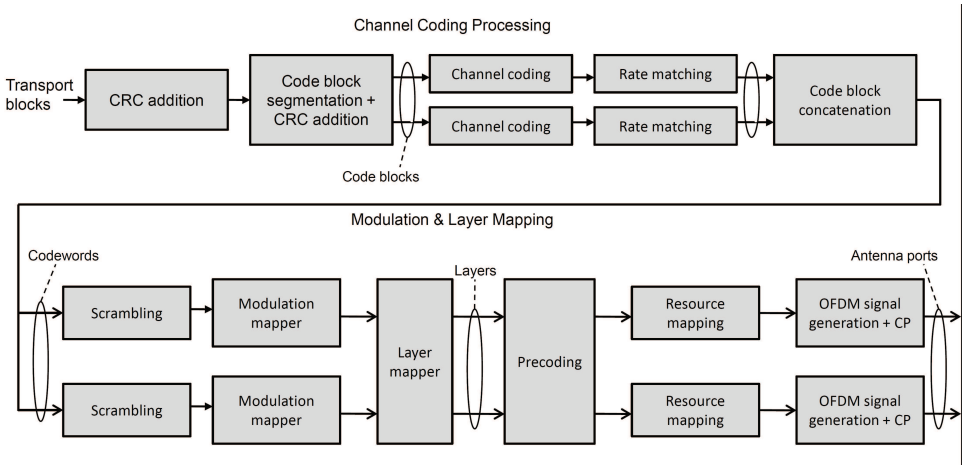

Figure 2.6: Channel coding, Rate matching and Modulation Mapping in LTE

To provide forward error detection a cyclic redundancy check (CRC) are 24 parity bits is attached to the transport block. This CRC is generated using the cyclic generator polynomials described in [9]. The code block segmentation is performed on the resulting transport block only if the number of CRC and transport block bits becomes greater than the maximum allowed size of the interleaver in the turbo code(6144). If the segmentation is performed then an additional CRC of 24 bits is attached again to each of the code block. After this rate 1/3 Turbo coding is performed on each code block.

Turbo Coding and Rate Matching LTE utilizes capacity achieving turbo codes with rate 1/3 for the downlink transmission. The turbo encoder in LTE consists of one systematic and two parallel concatenated 8-state convolutional encoders and one internal interleaver. As is shown in the Figure 2.7 (a) the box labeled as systematic bits contains the code block directly and the boxes labeled as parity bits 1 and 2 contain the bits from the constituent encoder 1 and 2 respectively. Each data block has its own interleaver and the interleaved data bits are written into the circular buffer. Then for an arbitrary code rate transmission the codewords are generated using the circular buffer (CB) and rate matching. Since the CB corresponds to the code rate 1/3 (also referred to mother code), therefore, the codewords with higher code rate than the mother code rate can be generated by transmitting only a portion of the CB. And the codewords with lower code rate than mother code can be generated by transmitting the CB several times. More details about the structure of LTE rate matching and the CB can be found in [9] [10].

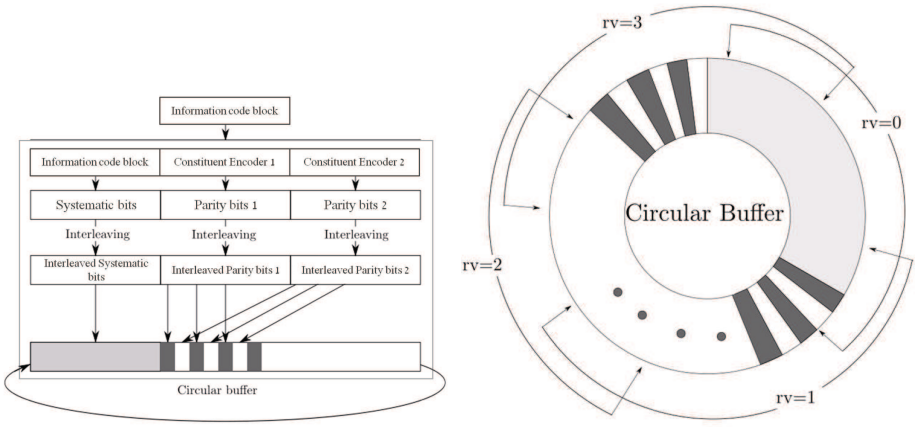

(a) Turbo Encoder in LTE (b) Redundancy Versions (rv) in LTE

Figure 2.7: Turbo Coding and IR-HARQ in LTE

2.3.3 HARQ in LTE

In LTE HARQ is supported at the PHY layer to provide higher improvements in the PHY throughput. If the first transmission is not successful, then the UE sends back a not-acknowledged (NACK) signal to the eNodeB on its UL control channel indicating that the codeword is received in error and is not decoded correctly. The eNodeB then transmits the either the same copy of codeword it sent in round 1 or sends a codeword such that it contains some repeated bits and mostly new parity bits. This is possible in LTE with the help of redundancy versions (RV) and virtual circular buffer. The design of rate matching and puncturing in LTE is very sophisticated and it can be used for implementing an arbitrary code size and HARQ benefits from the design of different redundancy versions. After receiving the certain number of retransmission, the effective signal is calculated at the receiver by applying the maximum ratio combining on the received log-likelihood ratios (LLRs) during different retransmissions. The gains received after the decoding can be actually divided into two categories, the coding gain which comes from the transmission of new parity bits in each retransmission and the receive SNR gain which comes from the repetition of coded bits in each retransmission. It is very well known that for turbo codes with contention free interleavers, most of the Hamming weight in the minimum distance resides in the parity bit streams. Therefore, the retransmissions are designed to have more new parity bits so that the effective minimum distance of the punctured code is improved and provides good performance at higher code rates. There are two types of HARQ supported in LTE,

- Chase Combining (CC) where in case of unsuccessful decoding at the receiver, the transmitter sends the copy of the same data as in previous transmissions.
- Incremental Redundancy (IR) where a combination of some old bits and some new parity bits is transmitted in the case of unsuccessful decoding at the transmitter.

For the IR-HARQ in LTE there are four different redundancy versions (RV) as shown in Figure 2.7 (b) which are created by reading out the bits from a different starting point in the CB. The adjacent RVs contain equal number of the repeated bits and if the same MCS is used for retransmission then each of the RV has the same size.

2.4 Bit Interleaved Coded Modulation (BICM)

Another important concept in the scope of this thesis is bit interleaved coded modulation (BICM). BICM was first proposed by Zehavi [11] and then later a detailed information theoretic analysis was performed by Caire et al [12].

BICM is being used in many of the latest standards, e.g., IEEE 802.11a, IEEE 802.16 and 3GPPs LTE because of its improved performance and ease of implementation compared to the coded modulation scheme. Figure 2.8 shows a generic baseband BICM channel model with iterative decoding. The vector of encoded bits c generated by the encoder is interleaved, generating $c' = \Pi(c)$.

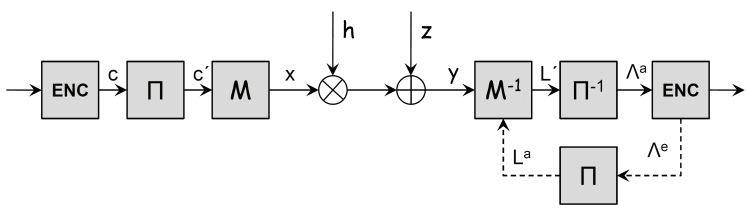

Figure 2.8: Baseband BICM-ID transmission model

The output of the interleaver is then given to the modulator where these inteleaved and coded bits are gathered in length-n codewords which are then mapped to complex symbols $x \in \chi$ using a binary memoryless mapping $\mathrm{M} : \{0,1\}^n \rightarrow \chi$ where χ is the constellation alphabet. Then these symbols $\mathbf{x} = [x_0, x_1, \cdots, x_N]$ are transmitted through the channel where N is the symbol block length. Then the received signal at time t can be given as,

$$y_t = h_t.x_t + z_t \tag{2.1}$$

where h_t is a complex channel gain and z_t is a zero mean real white Gaussian noise sample with variance N_0. We shall hereafter drop the index t, as in the rest of the chapter the individual channel symbols shall be considered.

2.4.1 BICM Capacity for QAM Constellation

The mutual information for the system for a finite size QAM constellation with $|\chi| = M$ takes the form,

$$\begin{aligned} I\left(Y;X|h\right) =& \mathcal{H}\left(X|h\right) - \mathcal{H}\left(X|Y,h\right) \\ =& \log M - \mathcal{H}\left(X|Y,h\right) \end{aligned} \tag{2.2}$$

where $\mathcal{H}\left(.\right) = -E\log p\left(.\right)$ is the entropy function. The second term of (2.2) is given as

$$\begin{aligned} \mathcal{H}\left(X|Y,h\right) =& \sum_{x\in\chi}\int_y\int_h p\left(x,y,h\right)\log\frac{1}{p\left(x|y,h\right)}dy \\ =& \sum_{x\in\chi}\int_y\int_h p\left(x,y,h\right)\log\frac{\sum_{x'\in\chi}p\left(y|x',h\right)}{p\left(y|x,h\right)}dy \end{aligned} \tag{2.3}$$

Note that conditioned on the channel, the only source of randomness is the noise. So (2.3) can be extended as

$$\begin{aligned}\mathcal{H}\left(X|Y,h\right) &= \frac{1}{M}\sum_{x\in\chi}\mathcal{E}_z \log \frac{\sum_{x'\in\chi}\exp\left[-\frac{1}{N_0}\left|hx+z-hx'\right|^2\right]}{\exp\left[-\frac{1}{N_0}\left|z\right|^2\right]} \\ &= \frac{1}{M}\sum_{x\in\chi}\mathcal{E}_z \log \frac{\sum_{x'\in\chi}\exp\left[-\frac{1}{N_0}\left|h(x-x')+z\right|^2\right]}{\exp\left[-\frac{1}{N_0}\left|z\right|^2\right]}\end{aligned}$$

then the mutual information for QAM constellation symbols can be written as,

$$I\left(Y;X|h\right) = \log M - \frac{1}{M}\sum_{x\in\chi}\mathcal{E}_z \log \frac{\sum_{x'\in\chi}\exp\left[-\frac{1}{N_0}\left|h\left(x-x'\right)+z\right|^2\right]}{\exp\left[-\frac{1}{N_0}\left|z\right|^2\right]} \tag{2.4}$$

Please note that the mutual information of (2.4) represents the case for single user system with no interference. Figure 2.9 shows the mutual information for the case of QPSK, 16-QAM and 64-QAM. This mutual information shall be used for the mutual information based PHY abstraction in the rest of the thesis.

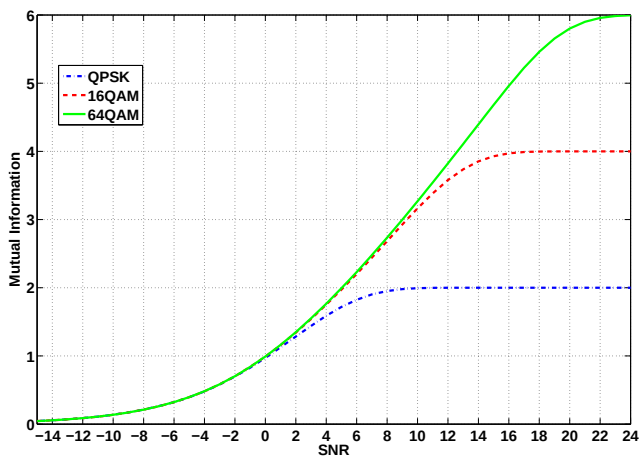

Figure 2.9: Mutual Information versus SNR for different QAM constellations

2.5 OpenAirInterface

OpenAirInterface is an open-source platform for experimentation in wireless systems with a strong focus on cellular technologies such as LTE and LTE-Advanced. The platform comprises of both hardware and software components and can be used for simulation/emulation as well as real-time experimentation. It comprises of the entire protocol stack from the physical to the networking layer. The objective of this platform is to fill the gap between the simulation and real time experimentation by providing the baselines for protocol validation, performance evaluation and pre-deployment system test. The key features are

- Extensive LTE Release 8.6 compliance with some features from LTE-Advanced
- Full protocol stack for both UE and eNB implementations
- Provides Linux networking interface to run any application on top
- Carrier aggregation possible
- Implements several important transmission modes (TM) of LTE
    - LTE TM 1 (SISO)
    - LTE TM 2 (STBC - Alamouti Codes)
    - LTE TM 5 (MU MIMO)
    - LTE TM 6 (Transmit Precoding)

OpenAirInterface comprises of a highly optimized C implementation including all of the elements of the 3GPP LTE Rel 8.6 protocol stack for UE and eNB (PHY, MAC, RLC, RRC, PDCP, NAS driver). Apart from real-time operation of the software modem on a hardware target, the full protocol stack can be run in emulation. The OpenAirInterface emulation environment allows for virtualization of network nodes within physical machines and distributed deployment on wired Ethernet networks. Nodes in the network communicate via direct-memory transfer when they are part of the same physical machine and via multicast IP over Ethernet when they are in different machines. In the first case the emulator can either be run with the full PHY layer or with PHY abstraction while in the latter case nodes interface at layer 2. The rest of the protocol stack (MAC and RLC) for each node instance uses the same implementation, as would the full system. Each node has its own IP interface that can be connected either to an application or a traffic generator. The emulator also comprises a simple mobility model and channel models including path loss, shadow fading and stochastic small scale fading.

2.6 PHY Abstraction

The purpose of PHY abstraction is to provide an accurate mapping between the link level and system level simulator in terms of the link quality measure. Traditionally this link quality measure is evaluated in terms of the BLER which is a function of signal-to-interference plus noise ratio (SINR) averaged over the several channel and noise realizations of one specific channel model. It is very important to mention that average SINR-to-BLER mapping may suffice assuming that every transmitted coded block encounters similar channel statistics. But this assumption usually does not hold in recent wireless mobile systems, due to several reasons:

- In OFDM-based systems, the frequency selectivity caused by multipath propagation introduces SINR variations across the subcarriers. The coded block is transmitted over several sub-carriers; therefore the post-processing (after equalization) symbol SINR values are not uniform.
- In multi-antenna systems the same coded block is transmitted across several spatial layers, each experiencing different channel thus giving rise to the variations in received SINR.
- The channels are also time selective, causing the channel gains of the sub-carriers to change in time, especially in the high mobility cases.
- Current systems include HARQ; delays in retransmissions and the time-varying channel introduce SINR variations across the transmitted symbols.

In this way, symbols with unequal SINR values may arrive at the receiver. The coded bits are fed to the decoder having different qualities, due to transmitting them on different spatial layers, in different OFDM symbols and on different OFDM subcarriers. This is equivalent to transmitting the FEC block through multiple-state channels. Predicting the BLER performance from a channel realization (the instantaneous SINR for each sub-carrier) becomes a key issue for accurate system-level evaluations, and this is the role of PHY abstraction.

2.6.1 PHY abstraction for OFDM-based Systems

Since all new and upcoming cellular standards use OFDM as the basic uplink and downlink transmission scheme so we are interested in studying the PHY abstraction schemes for OFDM-based systems. In OFDM-based systems the process of PHY abstraction can be redefined as the process which predicts the link quality (in terms of BLER) for a specific channel realization across all of the OFDM sub-carriers taking into account the power and resource allocation, modulation and coding scheme (MCS) and other parameters that

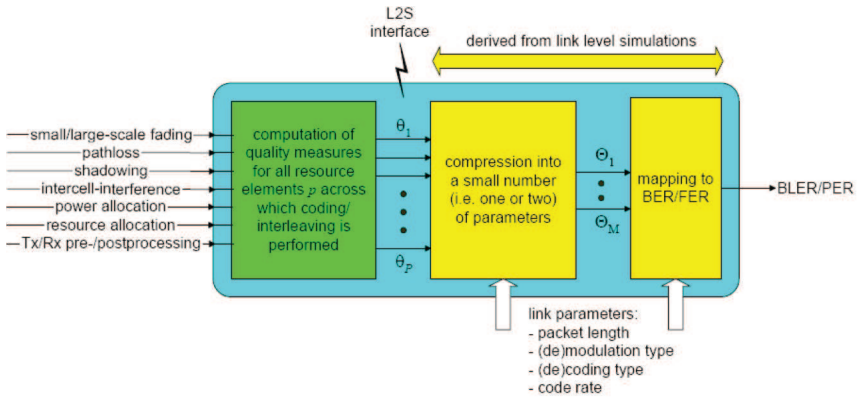

Figure 2.10: Link performance model

can influence the link performance. A link performance model given in [13] is illustrated in Figure 2.10.

The scheduler specifies how the resources are allocated to the users and at which power level, and the channel characteristics (e.g., frequency response) can be determined taking into account path loss, shadowing, fading and inter-cell interference. Based on this information, a set of quality measures θ_n is derived for all the resource elements $n = 1, \ldots, N$ which are occupied by the coded block (codeword). Usually, these quality measures are the SINR values after equalization at the receiver.

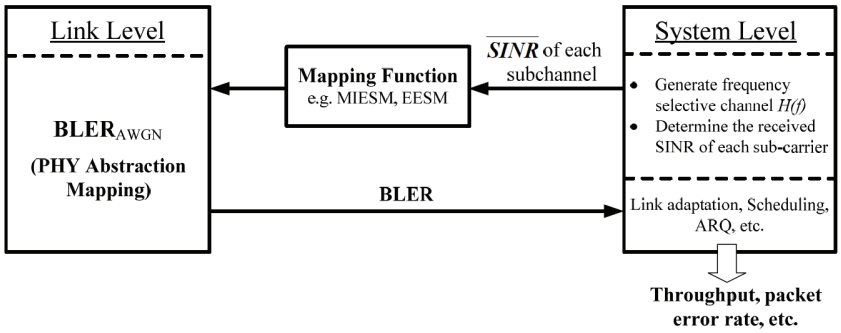

Figure 2.11: Link-to-System Mapping Procedure

The number N of resource elements can be very large for current MIMO-OFDMA systems, leading to many possible combinations of quality measure values (θ_n). Therefore, multidimensional mapping to BLER is impractical. The solution is to compress these values into a small number of parameters

(typically a single one), which would allow the mapping of the set of quality measures to a scalar value. After this, the compressed value is used to obtain the required link performance (BLER) using look-up tables (LUTs) or analytical expressions, which are previously created through link-level simulations. The mapping function depends on the employed channel code, interleaving, modulation and block length. The channel characteristics are generated at the system-level and are used to compute the post-processing SINR for each sub-carrier. The set of SINRs is considered as input to the PHY abstraction which maps this set to a link quality metric (LQM), which is a scalar value. Normally this LQM is an effective SINR (γ_{eff}), which is then mapped to the link level curves obtained in advance through simulations for an AWGN channel. This effective SINR can be thought of as an AWGN-equivalent SNR of the instantaneous channel realization and it can be calculated in different ways. This procedure is named effective SINR mapping (ESM). A similar Link-to-System (L2S) mapping procedure is used in the IEEE 802.16m Evaluation Methodology Document [14], as illustrated in Figure 2.11.

To conclude, the Link-to-System interfacing consists of two mapping mechanism:

- The first one maps the channel state information (CSI) of the instantaneous channel realization, usually a set of SINR values, to a link quality metric (LQM), a scalar value;
- The second one maps this LQM to the required link performance measure (usually the BLER), by using link level results previously generated for AWGN channels.

Part I

Methodologies

Chapter 3

LTE Single-User (SU) SISO & MISO Systems

3.1 Introduction

PHY abstraction also referred as link abstraction, link-to-system (L2S) interface or link prediction has gained quite a lot of attention from the research community in the last decade. This is due to the lucrative gains it offers in terms of resource and time consumption for large scale system evaluations. Usually it is thought of an interface which provides the necessary information from the link level simulator to the system level simulator to perform higher layer tasks, i.e., resource scheduling, link adaptation and radio resource management (RRM) and hence the name link-to-system interface. In the past average value interface (AVI) was the first PHY abstraction technique used for GSM systems under the assumption of slow or flat fading channels. This scheme was unable to capture the effects of the variations in the channel and thus was limited in its applicability for the evaluation of real systems. Then actual value interface (AcVI) was proposed in [15] which was able to account for multipath and the frequency hopping with the help of some auxiliary statistics.

However with the invention of capacity achieving Turbo codes and LDPC codes, use of OFDM as modulation scheme, support of multiple antennas at transmitter and receiver, forward error correction at layer 1 with the help of HARQ and use of fast link adaptation in recent standards such as 3GPP LTE has revolutionized the field of cellular communications. One of the very important features of new systems is the utilization of an instantaneous chan-

nel feedback to benefit from the adaptive modulation and coding schemes. This puts even more strict constraints for the PHY abstraction, other than to imitate already complicated PHY processes, in terms of accuracy for the fast fading channels, low complexity and speed. Therefore research in this specialized area is of utmost importance and has been welcomed by both industry and academia.

3.1.1 Related Work

During the last decade the need for more sophisticated PHY abstraction modeling has gained quite a bit of attention from the research community due to its importance for accurate system level evaluations. Mainly [16] [17] [18] [19] discuss the possible link performance models which are capable of capturing the effects of multi-state channels. Exponential effective SINR mapping (EESM) was first introduced for system level evaluations in [16] and since then onwards have been extensively used for link quality modeling. In [20] it is shown that EESM is a suitable choice for 3GPP LTE wireless systems and performs better than other link quality schemes but mutual-information based methods were not considered for the comparison. They also showed through simulations that the PHY abstraction is independent of the used channel model. In [18] authors discussed some of the possible link performance models and evaluated them in terms of complexity and performance. They showed through their results that for single antenna systems mutual-information based effective SINR mapping (MIESM) performs better in both complexity and performance than all other approaches. They also showed that for multi-antenna systems MIESM is able to describe the characteristics of modulation and coding schemes in a much better way than other schemes. In [21] authors have introduced one more calibration factor for EESM and have shown that it speeds up the abstraction process. In [22] authors have studied the abstraction for generalized spatial channel model (SCM) and in [23] abstraction for OFDM based mobile networks is discussed. In [19] the authors have used the observation that decoding of a codeword is independent of modulation so they have devised a two step method where received bit information rate is used as a link quality measure instead of SINR. This method is also based on mutual information and does not require the calibration for convolution and turbo decoders. They showed the superiority of MIESM over EESM using this approach. This result was strengthened by [13] (Wireless World Initiative New Radio- WINNER) and they chose MIESM as the link performance modeling methodology. PHY abstraction modeling for linear MIMO receivers (i.e. zero-forcing and minimum mean-squared error) and Maximum Likelihood (ML) receivers are given in [14]. Moreover the link quality expressions for simplified HARQ enabled transmissions are given in [14].

An interesting result is shown in [24] which states that the training for the link quality model of MIMO systems should not be done using SISO systems. They strengthen their point by showing results for a 2x2 open loop MIMO system using both EESM and MIESM and they have also shown that MIESM performs better than EESM. In [17] which is an intermediate report on a system level simulator, the authors proposed link quality modeling for cooperative communications considering a generic link which consists of the direct path and the relayed path which in effect makes it similar to the previously discussed link performance schemes. They do not discuss the effect of abstracting each (direct/indirect) link between transmitter and receiver and thus it is not really a true link performance metric for the claimed cooperative communications.

In [25] the author gives very interesting insight into link quality modeling for the relay assisted transmissions with different relay scenarios using decode-and-forward scheme. The author in [25] makes use of the fact that the relay assisted communication can be seen as virtual MIMO with distributed antennas and then he uses EESM for the link quality modeling.

3.1.2 Contributions

In this chapter most popular PHY abstraction techniques are presented with a strong emphasis on their point-to-point pragmatic implementation for various types of transmission and reception schemes in LTE systems. The two widely used PHY abstraction schemes are EESM and MIESM. Both of these schemes are based on the concept of effective SINR mapping which is explained in the next section. An important parameter for both of these schemes is the adjustment factor(s) for different types of transmission strategies and channel models. In this chapter we shall provide clear understanding of these adjustment factors and on their requirement for the accuracy of the model. We show that the adjustment factors need to be calibrated and validated to make sure that the PHY abstraction provides the realism by imitating the full PHY performance.

Most of the work in the literature presents the results for very limited systems whereas in this chapter we present a generic understanding on different aspects of PHY abstraction with the help of various antenna configurations including single-input single-output (SISO) channel, multiple-input single-output (MISO) channel with transmit diversity [26–31] and transmit beamforming techniques [32–41]. These schemes are referred as transmission mode 1, 2 and 6 in LTE systems respectively. This chapter provides a complete methodology of the calibration and validation of the mentioned PHY abstraction schemes and presents results with the help of OAI link level simulator.

Table 3.1: Downlink Transmission Modes in LTE

UE DL Transmission Mode	Transmission Scheme of PDSCH
Mode 1	Single-antenna port
Mode 2	Transmit Diversity
Mode 3	Open-Loop Spatial Multiplexing
Mode 4	Closed-Loop Spatial Multiplexing
Mode 5	Multi-User MIMO
Mode 6	Closed-Loop Rank-1 Precoding
Mode 7	Beamforming Single-antenna port port 5
Mode 8	Dual Layer Beamforming
Mode 9	Multi-user MIMO Rank>1 seamless switching between SU and MU-MIMO

3.2 LTE Signal & System Model

The system under consideration is an LTE single cell scenario with one eNodeB and U active UEs. The eNodeB is equipped with N_t antennas and the all of the UEs are equipped with one antenna only. It is assumed that there is no coordination between UEs for the communication to the eNodeB and all UEs have independent and identically distributed (iid) channels. It is further assumed that there is no intercell interference in the system. The scheduler can decide to serve K users out of the U available users depending on their channel conditions and the requested bandwidth. The eNodeB can be configured to serve the selected K UEs in different available LTE transmission modes on the downlink. These transmission modes are listed in the Table 3.1. Latest release 10 of LTE has up to 9 different downlink transmission modes depending on the different antenna configuration and transmit or receive strategy.

In this chapter the abstraction methodology for transmission mode 1, 2 and 6 is presented but the methodology for transmission mode 6 can be equivalently used for the transmission mode 7 as well.

3.2.1 LTE Transmission Mode 1

LTE transmission mode 1 is the most basic and simplest transmission mode in which a single antenna eNodeB communicates with single antenna UEs. The system model for this transmission mode is shown in Figure 3.1. For the model shown in Figure 3.1 the received signal at the k-th UE for n-th

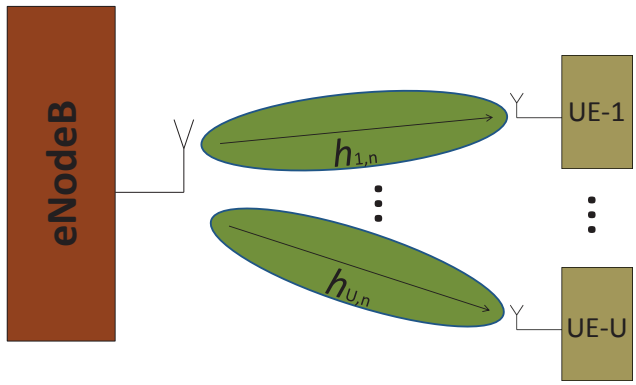

Figure 3.1: SISO: system model with one singe antenna eNodeB and U single antenna UEs

resource element can be written as

$$y_{k,n} = h_{k,n}x_{k,n} + z_{k,n}, \quad n = 1, 2, \cdots, N$$

where $h_{k,n} \in \mathbb{C}$ symbolizes the SISO channel from the desired eNodeB to the k-th UE, $z_{k,n}$ is zero mean circularly symmetric complex Gaussian (ZM-CSCG) white noise of variance N_0 at k-th UE. Complex symbol $x_{k,n}$ is assumed to be independent and belongs to a discrete M-QAM constellation with variance $\sigma_k^2 = 1$. For such a system model the received signal to noise ratio (SNR) at k-th UE on n-th resource element is given by

$$\gamma_{k,n} = \frac{|h_{k,n}|^2.\sigma_k^2}{N_0} = \frac{|h_{k,n}|^2}{N_0} \tag{3.1}$$

3.2.2 LTE Transmission Mode 2

In LTE transmission mode 2 employs transmit diversity which is a technique to combat multipath fading in wireless communication. LTE utilizes Alamouti space time block codes which were proposed in late 1990s [26]. The main idea is to send the copies of the same signal, coded differently, from multiple transmit antennas giving rise in the transmit diversity. In transmission mode 2, two complex symbols (i.e. x_1 and x_2) are transmitted over two symbol times from the two transmit antennas. Figure 3.2 shows the system model for LTE TM 2 where a dual antenna eNodeB is communicating with single antenna UEs. We assume that the channel is i.i.d but stays constant for the duration of the two symbol times. In the first symbol time x_1 and x_2

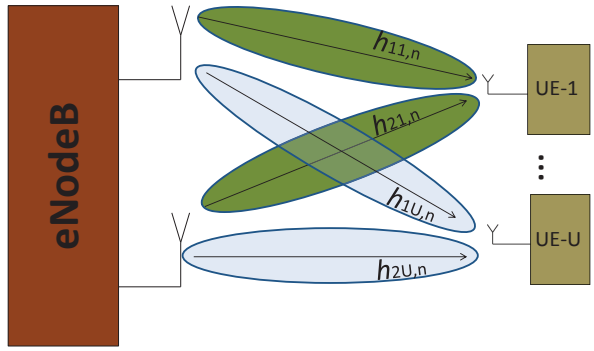

Figure 3.2: Transmit Diversity: system model with a dual antenna eNodeB and U single antenna UEs

are transmitted whereas in the second symbol time $-x_2^*$ and x_1^* are transmitted through antenna 1 and antenna 2 respectively. The received signal for transmission mode 2 at u-th UE on n-th resource element after two symbol times is given by

$$\mathbf{y}_{k,n} = \frac{1}{\sqrt{2}}\mathbf{X}_{k,n}\mathbf{h}_{k,n} + \mathbf{z}_{k,n}, \quad n = 1, 2, \cdots, N$$

$$\mathbf{X}_{k,n} = \begin{bmatrix} x_1 & x_2 \\ -x_2^* & x_1^* \end{bmatrix}, \mathbf{h}_{k,n} = \begin{bmatrix} h_{1k,n} \\ h_{2k,n} \end{bmatrix} \text{ and } \mathbf{z}_{k,n} = \begin{bmatrix} z_1 \\ z_2 \end{bmatrix}$$

where $\frac{1}{\sqrt{2}}$ is the power normalization factor for both antennas, $\mathbf{h}_{k,n} \in \mathbb{C}^{2\times 1}$ is the MISO channel from eNodeB to the k-th UE, $\mathbf{X}_{k,n}$ is 2×2 matrix in which each column represents the 2×1 vector of independent complex symbols x_1 and x_2 of variance σ_k^2 at k-th UE for two symbol periods, $\mathbf{z}_{k,n}$ is vector of ZMCSCG white noise of variance N_0 at k-th UE for two symbol periods. At the receiver joint processing for the two symbols is applied and the received SNR at k-th UE on n-th resource element can be calculated as,

$$\gamma_{k,n} = \frac{|h_{1k,n}|^2 + |h_{2k,n}|^2}{2.N_0} \tag{3.2}$$

Because of the power normalization factor the gain in the received SNR is lost in transmission mode 2 but the gain in diversity is still obtained.

3.2.3 LTE Transmission Mode 6

In LTE transmission mode 6 employs transmit beamforming where multiple antennas at the eNodeB are used to transmit the same signal appropriately

weighted for each antenna element so that the transmission can be directed in the direction of the desired user only. For transmission mode 6 in LTE, a high SNR is obtained at the receiver by using transmit precoder $\mathbf{p}$ which focuses the transmit energy to a specific user. Figure 3.3 shows the system model for LTE TM 6 where a dual antenna eNodeB performs transmit precoding towards single antenna UEs.

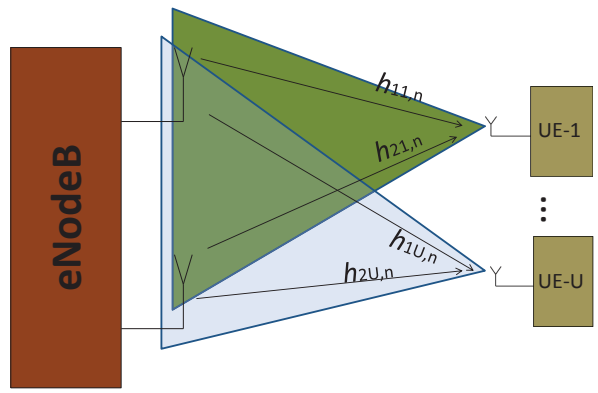

Figure 3.3: Transmit Precoding: system model with a dual antenna eNodeB and U single antenna UEs

The received signal for LTE TM 6 MISO transmission at k-th UE on n-th resource element is given by

$$y_{k,n} = \mathbf{h}_{k,n}^{\dagger}\mathbf{p}_{k,n}x_{k,n} + z_{k,n}, \quad n = 1, 2, \cdots, N$$

where $\mathbf{h}_{k,n}^{\dagger}\mathbf{p}_{k,n}$ is the effective precoded channel from eNodeB to the k-th UE, $\mathbf{p}_{k,n}$ is the precoder requested by k-th UE and $z_{k,n}$ is ZMCSCG white noise of variance N_0 at k-th UE. In LTE the user can request one of the four available precoders,

$$\mathbf{p}_{k,n} = \frac{1}{\sqrt{2}}\begin{bmatrix}1\\1\end{bmatrix}, \frac{1}{\sqrt{2}}\begin{bmatrix}1\\-1\end{bmatrix}, \frac{1}{\sqrt{2}}\begin{bmatrix}1\\\mathrm{j}\end{bmatrix}, \frac{1}{\sqrt{2}}\begin{bmatrix}1\\-\mathrm{j}\end{bmatrix}$$

The received SNR at the k-th UE on n-th resource element is given by

$$\gamma_{k,n} = \frac{|h_{1k,n} + qh_{2k,n}|^2}{2.N_0} \tag{3.3}$$

where $q \in \{\pm 1, \pm j\}$. Because of the beamforming effect, transmission mode 6 extends the range of the cell in LTE and because of the directed beams it also reduces the interference on the neighboring UEs.

3.3 PHY Abstraction in LTE

In LTE the main purpose of PHY abstraction is to accurately provide the performance of LTE air interface for the MAC layer. A more generic view of abstraction is shown in Figure 3.4. In LTE the air interface is based on the bit interleaved coded modulation with iterative decoding. The details about BICM in LTE are already given in Chapter 2. As explained in the

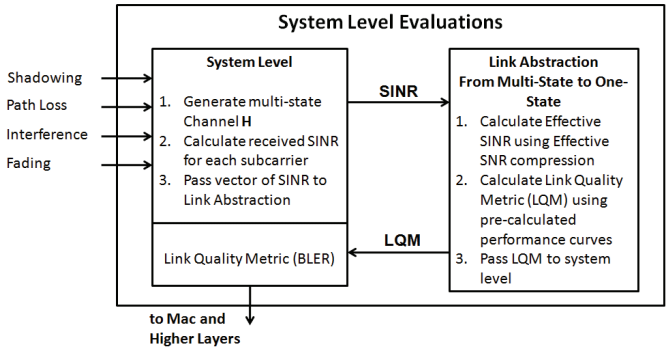

Figure 3.4: PHY Abstraction in LTE

previous chapter PHY abstraction usually consists of two main steps; link quality metric calculation and link performance modeling. Since the link quality metric has to reflect the state of the channel in a useful way that is why most of the times SNR (or SINR in case of Gaussian interference) is the best candidate for it. The link performance modeling consists of two further steps; compression of multiple link quality metrics into one effective link quality metric and its mapping onto AWGN based link performance curves of specific MCS to obtain the link quality indicator.

3.3.1 Link Quality Metric

The link quality metric can be defined as the quantity which is capable of capturing all the phenomenon effecting the link quality between the eNodeB and UE. The link quality metric should be able to capture the effects of interference, pathloss, multipath fading etc. and give a simple measure of the quality of the link. Normally the received SINR is the best candidate for the link quality metric and for the system model of this chapter, the link quality metrics can be obtained using (3.1), (3.2) and (3.3) for the case of transmission mode 1, 2 and 6 respectively.

3.3.2 Link Performance Modeling

An important step in link performance modeling for PHY abstraction is to calculate the effective SNR in a way that it is able to transform the multi-state channel in to a single state channel. For this purpose the basic proposed

scheme in the literature is effective SNR mapping which at first compresses the varying SNRs of a codeword to an effective SNR (γ_{eff}) value then this γ_{eff} is used to obtain the link quality indicator as an equivalent BLER from the AWGN performance curves of a particular modulation and code scheme (MCS).

$$\gamma_{\text{eff}}\left(\beta_1, \beta_2\right) = \beta_1 I^{-1}\left[\frac{1}{N}\sum_{n=1}^{N} I\left(\frac{\gamma_n}{\beta_2}\right)\right], \tag{3.4}$$

$$\gamma_{\text{eff}} \rightarrow \text{BLER}_{\text{A}}\left(\text{MCS}\right) \tag{3.5}$$

where BLER_{A} (MCS) is the BLER of specific MCS for an AWGN channel, β_1 and β_2 are called adjustment factors to compensate for different modulation orders and code rates. Further details about these adjustment factors is given in the next section. In (3.4) N is the number of channel symbols in a given codeword and $I(\gamma_n)$ is a mapping function which transforms SINR of each channel symbol to some "information measure" where it is linearly averaged over the codeword. The choice of this information measure in ESM is of very much importance. It should be able to reflect the effects of frequency selectivity experienced by each channel symbol within the limits of a communication channel which in the case of LTE is based on the BICM capacity for QAM constellation. Due to this restriction the very famous Shannon's capacity can not be used as an information measure in LTE as it is an unbounded measure of information being a function of S(I)NR. It is shown in Figure 3.5. Therefore the ideal choice for LTE systems will either be the BICM capacity function or some equivalent function which is similar to BICM capacity in terms of performance.

There has been many investigations in the literature for finding the proper information measure which is not only easy to implement but also accurate. In this respect the two most studied link abstraction methodologies are the EESM and MIESM where in the former an exponential function is used as an information measure and in the latter normalized BICM constrained capacity is used as an information measure. These are shown in Figure 3.5.

EESM

For EESM the information measure function $I(\gamma_n)$ is calculated using Chernoff union bound of error probabilities [16] and can be given as,

$$I(\gamma_n) = 1 - \exp(-\gamma_n). \tag{3.6}$$

and the reverse information function is easily computed from (3.6). Then γ_{eff} for the EESM can be written as,

$$\gamma_{\text{eff}}\left(\beta_1, \beta_2\right) = -\beta_1 \ln\left[\frac{1}{N}\sum_{n=1}^{N} \exp\left(-\frac{\gamma_n}{\beta_2}\right)\right]. \tag{3.7}$$

In (3.7) the compression is performed on N channel symbols and then the compressed value is transformed back into the SNR domain to obtain $\gamma_{\text{eff}}(\beta_1, \beta_2)$ for the purpose of look-up from the corresponding AWGN look-up tables to provide the link quality indicator.

MIESM

In the case of MIESM there are no closed form analytical formulations of information measure and thus one has to rely on numerical approximations. For the BICM the approximation of the information measure function and the reverse information function comes from the normalized mutual information for discrete QAM constellations. For the ease of implementation and calculation of the mutual information for each channel symbol, these values are pre-computed for different QAM modulations over a wide range of input SNR and are stored in the form of look-up tables. In general the normalized BICM mutual information for an arbitrary channel symbol γ_n and M-QAM modulation can be given as,

$$I_M(\gamma_n) = \frac{1}{\log M}\left\{\log M - \frac{1}{M}\sum_{x\in\chi}\mathcal{E}_z \log \frac{\sum_{x'\in\chi}\exp\left[-\left|\gamma_n\left(x-x'\right)+z\right|^2\right]}{\exp\left[-|z|^2\right]}\right\} \tag{3.8}$$

where χ is the set of the QAM constellation points with $|\chi| = M$ and $z \in \mathcal{CN}(0,1)$. To complete the process of the PHY abstraction the I_M is calculated for all of the N channel symbols and is then compressed (averaged) to a single mutual information value. This mutual information value is then used to perform the reverse information mapping to obtain the $\gamma_{\text{eff}}(\beta_1, \beta_2)$ for reading the BLER from AWGN look-up tables. Figure 3.5 shows the normalized mutual information for different QAM modulations and the information measure for EESM.

For the PHY abstraction the link quality metric can be calculated using (3.1), (3.2) and (3.3) for LTE transmission modes 1, 2 and 6. Then any of the two explained methods can be used to obtain $\gamma_{\text{eff}}(\beta_1, \beta_2)$ so that it can be used to read BLER from the previously calculated AWGN performance curves corresponding to the specific MCS, i.e.,

$$\text{BLER}(\boldsymbol{\gamma}, \text{MCS}) \simeq \text{BLER}_{\text{A}}(\gamma_{\text{eff}}(\beta_1, \beta_2), \text{MCS}) \tag{3.9}$$

Where $\boldsymbol{\gamma}$ represents the $N \times 1$ vector of γ_n and BLER_{A} represents the AWGN block error rate obtained for a specific MCS. In LTE there are 29 different MCS with a wide range of code rates and 3 possible modulation schemes; QPSK, 16-QAM and 64-QAM. Figure 3.6 shows the AWGN performance curves for these MCS which are obtained from the OAI LTE link level sim-

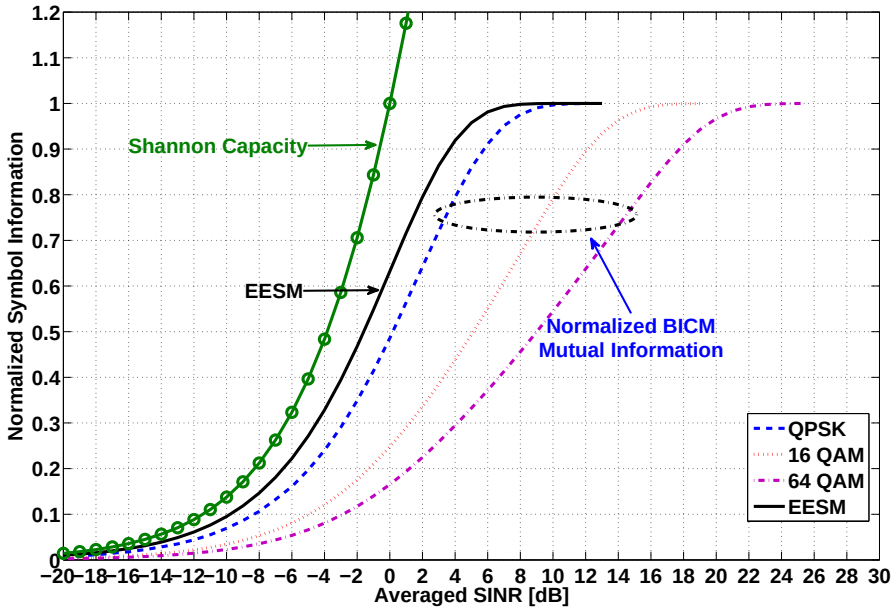

Figure 3.5: Comparison of Normalized Mutual Information functions and EESM function

ulator for mapping the effective link quality metric to an equivalent link quality indicator.

3.4 Calibration of Adjustment Factors

An extremely important feature of PHY abstraction is that it must be very accurate in providing as much realism in the performance of a system as a simulation with full PHY processing. Therefore, before we implement the PHY abstraction for the system level evaluations it has to be validated. For this purpose we used Eurecom's OpenAirInterface link level simulator and applied both ESM methods. Figure 3.5 shows the normalized mutual information functions for QPSK, 16-QAM and 64-QAM and the information function from (3.6) for EESM. It can be seen that the EESM function is very similar to that of the QPSK normalized mutual information function which is why the calibration is not a critical issue for the case of QPSK but for the case of 16-QAM and 64-QAM, calibration is a necessary step if EESM is to be employed in the system.

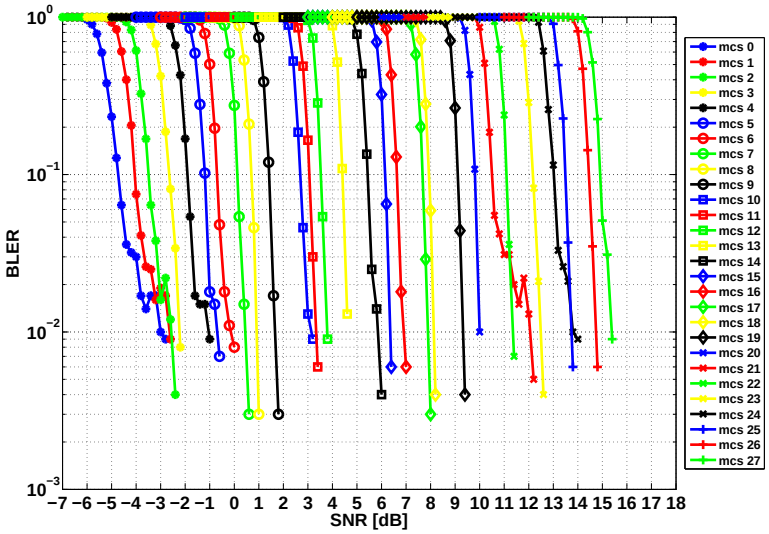

Figure 3.6: AWGN Link Performance Curves in LTE with 5 MHz Bandwidth for MCS 0 - 27

3.4.1 Link Level Simulations

The main idea of validation is to check whether the PHY abstraction is good enough for any random channel realization or not. In other words can the PHY abstraction be applied in any random scenario and be able to transform the effects of a multi-state channel into a single-state channel by providing an accurate link quality indicator.

The answer can be found with the help of link level simulations for the three described transmission modes. If it is made sure that the link level simulations are performed for a highly frequency selective channel with a very large number of channel and noise realization then it shall be able to capture the effect of highly variant channels for the PHY abstraction. The complete parameters of these simulations are described in Table 3.2.

For each of the link level simulations, a huge number of i.i.d channel realizations are generated and during the simulation of each channel realization the channel is kept constant. Then link level simulation is performed for 10000 packets or 5000 erroneous packets with random AWGN noise. These simulations took a very long time to finish but these were necessary to prove the validation of the PHY abstraction schemes. We could have applied the PHY abstraction of the channel realizations directly in the link level simulator while these simulations were running but that would have limited the applicability and the scope of these simulations as we could perform PHY

Table 3.2: Simulation Parameters for Link Level Simulator

OpenAirInterface Link Level Parameters	
Transmission Mode	1, 2, 6
Transmission Bandwidth	5 MHz
FFT Size	512
Subcarrier Spacing	15 KHz
Useful Subcarriers	300
Subframe Length	1 ms
Cyclic Prefix	Normal
Physical Resource Blocks	25
Channel	8-tap Rayleigh Channel Model
Delay Spread	1e-6 second
Channel Estimation	Real & Ideal
Decoder	Max-log Map
MCS	0 - 22

abstraction just once during the execution of the simulations. But instead we chose to save the estimates of channel realization and necessary information from these simulations as a channel trace into an external file which can be used for further analysis. This way the trace files can be easily used for experimenting on the different aspects of PHY abstraction and for future references. Therefore, from these simulations we saved the trace files containing each of the channel realization, its corresponding BLER and other parameters necessary for the PHY abstraction. Then we applied both of the ESM PHY abstraction schemes on the saved channel realizations and tried to map the instantaneous BLER onto pre-computed AWGN curves. The complete algorithm for generating the trace files from the link level simulations for each of the MCS is given in Algorithm 1 [42].

3.4.2 Sufficient number of Channel estimates for Trace Files

An important aspect while saving the channel trace file from link level simulations is the cardinality of it. That is how much number of channel estimates are sufficient enough to perform an efficient PHY abstraction. With the assumption that the channel stays constant for the duration of 1ms, i.e. for a subframe still it is required to have 1200 estimates for the bandwidth of 20MHz. However this number can be further reduced by utilizing the intelligent structure of cell-specific reference symbols (CRS) which are used for channel estimation in LTE. They are very optimally and intelligently placed in a diamond shape in each of the subframe so that even the most simple linear interpolation both in time and frequency domain is enough for estimating the channels on other subcarriers. For this reason we store these

Algorithm 1 Algorithm for the Generating the Trace files from Link Level Simulation for PHY Abstraction

```
for c = 1 : 1 : N_ch (loop over channel realizations) do
  Generate h_c (and if required) p_c
  for j = 1 : 0.2 : J(loop over SNR points) do
    e = 0 (for instantaneous error rate)
    for k = 1 : 1 : K (i.i.d AWGN realizations) do
      Generate z_k of variance σ_j^2
      Perform LTE transceiver operations
      Calculate decoding decision: BLER(h_c, z_k)
      Update e = e + BLER(h_c, z_k)
    end for
    Calculate BLER(h_c, σ_j^2) = e/K
    Store BLER(h_c, σ_j^2) to an external trace file
    Store SNR_j, σ_j^2 to an external file
    if BLER(h_c^†, σ_j^2) ≤ 1e^-3 then
      break SNR loop
    else
      Set SNR_{j+1} = SNR_j + 0.2
    end if
  end for
  Store h_c (and if required) p_c to an external trace file
end for
```

CRS channel estimates for the validation of PHY abstraction. There are two subcarriers for each antenna port in a PRB which means that for the bandwidth of 5MHz we store $2 \times 25 = 50$ estimates for SISO transmission and $4 \times 25 = 100$ estimates for MISO transmission.

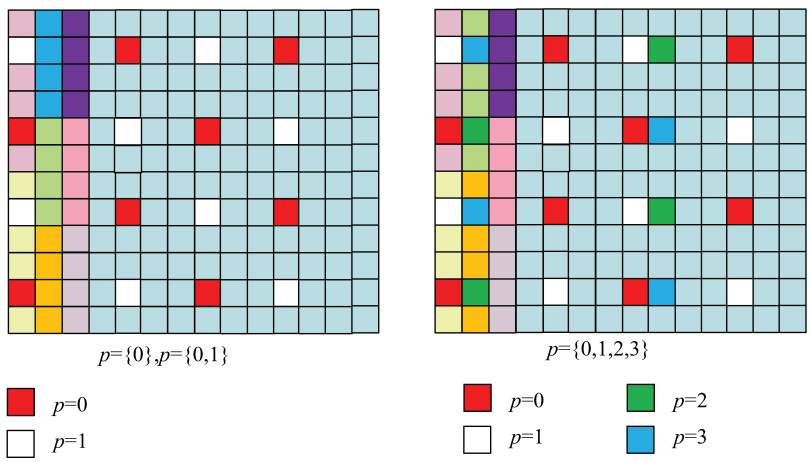

Figure 3.7: Symbol Reference Signals (SRS) with NCP used for the channel estimation in LTE. For antenna port 0,1 on the left side and for antenna port 0, 1, 2 and 3 on the right.

3.4.3 PHY Abstraction without Adjustment Factors

To find out the importance of adjustment factors first we assumed that $\beta_1 = \beta_2 = 1$, i.e., there are no adjustment factors in (3.4). With such an assumption it is expected that the PHY abstraction employing normalized mutual information functions as information measure in (3.4) from (3.8) should be fine. This is due to the reason that γ_{eff} obtained from these normalized mutual information functions already corresponds to an averaged normalized BICM channel capacity and hence there is no need of any calibration of the adjustment factors. But for the case of EESM the calibration must be performed because it is an approximation of the normalized BICM channel capacity and very likely it might deviate from the actual value. The deviation can be calculated as a mean squared error value either between the simulated BLER points and predicted BLER points, i.e.,

$$\text{MSE} = \frac{1}{N_{ch} J} \sum_{c=1}^{N_{ch}} \sum_{j=1}^{J} \left| \overline{\text{BLER}}\left(\mathbf{h}_c, \sigma_j^2\right) - \overline{\text{BLER}}_{\text{A}}\left(\gamma_{\text{eff}}\right) \right|^2 \tag{3.10}$$

or between the predicted SNR obtained for the $\overline{\text{BLER}}\left(\mathbf{h}_c, \sigma_j^2\right)$ from reference AWGN curves and the γ_{eff} for current channel realization $\left(\mathbf{h}_c, \sigma_j^2\right)$, i.e.,

$$\text{MSE} = \frac{1}{N_{ch}J}\sum_{c=1}^{N_{ch}}\sum_{j=1}^{J}\left|\gamma_{\text{A}}\left[\overline{\text{BLER}}\left(\mathbf{h}_c, \sigma_j^2\right)\right] - \gamma_{\text{eff}}\right|^2 \tag{3.11}$$

where in (3.10) N_{ch} is the number of channel realizations, $\overline{\text{BLER}}\left(\mathbf{h}_c, \sigma_j^2\right)$ is the block error probability stored for the c-th channel and j-th SNR point, $\overline{\text{BLER}}_{\text{A}}\left(\gamma_{\text{eff}}\right)$ is the predicted block error rate of the respective AWGN curve which is based on the γ_{eff}. Whereas in (3.11) $\gamma_{\text{A}}\left[\overline{\text{BLER}}\left(\mathbf{h}_c, \sigma_j^2\right)\right]$ is the predicted SNR for c-th channel and j-th SNR point from the link level simulation and γ_{eff} is the corresponding effective SNR obtained from the ESM PHY abstraction schemes. In the rest of the chapter and thesis we shall use the MSE from (3.11) for the validation purposes.

Table 3.3: Mean Squared Error (MSE) Values for PHY abstraction of TM 1, 2 and 6 with Ideal Channel Estimation

MCS	TM 1		TM2		TM6	
	MIESM	**EESM**	**MIESM**	**EESM**	**MIESM**	**EESM**
0	0.00845	0.00800	0.01912	0.01969	0.02806	0.02882
1	0.12780	0.11079	0.03062	0.01256	0.03062	0.03238
2	0.21208	0.15241	0.02068	0.01256	0.01607	0.01055
3	0.01569	0.00972	0.03522	0.02004	0.05067	0.02757
4	0.08193	0.02743	0.04810	0.02230	0.03330	0.01646
5	0.21651	0.05721	0.09664	0.04887	0.13142	0.06498
6	0.31502	0.09233	0.23345	0.10487	0.14630	0.07249
7	0.44880	0.11138	0.16165	0.08041	0.28938	0.12268
8	0.58452	0.08906	0.32268	0.11236	0.31194	0.12487
9	0.89817	0.13383	1.02994	0.33643	0.73582	0.26321
10	0.07188	0.36218	0.10805	0.08999	0.11431	0.15981
11	0.09870	0.52267	0.14731	0.06849	0.12385	0.12216
12	0.17014	0.88513	0.14099	0.21051	0.18981	0.29276
13	0.29681	2.02549	0.32245	0.49950	0.19109	0.43130
14	0.51801	1.83117	0.48831	0.45092	0.42177	0.62784
15	0.47026	3.23903	0.93283	0.59642	0.71872	1.12717
16	0.55302	3.37197	0.58283	1.16952	1.05429	1.31727
17	0.28176	6.97156	0.59969	2.36247	0.42909	3.14923
18	0.51119	8.81638	0.57480	4.01219	0.62866	3.67671
19	0.91280	13.58936	1.14600	5.35963	0.69547	4.68949
20	0.69745	13.60889	1.66675	3.92301	1.10408	9.15578
21	1.05521	15.70319	1.91880	6.32198	0.95086	7.36687
22	1.88587	19.86025	2.08107	8.38557	1.97902	11.26809

In Table 3.3 and 3.4 the MSE error values for the transmission mode 1, 2 and 6 are presented for a wide variety of MCS using both EESM and MIESM approaches for ideal and real channel estimation. The results in Table 3.3 and 3.4 show that PHY abstraction with no adjustment factors perform within a reasonable amount of error range only in the case of MIESM and transmission mode 1. For all other transmission modes and abstraction techniques, the adjustment factor are necessary for the PHY abstraction to be accurate and have lower level of MSE even in the case of ideal channel estimation. For MIESM this result is slightly different than the usual expectations where in the literature it has been claimed that no calibration of adjustment factors is required for the MIMO systems. The reason for a different result is that in the MIMO case the combined LLRs of the received bits at the decoder are the combination of the bit quality received from different mutiple channels and when we are comparing this LLR with the SISO AWGN curves then the predicted BLER shall deviate from the measured BLER. Therefore the calibration of adjustment factors for the case of MIMO channels has to be performed even for MIESM in LTE systems.

Table 3.4: Mean Squared Error (MSE) Values for PHY abstraction ($\beta_1 = \beta_2 = 1$) of TM 1, 2 and 6 with Real Channel Estimation

MCS	TM 1		TM2		TM6	
	MIESM	**EESM**	**MIESM**	**EESM**	**MIESM**	**EESM**
0	0.03522	0.06557	2.0508	1.93288	3.02906	2.67547
1	0.09585	0.03805	2.91195	2.47222	2.91195	2.47222
2	0.14284	0.07841	2.0125	1.7958	2.29706	1.88138
3	0.10339	0.12498	2.24767	1.99516	2.28116	1.77651
4	0.01936	0.01988	1.93121	1.63873	1.99104	1.41858
5	0.06068	0.01805	2.2644	1.74546	2.23588	1.58335
6	0.13045	0.01644	2.26935	1.74087	2.15215	1.37451
7	0.212	0.02269	2.67041	1.65489	2.4042	1.35381
8	0.27117	0.02715	2.90936	1.88103	2.47615	1.35297
9	0.26503	0.05717	3.06781	1.64914	2.70605	1.11496
10	0.01307	1.42428	2.2695	0.72383	1.84343	0.49292
11	0.08988	2.05075	2.7936	1.13846	2.07848	0.41211
12	0.03862	3.21134	2.62477	0.55144	1.8545	0.60692
13	0.10495	4.76155	2.68578	0.56758	1.99882	0.85654
14	0.17942	4.7664	2.74274	1.03837	2.19197	2.06321
15	2.24155	6.36159	3.0917	0.74722	2.77398	1.59631
16	0.47506	7.77526	3.3929	0.75006	3.0259	2.71877
17	0.14298	11.24418	3.3967	2.96176	2.07854	2.50113
18	0.19349	14.25836	2.84884	1.95397	2.67095	4.0475
19	0.38208	23.36054	3.21012	4.38324	2.85916	6.40636
20	0.32888	27.36012	14.35266	4.37539	2.84957	8.63553
21	3.56453	29.30248	4.02345	2.68353	3.39659	8.22266
22	2.46121	33.54749	5.33967	4.2515	3.79212	9.94241

3.4.4 PHY Abstraction with Adjustment Factors

Due to the highly non-linear nature of the information measures used in both ESM methods there exists no analytical formulation for the optimum adjustment factors. Therefore the optimization on the adjustment factors is performed numerically over the large data set obtained from the link level simulations, i.e.,

$$(\beta_1, \beta_2) = \underset{(\beta_1,\beta_2)}{\operatorname{argmin}} \left[\frac{1}{N_{ch} J} \sum_{c=1}^{N_{ch}} \sum_{j=1}^{J} \left| \gamma_{\mathrm{A}} \left[\overline{\mathrm{BLER}} \left(\mathbf{h}_c, \sigma_j^2 \right) \right] - \gamma_{\mathrm{eff}} \left(\beta_1, \beta_2 \right) \right|^2 \right]. \tag{3.12}$$

For the optimized values of β_1 and β_2, both of the ESM methods are applied to the stored channel trace from link level simulations. We also performed the optimization (3.12) with the assumption $\beta_1 = \beta_2$. This means that there is only one adjustment factor in (3.4) to compensate for both coding and modulation. This reduces one degree of freedom (DOF) for the minimization of the MSE in (3.12) but at the same time it also reduces the complexity of the optimization problem. In the next subsection we shall see what kind of results are obtained for the mentioned transmission modes by using single and dual adjustment factors with both ideal and real channel estimation.

3.4.5 Results With Adjustment Factors

After calibration of optimum adjustment factors we applied both of the ESM PHY abstraction techniques on the saved outputs of the link level simulations. In the following section, we provide the results for both ideal and real channel estimation in the case of transmission mode 1, 2 and 6. Figure 3.8 shows the mean squared values obtained for EESM and MIESM for the case of single and dual adjustment factor optimization. It can be observed that in the case of ideal channel estimation there is not much of an improvement in the MSE for using dual adjustment factors than using a single adjustment factor. Also Figure 3.9 shows the values of both dual and single adjustment factors and it can be observed that for the ideal channel estimation there is not much difference in the calibrated values of the adjustment factors and thus the calibration of the single adjustment factor is sufficient enough for reasonable[1] MSE.

We show the validation results corresponding to the discussed transmission modes for the ideal channel estimation, two adjustment factors and for EESM in Figure 3.10, 3.11 and 3.12. It can be noticed that the BLER points obtained from link level simulations are very efficiently mapped onto the re-

[1] By reasonable we mean the MSE in dB should be so small that no two adjacent MCS should be confused with each other. This can be observed in Figures 3.10, 3.11 and 3.12 that all BLER points are usually around the intended MCS curve.

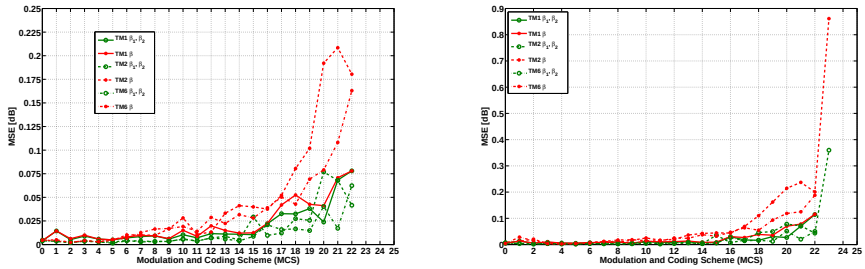

(a) Mean Squared Error for EESM (b) Mean Squared Error for MIESM

Figure 3.8: For Transmission Mode 1, 2 and 6 using ideal channel estimation, MSE for different MCS using EESM and MIESM with single and dual adjustment factors

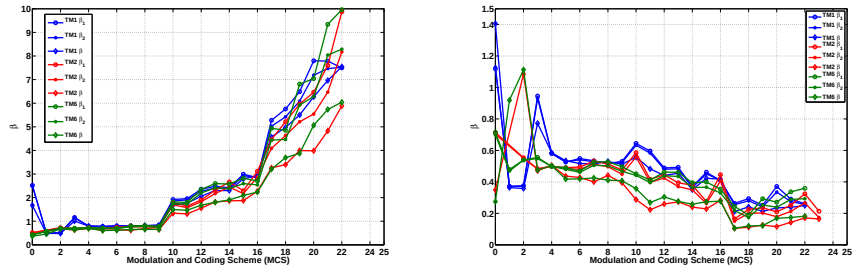

(a) Calibration Factors For EESM (b) Calibration Factors For MIESM

Figure 3.9: For Transmission Mode 1, 2 and 6 using ideal channel estimation, comparison of single and dual adjustment factors for EESM and MIESM

spective AWGN curves. The reason for the low performance for higher MCS is that in the case of 64-QAM modulation the bits are unequally protected which means that some of the bits have higher received SNR whereas in the abstraction methods all bits are treated as having equal received SNR.

However, for real channel estimation, the results are slightly different and are shown in Figure 3.13 and 3.14. It can be observed that the MSE in the case of single and dual adjustment factors is quite different and there is an improvement in the accuracy of the model if the dual adjustment factors are used. Also the optimum adjustment factors are different for all three transmission modes and have to be calibrated very carefully. The reason for better results with two adjustment factors in the real channel estimation case is that due to the channel estimation errors the mapping of s multi-state channel onto a single-state channel can deviate from the predicted AWGN performance and the use of dual adjustment factors can provide better compensation for

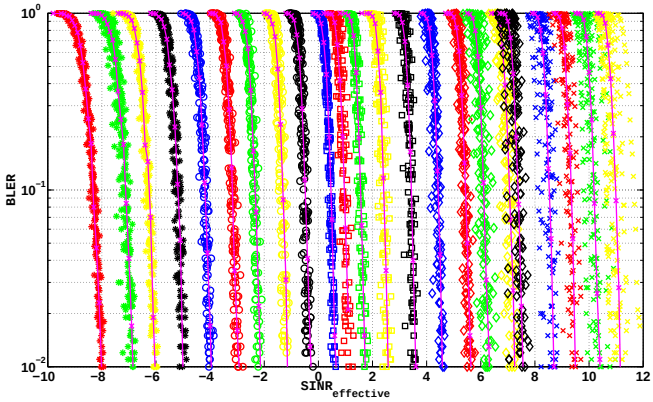

Figure 3.10: LTE Transmission Mode 1 - EESM with two calibration factors for MCS 0 - 22

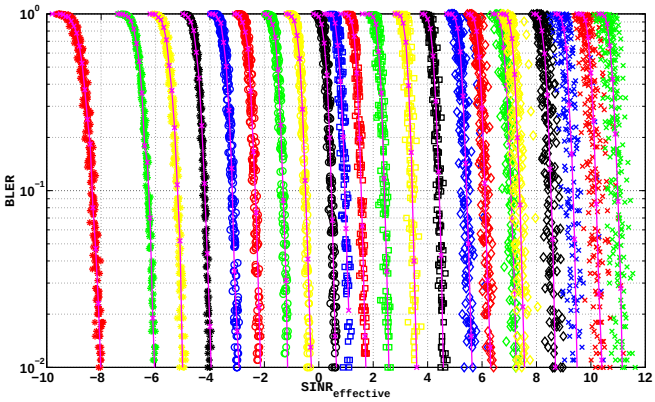

Figure 3.11: LTE Transmission Mode 2 - EESM with two calibration factors for MCS 0 - 22

both coding and modulation.

Comparison of EESM and MIESM

Another interesting point shall be to compare the performance of EESM and MIESM to provide a fundamental rule for these ESM techniques. Since we have performed extensive simulations with both of the methods, so it shall be straight forward to compare both of these methods with the same data sets from the link level simulations. We applied both of the schemes on all of the data sets for the discussed transmission modes with both real and ideal channel estimation. We show results for the real channel estimation case in Figure 3.15 for a wide variety of MCS in terms of the obtained MSE after

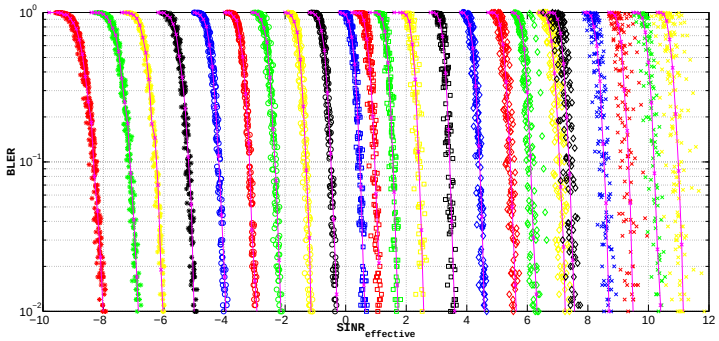

Figure 3.12: LTE Transmission Mode 6 - EESM with two calibration factors for MCS 0 - 22

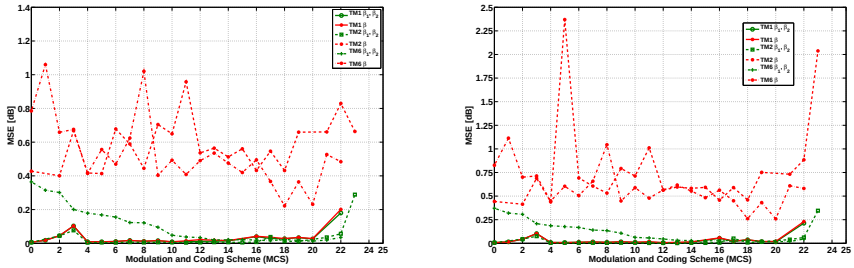

(a) Mean Squared Error for EESM (b) Mean Squared Error for MIESM

Figure 3.13: For Transmission Mode 1, 2 and 6 using real channel estimation, MSE for different MCS using EESM and MIESM with single and dual adjustment factors

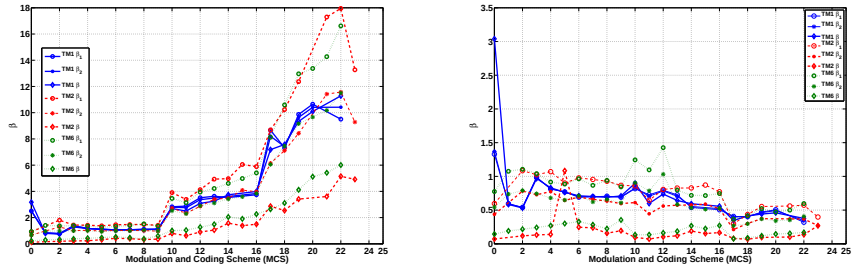

(a) Calibration Factors For EESM (b) Calibration Factors For MIESM

Figure 3.14: For Transmission Mode 1, 2 and 6 using real channel estimation, comparison of single and dual adjustment factors for EESM and MIESM

the validation of both ESM methods. It can be seen that if the adjustment factors are properly calibrated then both of the ESM methods can provide almost the same MSE. The results for the ideal channel estimation are also similar so we did not include them here. But in the end it can be stated with confidence that with proper calibration of adjustment factors, both of these methods perform equivalently. However, EESM has an advantage of closed form expression for the calculation of effective SNR, making it easier to implement.

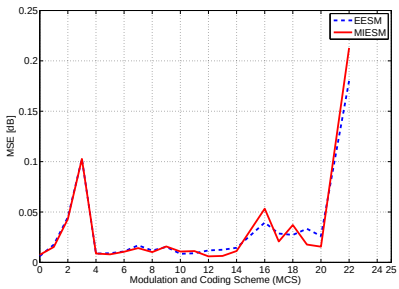

(a) Performance comparison of MIESM and EESM for transmission mode 1

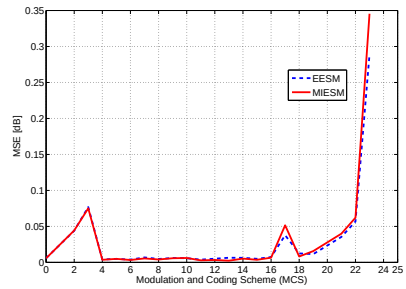

(b) Performance comparison of MIESM and EESM for transmission mode 2

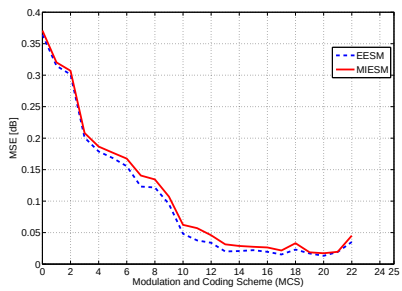

(c) Performance comparison of MIESM and EESM for transmission mode 6

Figure 3.15: Performance comparison of MIESM and EESM for transmission mode 1, 2 and 6 using real channel estimation and dual adjustment factors.

3.4.6 Global Optimality of Adjustment Factors

Finally the very important question arises about the global optimality of the adjustment factors. It is of high interest to show that the calibrated adjustment factors are globally optimal for each of the MCS. For finding the optimum values of the adjustment factors an initial value and, the maximum and minimum values of the search regions for β_1 and β_2 are chosen. The next important thing is to choose the step size and there is a tradeoff between the

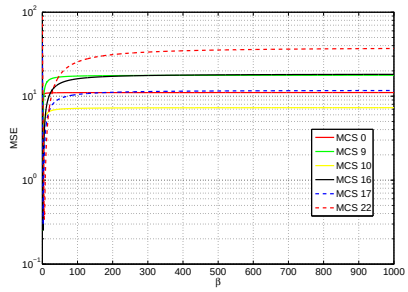

(a) MSE Caclulation for different β (0-1000) using EESM

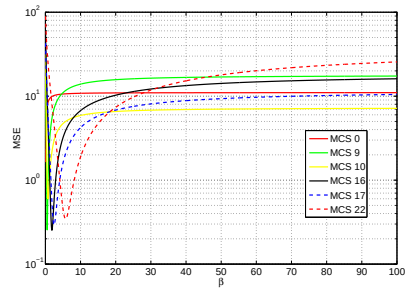

(b) MSE Caclulation for different β (0-100) using EESM

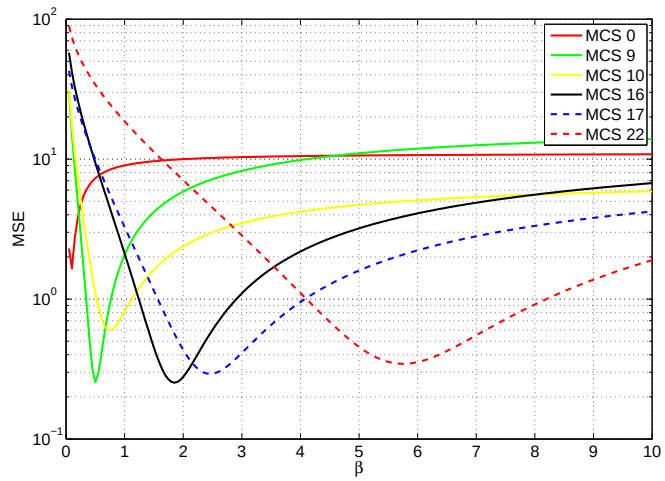

(c) MSE Caclulation for different β (0-10) using EESM

Figure 3.16: Global optimality of the MSE optimization problem

complexity and accuracy of the selection. However we decided to choose a small step size of 0.05. Then the optimization problem of (3.12) is applied over the saved data set from link level simulations for each of the MCS and the adjustment factors are swept from minimum to the maximum in given step size and the MSE is calculated for each value of both adjustment factors. Then those values of β_1 and β_2 are chosen which give the minimum MSE. Similarly for the case of only one β value maximum and minimum of β is chosen and the optimization of (3.12) is performed with $\beta_1 = \beta_2 = \beta$. It is clear from the results shown in the previous section that the chosen adjustment factors are optimum and provide the minimum MSE. But a clear proof is provided with the help of Figure 3.16 which shows the single calibrated beta values over a wide range of different MCS using EESM. It is clear that for all of the MCS there always exists only one optimum β value. To make sure that there is no other minimum the function we increased the

maximum range from 10 to 100 and 1000. The results for these maximum ranges are also shown in Figure 3.16 and it can be observed that there exists no other minimum of the function. The similar procedure was performed for dual adjustment factors and similar results were obtained for the calibrated adjustment factors.

3.5 Summary

In this chapter we have presented the complete methodology about the validation of the PHY abstraction in LTE systems using OpenAirInterface. We have provided the detailed training and validation of PHY abstraction with the help of a link level simulator for different transmission modes of LTE corresponding to different antenna configurations. It was shown that with proper calibration both EESM and MIESM perform equivalently and thus anyone of them could be used for the system evaluations. Furthermore, it was shown that the calibration is a necessary step for the PHY abstraction to be accurate especially in the case of MIESM and multi-antenna configurations. In the end it was shown that the calibrated adjustment factors were globally optimal and provided the minimal MSE values for all of the MCS. It is very clear from the results that methodology is very accurate and indeed can be directly used for system level evaluations. Further in the Appendix A we present the calibrated adjustment factors for the discussed transmission modes which can be used in system level simulators.

3.A Calibration Factors and MSE

Tables 3.5, 3.6 and 3.7 represent the adjustment factors using EESM for transmission mode 1, 2 and 6 respectively. Similarly Tables 3.8, 3.9 and 3.10 represent the adjustment factors using MIESM for transmission mode 1, 2 and 6 respectively. These adjustment factors are calibrated with real channel estimation.

Table 3.5: Transmission Mode 1 using EESM

MCS	β_1	β_2	**MSE**	$\beta_1 = \beta_2$	**MSE**
0	2.50200	2.52163	0.00614	3.17266	0.00638
1	0.84047	0.83231	0.01761	0.79766	0.01820
2	0.78195	0.77472	0.04481	0.74258	0.04521
3	1.37929	1.36536	0.10277	1.28672	0.10344
4	1.16871	1.16829	0.00872	1.16631	0.00872
5	1.11906	1.11186	0.00909	1.09287	0.00930
6	1.06303	1.06287	0.01086	1.06250	0.01086
7	1.07447	1.07292	0.01693	1.07041	0.01693
8	1.11403	1.09946	0.01178	1.07881	0.01252
9	1.09223	1.10650	0.01536	1.12725	0.01577
10	2.82502	2.79174	0.00852	2.68711	0.00925
11	2.87556	2.75655	0.00903	2.50146	0.01472
12	3.51254	3.36651	0.01189	3.08525	0.02212
13	3.62920	3.49011	0.01256	3.25283	0.01826
14	3.53638	3.60903	0.01445	3.74209	0.01637
15	2.35980	2.73517	0.36966	3.17852	0.44267
16	3.74126	3.84009	0.03952	3.99219	0.04159
17	8.66532	8.20312	0.02863	7.18301	0.03623
18	7.31772	7.41739	0.02724	7.57412	0.02817
19	9.86882	9.64081	0.03334	9.33271	0.03520
20	10.64939	10.40911	0.02605	10.09463	0.02807
21	6.75208	8.11765	0.34621	9.41289	0.44151
22	9.50664	10.41923	0.18020	11.28281	0.20101

Table 3.6: Transmission Mode 2 using EESM

MCS	β_1	β_2	**MSE**	$\beta_1 = \beta_2$	**MSE**
0	0.92257	0.67252	0.00588	0.12139	0.42774
2	1.80445	1.28633	0.04400	0.19541	0.40069
3	1.43175	1.01624	0.07687	0.22090	0.66787
4	1.42093	1.03066	0.00394	0.23564	0.41717
5	1.37381	0.97590	0.00488	0.31299	0.41358
6	1.45392	1.02560	0.00378	0.42373	0.67791
7	1.47255	1.01840	0.00689	0.39258	0.58927
8	1.47451	1.00547	0.00476	0.32793	0.44468
9	1.41235	0.97093	0.00599	0.35654	0.70453
10	3.90797	2.72573	0.00579	0.79502	0.64950
11	3.38557	2.33283	0.00383	0.62441	0.95780
12	4.13059	2.86181	0.00507	0.90195	0.53634
13	4.93355	3.40452	0.00647	1.04883	0.56436
14	4.97277	3.47957	0.00629	1.57578	0.51257
15	6.04951	4.08916	0.00495	1.38467	0.56047
16	5.88896	3.97628	0.00737	1.49580	0.43234
17	8.68076	6.14541	0.03771	2.86875	0.54606
18	10.23746	7.11017	0.01246	2.53779	0.43182
19	12.37069	8.42369	0.01147	3.41221	0.65920
20	5.50538	4.04812	1.44425	2.79697	1.95872
21	17.29612	11.42082	0.03537	3.60771	0.66077
22	17.95050	11.57171	0.05672	5.14805	0.82959
23	13.27095	9.28462	0.28886	4.91787	0.66342

Table 3.7: Transmission Mode 6 using EESM

MCS	β_1	β_2	**MSE**	$\beta_1 = \beta_2$	**MSE**
0	0.93374	0.66288	0.36439	0.22627	0.78530
1	1.40389	0.96402	0.31481	0.29404	1.05968
2	1.36670	0.98545	0.30117	0.33535	0.65842
3	1.38679	0.99386	0.20086	0.37646	0.67562
4	1.35707	0.99981	0.17879	0.42607	0.41506
5	1.26353	0.92678	0.16842	0.47217	0.55619
6	1.32360	0.98978	0.15541	0.53184	0.46950
7	1.40164	0.99600	0.12315	0.46357	0.62411
8	1.51843	1.05538	0.12167	0.37715	1.01992
9	1.34868	0.97777	0.09525	0.60176	0.40311
10	3.45839	2.52504	0.04816	1.00518	0.49288
11	3.13726	2.29338	0.03763	1.04209	0.40827
12	3.94768	2.89631	0.03385	1.27129	0.49046
13	4.21966	3.10812	0.02008	1.48730	0.53496
14	4.60750	3.41916	0.02074	2.04482	0.47580
15	4.97894	3.58671	0.02211	1.90596	0.41997
16	5.40755	3.84166	0.01947	2.26533	0.49488
17	8.12814	6.05254	0.01524	2.63701	0.36690
18	10.59221	7.45821	0.02309	3.11152	0.22210
19	12.96427	9.15812	0.01687	4.12158	0.36411
20	13.37323	9.66330	0.01314	5.12168	0.23121
21	14.27206	10.17852	0.01931	5.41904	0.52666
22	16.61779	11.50519	0.03512	6.00830	0.48425

Table 3.8: Transmission Mode 1 using MIESM

MCS	β_1	β_2	**MSE**	$\beta_1 = \beta_2$	**MSE**
0	1.32955	1.36875	0.00750	3.03896	0.00692
1	0.59522	0.59304	0.01529	0.58398	0.01538
2	0.54024	0.53870	0.04302	0.53115	0.04306
3	0.98698	0.98239	0.10267	0.96904	0.10291
4	0.81305	0.81637	0.00876	0.83057	0.00889
5	0.76976	0.76847	0.00794	0.76484	0.00796
6	0.69258	0.69842	0.01057	0.71211	0.01115
7	0.69713	0.69885	0.01415	0.70156	0.01418
8	0.70546	0.69967	0.01018	0.69072	0.01050
9	0.69111	0.69826	0.01578	0.70918	0.01605
10	0.81904	0.82660	0.01075	0.89795	0.01100
11	0.72664	0.70559	0.01124	0.59902	0.01668
12	0.79491	0.78404	0.00600	0.73799	0.00764
13	0.72562	0.70670	0.00639	0.64326	0.01028
14	0.53980	0.55393	0.01129	0.59424	0.01521
15	0.33134	0.36893	0.57483	0.41836	0.63788
16	0.50550	0.52225	0.05330	0.55693	0.05762
17	0.40602	0.39752	0.02071	0.34561	0.02369
18	0.40281	0.40494	0.03708	0.41318	0.03733
19	0.47012	0.46239	0.01770	0.44160	0.01950
20	0.50510	0.49247	0.01558	0.45947	0.02003
21	0.23540	0.26900	0.60484	0.30762	0.69461
22	0.32045	0.34504	0.21285	0.37695	0.23012

Table 3.9: Transmission Mode 2 using MIESM

MCS	β_1	β_2	**MSE**	$\beta_1 = \beta_2$	**MSE**
0	0.59632	0.43775	0.00573	0.07129	0.44339
2	1.08475	0.78208	0.04437	0.11787	0.41393
3	1.02431	0.72875	0.07511	0.13174	0.68835
4	1.07020	0.77458	0.00361	0.13994	0.43896
5	0.90170	0.64485	0.00491	1.08389	2.36940
6	0.97719	0.69174	0.00332	0.24629	0.69209
7	0.95464	0.66097	0.00547	0.23730	0.60609
8	0.92764	0.63289	0.00404	0.15742	0.53167
9	0.86721	0.59652	0.00572	0.19453	0.79222
10	0.85986	0.61175	0.00612	0.09531	0.71265
11	0.64558	0.44551	0.00284	0.07158	1.01123
12	0.80631	0.56047	0.00333	0.10332	0.56289
13	0.82673	0.57314	0.00231	0.11885	0.59614
14	0.82888	0.57553	0.00526	0.18916	0.58208
15	0.87122	0.58849	0.00359	0.15293	0.59291
16	0.77245	0.52159	0.00650	0.16621	0.45732
17	0.29771	0.21241	0.05151	0.07979	0.58986
18	0.43477	0.30139	0.00816	0.06855	0.46021
19	0.55321	0.37373	0.01569	0.09502	0.75149
20	0.61027	0.32029	4.12362	0.60449	11.94598
21	0.56111	0.37067	0.03984	0.10098	0.73146
22	0.57292	0.36706	0.06210	0.13730	0.88452
23	0.39737	0.27118	0.34545	0.26797	2.03803

Table 3.10: Transmission Mode 6 using MIESM

MCS	β_1	β_2	**MSE**	$\beta_1 = \beta_2$	**MSE**
0	0.77532	0.54448	0.37079	0.14473	0.82650
1	1.07544	0.73731	0.32028	0.19150	1.11373
2	1.10571	0.79165	0.30696	0.21650	0.70072
3	1.04099	0.74407	0.20822	0.24180	0.71320
4	0.91638	0.68042	0.18665	0.27021	0.44771
5	0.88644	0.64906	0.17691	0.30068	0.60414
6	0.96405	0.71349	0.16751	0.32861	0.50532
7	0.86709	0.62109	0.14058	0.28271	0.65730
8	0.94066	0.65815	0.13443	0.22422	1.04442
9	0.84430	0.60940	0.10719	0.35410	0.44835
10	1.24478	0.90549	0.06235	0.13379	0.58910
11	1.09665	0.78708	0.05709	0.13506	0.47862
12	1.42604	1.03176	0.04578	0.16250	0.56541
13	0.79541	0.58431	0.03135	0.18564	0.61692
14	0.71847	0.53379	0.02877	0.26777	0.55334
15	0.71604	0.51224	0.02749	0.22578	0.48371
16	0.74561	0.52767	0.02642	0.27158	0.56280
17	0.36431	0.26848	0.02158	0.07578	0.45022
18	0.41536	0.29642	0.03314	0.08809	0.26089
19	0.52175	0.36879	0.01865	0.11836	0.43116
20	0.47096	0.34148	0.01721	0.14600	0.25952
21	0.49977	0.35279	0.01950	0.15439	0.60924
22	0.59728	0.40633	0.04522	0.16816	0.58094

Chapter 4

LTE Multi-User MIMO with Interference Aware Receiver

4.1 Introduction

In this chapter we study the PHY abstraction for interference limited systems and advanced receiver algorithms. This is a challenging task especially for MIMO communications. MIMO communication provides a linear gain in the capacity of a system proportional to the minimum of the number of antennas at the transmitter and the receiver without having to actually increase the bandwidth or power [43] [44]. MIMO systems generally fall into two categories, SU MIMO and MU MIMO [45]. MU MIMO has several benefits over the SU MIMO and inherently solves many of the main problems of SU MIMO [46] [47]. The main principle in MU MIMO communication is that more than one user can be served using same time and frequency resources thus increasing directly the spectral efficiency and capacity of the system.

However, the performance of MU MIMO mainly depends on the channel state information at the transmitter (CSIT) and the detection algorithm at the receiver. Real life implementation of MU MIMO in LTE and LTE-Advanced suffers from multi-user interference (MUI) due to the imperfect CSIT and use of sub optimal single user detection at the receiver. It is shown in [48] that for LTE release 8 MU MIMO does not meet the expectations of theoretical gains because of the extremely low resolution feedback for providing CSIT and because of the design of transmit precoder's code book which is based on equal gain transmission. This has been improved in

the latest releases of LTE.

In the latest release of 3GPP there is an improved hierarchical codebook design for MU-MIMO which provides better channel separation for MU MIMO users but due to the quantization of CSIT there remains a huge amount of residual MUI in the system which comes from a finite constellation. Therefore, use of linear receivers is sub-optimal for the detection in such cases. The optimal solution for this kind of interference is to pre-cancel the interference at the transmitter using dirty paper coding [49] but it is not feasible in practical systems due to its huge complexity and requirements on the feedback for the perfect CSIT. A good solution was presented in [50] where the authors show that low complexity optimal (capacity achieving) interference aware (IA) receivers are feasible with implementable complexity. This kind of receiver exploits some prior knowledge of interference in decoding procedure, i.e., in the case of IA receiver, it requires the knowledge about the constellation order of the interfering user. Once this information about the interference is obtained, it exploits the structure of interference in the process of detection.

Although the gains offered by MU MIMO with improved codebook design and IA receiver are significant on the single communication link [51] the true potential of such receiver is tested at system level. However, system level evaluations normally require heavy computations for extremely long duration of time due to the characterization of the radio links between each user and the base station. The link level simulations of all such links is the bottle neck in these evaluations. Therefore, to reduce the complexity and duration of system level simulations we need to have an accurate PHY abstraction model.

4.1.1 Related Work

Detailed literature review about the PHY abstraction models has already been given in previous chapter. An important work in the field of MIMO communications was presented in [52] where the authors have presented a semi-analytical performance prediction model based on MIESM for iterative MMSE-Interference Cancellation detection and LMMSE semi-blind channel estimation. Their model heavily relies on the Gaussian approximation on MMSE-IC and channel estimation error. Furthermore, they presented the results only for SU MIMO case. Another important work was presented in [53] for MIMO-OFDM systems with ML receivers. Their model is also based on a variant of MIESM (based on work by [19]) and they model the effects of channel mismatch and correlation in the abstraction model. They show results for the rate compatible punctured convolution codes and different MIMO antenna configurations. There has not been much work published

about the PHY abstraction of MU MIMO in the framework of LTE. To the best knowledge of author there has been no work for the case of interference limited MIMO-OFDM systems employing turbo codes and especially for the MU MIMO in the framework of LTE. However, in [54] it was shown by the authors how the concept of PHY abstraction can be used for the throughput calculation of different transmission modes in LTE with the help of stored frequency response of MIMO channels. The results from [54] were the motivation for us to extend the PHY abstraction for the link-to-system simulators.

4.1.2 Contributions

The most important feature of PHY abstraction models is to be able to not only capture the transceiver features very accurately but also be able to provide high level of accuracy for the system level simulator. In this chapter we investigate the PHY abstraction with the help of MU MIMO in great detail and improve the methodology presented in [55] both in terms of complexity and accuracy. We propose a novel mutual information based interference aware PHY abstraction (IAPA) model for MU MIMO in LTE when low complexity IA receivers are used. We show that the proposed PHY abstraction model is capable of exploiting the interference and provide accurate link quality indicator. For the comparison we show how standard PHY abstraction models can be used for interference aware receivers in LTE and compare their results with our proposed PHY abstraction model. Further, in this chapter we generalize the proposed PHY abstraction model for interference limited scenarios other than MU MIMO in LTE as well.

4.1.3 Organization

The chapter is organized as follows, Section 4.2 presents an overview of MU MIMO in LTE up to the latest release 10. In Section 4.3 we present the system model and expressions for the achievable mutual information of QAM constellations under interference for MU MIMO. In Section 4.4 we discuss how state-of-the-art PHY abstraction models can be used for the IA receivers and present our proposed interference aware PHY abstraction (IAPA) model for MU MIMO in LTE. In Section 4.5 we explain how our proposed PHY abstraction model can be used for interference limited scenarios other than MU MIMO in LTE. In Section 4.6 we present results of PHY abstraction for MU MIMO in LTE using OpenAirInterface platform for a frequency selective channel. Finally in Section 4.7 we conclude the chapter with a summary.

4.2 Multi-User MIMO in LTE

MU MIMO is supported in transmission mode 5, 8 and 9 and is discussed next in detail for the different releases of LTE.

4.2.1 MU-MIMO in Release 8

In LTE release 8 MU-MIMO is only supported in the downlink transmission mode 5 where an eNodeB can schedule two UEs simultaneously using the same time and frequency resources with single data stream i.e. rank-1 transmission. LTE release 8 was mainly designed to support the SU-MIMO transmission and support for MU-MIMO was kept at minimum in it [4]. Because of this reason there is no separate codebook for the precoding in downlink transmission mode 5 and the system has to rely on the low-resolution codebook-based precoding of transmission mode 4 (rank-1) which was initially designed to provide a compromise between performance and feedback overhead. The codebook $\mathcal{P}$ for two transmit antennas in LTE is given by,

$$\mathcal{P} = \frac{1}{\sqrt{2}} \left\{ \begin{bmatrix} 1 \\ 1 \end{bmatrix}, \begin{bmatrix} 1 \\ -1 \end{bmatrix}, \begin{bmatrix} 1 \\ j \end{bmatrix}, \begin{bmatrix} 1 \\ -j \end{bmatrix} \right\} \tag{4.1}$$

The information about the precoder can be sent back to the eNodeB in a special field named as precoding matrix indicator (PMI). This PMI requires two (for 2 antenna ports) to four (for 4 antenna ports) bits of feedback from the UEs and is reported for the whole bandwidth, i.e., wideband PMI. There is no subband PMI in transmission mode 5.

The main difference in transmission mode 4 and 5 in LTE release 8 is the signaling of an additional power offset between PDSCH and the CRS. This power offset is required because the CRS in all releases of LTE are always QPSK modulated and for the correct demodulation of the signals transmitted by means of higher order modulation (16-QAM and 64-QAM), the UE needs to know the power offset between the CRS and PDSCH. Of course this relationship has to be refined if the transmission is performed with more than one stream because in that case the offset shall correspond to the power offset between the CRS and per-layer PDSCH power.

For the case of MU MIMO, the total power is also divided between the transmissions to the co-scheduled UEs which results in low PDSCH power for each transmission. Since in release 8 the UEs are not aware of the presence of the parallel transmission to the co-scheduled UEs so there is an additional power offset of -*3dB* to be used by the UE in addition to the CRS/PDSCH power offset signaled by higher layers. Since there is just one additional -*3dB* power offset defined in release 8, therefore, MU MIMO is limited to rank-1 transmission of two co-scheduled UEs in transmission mode 5.

4.2.2 MU-MIMO in Release 9 and 10

The support for MU-MIMO was extended to transmission mode 8 and 9 in further releases of LTE with user-specific demodulation reference symbols (DMRS) [56]. These reference symbols are initialized using only the cell identity in order to enable the two orthogonally code-multiplexed DMRS ports to be used for different UEs (MU MIMO) as shown in Figure 4.1. The orthogonal code-multiplexed RSs are generated by means of length-2 Walsch-Hadamard Orthogonal Cover Codes (OCC), i.e.,$\{(1,\ 1), (1,\ -1)\}$ which can be used for the transmission to two UEs in MU MIMO mode. For more than two ports a pseudo random sequence is applied to the DMRS and the placement of these DMRS is shown in the LTE frame structure in Figure 4.2. The pusedo-random sequence is not terminal specific in the sense that each terminal has its own sequence. Rather there are only two sequences available and information on what pseudo random sequence is used for a certain DMRS to a certain terminal is provided in the scheduling assignment together with the information about OCC. This allows multi-stream MU MIMO, rank-2 transmission in release 9 and up to rank 4 in release 10.

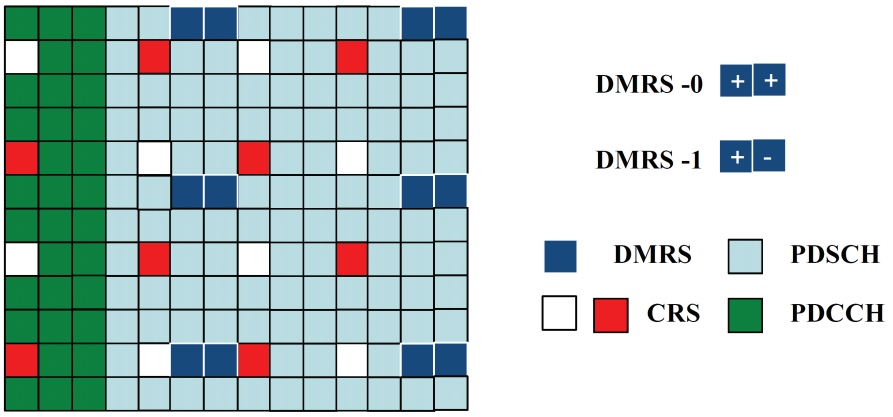

Figure 4.1: Demodulation Reference Signal structure for the case of two antenna ports

Another improvement for MU-MIMO in the latest releases is that the UE-specific RS are precoded the same way as the data which means that the precoding for the MU-MIMO is more flexible and can be decided independent of the 3GPP specifications. Although MU MIMO in the latest releases is also invisible for the UEs but at the same time nothing prevents a UE from assuming that there are transmissions on the other layers corresponding to the other demodulation reference signals. In this case UEs can apply receiver side signal processing to estimate and suppress the potential inter-

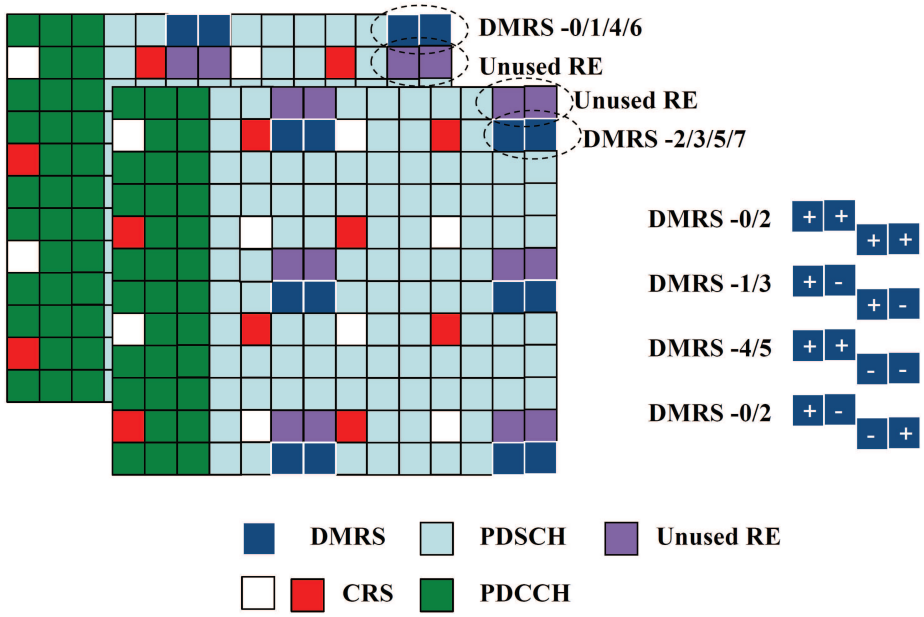

Figure 4.2: Demodulation Reference Signal structure for more than two antenna ports

ference. Further the feedback is much more refined in these releases and is supported for subband and wideband reporting on the uplink.

An important improvement in latest releases of LTE is that the UE can actually estimate the interference channel by applying the other OCC. Thus the UE does not need to have any additional information in the control signals about the precoder of the interferer and it can detect the presence of other user by analyzing the energy of the interference channel.

4.3 System Model

MU-MIMO was first introduced in LTE release 8 therefore to be backward compatible we shall focus on transmission mode 5 in this chapter. But the methodology presented in this chapter is also valid for the latest releases of LTE. We consider LTE small cell scenario with a few users and the baseline configuration of LTE for MU MIMO downlink channel where an eNodeB, equipped with $n_t = 2$ transmit antennas, serves two single antenna UEs (i.e., $n_r = 1$) on the same time and frequency resource with a single data stream. The received signal at UE-1 for n-th resource element is given by

$$y_{1,n} = \mathbf{h}_{1,n}\mathbf{p}_{1,n}x_{1,n} + \mathbf{h}_{1,n}\mathbf{p}_{2,n}x_{2,n} + z_1, \quad n = 1, 2, \cdots, N$$

where N is the number of total resource elements, $\mathbf{h}_{1,n} \in \mathbb{C}^{1\times 2}$ symbolizes the spatially uncorrelated flat Rayleigh fading MISO channel from the eNodeB to UE-1. Its elements can be modeled as i.i.d ZMCSCG random variables with a variance of 0.5 per dimension. The z_1 is ZMCSCG white noise of variance N_0 at UE-1. Complex symbols $x_{1,n}$ and $x_{2,n}$ are assumed to be independent and of variances σ^2. These symbols belong to discrete QAM constellations, i.e., $\chi_{1,n}$ and $\chi_{2,n}$ respectively. $\mathbf{p}_{1,n}$ and $\mathbf{p}_{2,n}$ are 2×1 precoder vectors requested by UE-1 and UE-2 for the n-th resource element, respectively. The available precoders in LTE release 8 are given in (4.1). UE-1 selects the precoding vector $\mathbf{p}_{1,n}$ which results in the maximization of its desired effective channel magnitude $||\mathbf{h}_{1,n}\mathbf{p}_{1,n}||$, i.e.,

$$\mathbf{p}_{1,n} = \underset{\mathbf{p}\in\mathcal{P}}{\operatorname{argmax}} \{|\mathbf{h}_{1,n}\mathbf{p}|\} \tag{4.2}$$

and feeds it back to the eNodeB for it to be scheduled. In the rest of the chapter dependency on the resource element index n can be ignored, since the processing is assumed to be performed on a resource element basis for each received OFDM symbol.

4.3.1 Scheduler

There is no rule defined specifically for the UEs to be scheduled in SU and MU MIMO mode in the 3GPPs specifications. In general the scheduler should serve the users in the MU MIMO mode on the downlink when it is possible to generate independent parallel channels from cross coupled channels (i.e., eliminating multi-user interference). This is only possible if the users are scheduled with orthogonal precoders with respect to each other which provides the spatial separation between the channels of the co-scheduled users. Therefore we assume that from the available set of users there exists a second UE who has asked for the scheduler $\mathbf{p}_2$ chosen on the principle of (4.2) and is orthogonal to the precoder selected by UE-1, i.e. $\mathbf{p}_1 = \perp\mathbf{p}_2$. For example if UE-1 has selected and asked for $\mathbf{p}_1 = [1 \quad q]^{\mathrm{T}}$ and UE-2 has asked for $\mathbf{p}_2 = [1 \quad -q]^{\mathrm{T}}$ where $q \in \{\pm 1, \pm j\}$ only then both of them shall be scheduled for MU MIMO transmission. Using this approach it can be made sure that each UE is actually aware of the precoder of the interfering user but the knowledge about the constellation used for the UE-2 is still unknown and it is shown in [57] that assuming the same constellation as the desired UE has negligible effect on the decoding performance. Therefore, we shall use the same constellation as the desired UE in rest of this chapter. Then this extra information about precoder and constellation can be exploited in the detection process by the interference aware receiver.

In the following we assume that both of the co-scheduled users are served with the same modulation order, i.e., $\chi_1 = \chi_2$. In LTE the channel can

be estimated at each of the UE with the help of CRS also known as pilot symbols and we assume ideal channel estimation for pilot symbols at the receivers. Then the effective channel at UE-1 can be represented by $\alpha_1 = \mathbf{h}_1\mathbf{p}_1$ and $\delta_1 = \mathbf{h}_1\mathbf{p}_2$. The signal received at UE-1 (on n-th resource element) can be represented as,

$$y_1 = \alpha_1 x_1 + \delta_1 x_2 + z_1. \tag{4.3}$$

As explained in the previous section that in the latest release of LTE, because of the orthogonal code-multiplexing of the DMRS, the effective channel of the interferer can be estimated at the desired UE. This means if a non-codebook based precoding is used even then the precoder of the interferer can also be estimated with the help of DMRS.

4.3.2 Interference Aware Receiver

Interference aware receiver is a low complexity matched filter (MF) based maximum likelihood (ML) detector which reduces one complex dimension of the system without introducing any suboptimality and is also characterized by exploiting the interference structure in the detection process. In the current scenario there is MUI present in the system and the knowledge about it can be exploited in the detection process. After the matched filtering (4.3) can be written as,

$$y_1' = \frac{\alpha_1^\dagger}{|\alpha_1|} y_1 \tag{4.4}$$

$$= |\alpha_1| x_1 + \underbrace{\frac{\alpha_1^\dagger \delta_1}{|\alpha_1|}}_{\zeta_1} x_2 + \underbrace{\frac{\alpha_1^\dagger}{|\alpha_1|} z_1}_{z_1'}, \tag{4.5}$$

where $|\alpha_1|$ is the gain of the desired channel and ζ_1 is the interference for the desired user after matched filtering. Note that the variance of z_1' is still N_0. To compute the LLRs Λ we apply the classical ML criterion with subsequent Max-log approximation. Then the minimum distance λ is given as,

$$\lambda = \max_{x_1 \in \chi_1, x_2 \in \chi_2} \left\{ -||y_1 - \alpha_1 x_1 - \delta_1 x_2||^2 \right\}. \tag{4.6}$$

With further simplification we can obtain,

$$\begin{aligned} \lambda = \max_{x_1 \in \chi_1, x_2 \in \chi_2} \{ & - ||\alpha_1||^2 |x_1|^2 - ||\delta_1||^2 |x_2|^2 \\ & + 2 \left[\Re(y_1') \Re(x_1) + \Im(y_1') \Im(x_1) \right] \\ & + 2 \left[|\eta_1| \Re(x_2) + 2 |\eta_2| \Im(x_2) \right] \}, \end{aligned} \tag{4.7}$$

with

$$\eta_1 = \Re(\zeta_1)\Re(x_1) + \Im(\zeta_1)\Im(x_1) - \Re(y_2') \tag{4.8}$$
$$\eta_2 = \Re(\zeta_1)\Im(x_1) + \Im(\zeta_1)\Re(x_1) - \Im(y_2') \tag{4.9}$$

where $y_2' = \frac{\delta_1^\dagger}{|\delta_1|} y_1$, $\Re$ and $\Im$ represent the real and imaginary parts of the signals respectively. Note that in (4.8) one complex dimension is reduced on the search of alphabets as the maximization becomes independent of the sign of x_2. The optimum values of the $\Re(x_2)$ and $\Im(x_2)$ can be obtained by equating the derivative of (4.8) to zero. The complexity can be further reduced when these expressions are derived for particular constellation. For further details about the interference aware receiver structure the readers are referred to [58].

4.3.3 Information theoretic View

The mutual information of UE-1 for finite size QAM constellation with $|\chi_1| = M_1$ takes the form as

$$\begin{aligned} I\left(Y_1; X_1 \middle| |\alpha_1|, \zeta_1\right) &= \mathcal{H}\left(X_1 \middle| |\alpha_1|, \zeta_1\right) - \mathcal{H}\left(X_1 | Y_1, |\alpha_1|, \zeta_1\right) \\ &= \log M_1 - \mathcal{H}\left(X_1 | Y_1, |\alpha_1|, \zeta_1\right) \end{aligned} \tag{4.10}$$

where $\mathcal{H}(.) = -\mathcal{E} \log p(.)$ is the entropy function. The second term of (4.10) is given as

$$\begin{aligned} &\mathcal{H}\left(X_1 | Y_1, |\alpha_1|, \zeta_1\right) \\ &= \sum_{x_1} \int_{y_1} \int_{|\alpha_1|} \int_{\zeta_1} p\left(x_1, y_1, |\alpha_1|, \zeta_1\right) \log \frac{1}{p\left(x_1 | y_1, |\alpha_1|, \zeta_1\right)} dy_1 d|\alpha_1| d\delta_1 \\ &= \sum_{x_1} \sum_{x_2} \int_{y_1} \int_{|\alpha_1|} \int_{\zeta_1} p\left(x_1, x_2, y_1, |\alpha_1|, \zeta_2\right) \\ &\quad \times \log \frac{\sum_{x_1'} \sum_{x_2'} p\left(y_1 | x_1', x_2', |\alpha_1|, \zeta_2\right)}{\sum_{x_2'} p\left(y_1 | x_1, x_2', |\alpha_1|, \zeta_1\right)} dy_1 d|\alpha_1| d\delta_1 \end{aligned} \tag{4.11}$$

Note that conditioned on the channel, the precoder is not random. So there is only one source of randomness i.e. the noise. So (4.11) can be

$$I(Y_1; X_1 | \, |\alpha_1| \, , \zeta_1, N_0) = \log M_1 \tag{4.12}$$
$$- \frac{1}{M_1 M_2} \sum_{\mathbf{x}} \mathcal{E}_{z_1'} \log \frac{\sum_{\mathbf{x}'} \exp \left[-\frac{1}{N_0} \left| |\alpha_1| \, (x_1 - x_1^{'}) + \zeta_2 (x_2 - x_2^{'}) + z_1' \right|^2 \right]}{\sum_{x_2''} \exp \left[-\frac{1}{N_0} \left| \zeta_1 (x_2 - x_2'') + z_1' \right|^2 \right]}$$

extended as

$$\mathcal{H} \left(X_1 | Y_1, |\alpha_1| \, , \zeta_1 \right)$$
$$= \frac{1}{M_1 M_2} \sum_{\mathbf{x}} \mathcal{E}_{z_1'} \log_2 \frac{\sum_{\mathbf{x}'} \exp \left[-\frac{1}{N_0} \left| |\alpha_1| \, x_1 + \zeta_1 x_2 + z_1' - |\alpha_1| \, x_1^{'} - \zeta_2 x_2^{'} \right|^2 \right]}{\sum_{x_2''} \exp \left[-\frac{1}{N_0} \left| \zeta_1 x_2 + z_1' - \zeta_1 x_2'' \right|^2 \right]}$$
$$= \frac{1}{M_1 M_2} \sum_{\mathbf{x}} \mathcal{E}_{z_1'} \log \frac{\sum_{\mathbf{x}'} \exp \left[-\frac{1}{N_0} \left| |\alpha_1| \, (x_1 - x_1^{'}) + \zeta_2 (x_2 - x_2^{'}) + z_1' \right|^2 \right]}{\sum_{x_2''} \exp \left[-\frac{1}{N_0} \left| \zeta_1 (x_2 - x_2'') + z_1' \right|^2 \right]}$$

where $M_2 = |\chi_2|$, $\mathbf{x} = [x_1 \; x_2]^T$ and $\mathbf{x}^{'} = \left[x_1^{'} \; x_2^{'} \right]^T$.

Then the mutual information for finite QAM constellation at UE-1 with a non-Gaussian interferer is given in (4.12). The mutual information expressions for UE-2 can also be derived similarly. In the rest of the paper we shall use this MF based low complexity interference aware receiver for MU MIMO and present a novel PHY abstraction model for such a receiver,

4.4 PHY abstraction for Interference Aware Receiver

PHY abstraction using ESM consists of the three main steps as shown in Figure 6.1.

- *Information Mapping and Compression:* This step is most important as it selects the appropriate link quality metric depending on the receiver type. Typical choice is to use post processed SINR. Then based on the selected link quality metric, an information mapping function is chosen to transform the SINRs of each subcarrier to an information measure. This information measure is then linearly averaged over all of the subcarriers for the given codeword, producing an average information per symbol.

$$W_{\text{abs}} = \frac{1}{N} \sum_{n=1}^{N} I \left(\frac{\gamma_n}{\beta} \right) \tag{4.13}$$

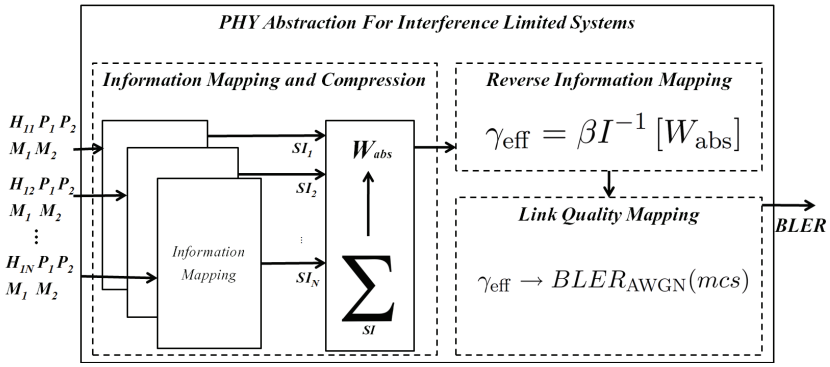

Figure 4.3: PHY abstraction model for MU MIMO using Interference Aware receivers in LTE

Where N is the number of subcarriers in a codeword, γ_n is the post-processed SINR across each subcarrier and $I(\gamma_n)$ is a mapping function. β is called an adjustment factor and its true value is to be optimized for each MCS in LTE.

- *Reverse Information Mapping:* In this step a mapping function is selected which has one-to-one relationship between the average information per symbol for the given codeword W_{abs} and the effective SINR γ_{eff}. This function is chosen very carefully as its sole purpose is to yield the accurate γ_{eff} based on the W_{abs} so that the link quality indicator from the AWGN performance curves can be selected.

$$\gamma_{\text{eff}} = \beta I^{-1}[W_{\text{abs}}] \tag{4.14}$$

- *Link Quality Mapping:* This is the final step of PHY abstraction which provides us with the required link quality indicator. The input to this step is γ_{eff} which was calculated from reverse information mapping such that this γ_{eff} produces the same error rate as it would have produced in the AWGN channel conditions. So in this step we read the link quality indicator as BLER based on γ_{eff} from previously computed AWGN performance curves of particular MCS.

$$\gamma_{\text{eff}} \rightarrow BLER_{\text{AWGN}}(mcs) \tag{4.15}$$

Now we describe the two popular PHY abstraction models very briefly and present our proposed interference aware prediction model in detail.

4.4.1 EESM

For the linear receivers such as minimum mean squared error (MMSE) or zero forcing (ZF), EESM [16] utilizes the post-processed SINR for each of

the subcarrier, but for the interference aware receiver post-processed SINR is not available. However, for interference aware receivers SINR after matched filtering of UE-1 for the n-th resource element can be calculated as,

$$\gamma_{1,n} = \frac{|\alpha_{1,n}|^2 \sigma^2}{|\delta_{1,n}|^2 \sigma^2 + N_0}, \tag{4.16}$$

where the $\alpha_{1,n}$ and $\delta_{1,n}$ come from equation (4.5). Important thing to note here is that the absorption of interference into Gaussian noise is already sub-optimal as the interference is not Gaussian and the PHY abstraction will correspond to a suboptimal solution in the case of EESM. The mapping function $I(\gamma_{1,n})$ is calculated using Chernoff union bound of error probabilities, i.e.,

$$I_{\text{EESM}}(\gamma_{1,n}) = 1 - \exp(-\gamma_{1,n}) \tag{4.17}$$

and

$$I^{-1}_{\text{EESM}}(\gamma_{1,n}) = -\ln\left(1 - I_{\text{EESM}}(\gamma_{1,n})\right). \tag{4.18}$$

Then,

$$W_{\text{EESM}} = 1 - \frac{1}{N}\sum_{n=1}^{N} \exp\left(-\frac{\gamma_{1,n}}{\beta}\right), \tag{4.19}$$

$$\gamma_{\text{eff}} = -\beta \ln\left[1 - W_{\text{EESM}}\right] \tag{4.20}$$

using (4.20) an effective SINR (γ_{eff}) is calculated for the given codeword. Based on this γ_{eff} the equivalent BLER from the pre-calculated AWGN performance curves corresponding to the specific MCS is obtained and given to the system level simulators.

4.4.2 MIESM

Similarly for MIESM the SINR for each subcarrier ($\gamma_{1,n}$) is calculated using (4.16) for the interference aware receivers and the PHY abstraction in the case of MIESM will also lead to the suboptimal solution as the interference is absorbed into the Gaussian noise. In this case the received signal is $y_{1,n} = \alpha_{1,n}x_{1,n} + z_1^o$ with $z_1^o = \delta_{1,n}x_{2,n} + z_1$. For this received signal the approximations of mapping and the reverse mapping functions come from the mutual information for discrete QAM constellation $I(Y_1; X_1|\gamma_{1,n})$ from Chapter 2 (BICM Capacity) where χ_1 is the set of the QAM constellation points with $|\chi_1| = M_{1,n}$ and it is assumed that $z_1^o \in \mathcal{CN}(0,1)$.

$$I_{\text{MIESM}}\left(\gamma_{1,n}, M_1\right) = I(Y_1; X_1|\gamma_{1,n}) \tag{4.22}$$

Based on (4.22) mutual information for each subcarrier with $\gamma_{1,n}$ is calculated and averaged over all subcarriers to yield average mutual information per symbol W_{MIESM} for the given codeword.

$$W_{\text{MIESM}} = \frac{1}{N}\sum_{n=1}^{N} I_{\text{MIESM}}\left(\frac{\gamma_{1,n}}{\beta}, M_{1,n}\right) \tag{4.23}$$

But unfortunately the closed form analytical expressions for calculating the mutual information of each subcarrier for a random channel realization do not exist so these are precomputed and stored in the form of LUTs. With the help of these LUTs the mutual information for $\gamma_{1,n}$ can be obtained. Then γ_{eff} is calculated using the reverse information mapping function which is also given by the same LUT based on (4.22).

$$\gamma_{\text{eff}} = \beta I_{\text{MIESM}}^{-1}\left[W_{\text{MIESM}}\right] \tag{4.24}$$

Finally using γ_{eff}, a link quality indicator is predicted in the form of BLER from the previously calculated AWGN reference curves for specific MCS to complete the PHY abstraction using MIESM.

4.4.3 Interference-Aware PHY abstraction (IAPA)

Interference aware receivers use the knowledge of interference in the detection process by exploiting the fact that this interference is coming from a finite QAM constellation. Therefore, it can not be considered Gaussian and SINR from (4.16) is not an accurate link quality metric. The proper link quality metric should be able to represent the effects of interference in correct manner. For this reason we propose to use a two dimensional link quality metric which consists of signal-to-noise ratio (SNR: $\gamma_{1,n}^{o}$) and interference-to-signal ratio (ISR: $\lambda_{1,n}$) for the UE-1 across all of its subcarriers.

$$\gamma_{1,n}^{o} = \frac{\left|\alpha_{1,n}\right|^2 \sigma^2}{N_0} \tag{4.25}$$

and

$$\lambda_{1,n} = \frac{\left|\zeta_{1,n}\right|^2}{\left|\alpha_{1,n}\right|^2}, \tag{4.26}$$

where the $\alpha_{1,n}$ and $\zeta_{1,n}$ come from equation (4.5). For the information mapping, the required function can be obtained from equation (4.12) which represents the mutual information of finite QAM constellation under an interference. Based on the defined link quality metric $\gamma_{1,n}^{o}$, $\lambda_{1,n}$, modulation order of the desired UE ($M_{1,n}$) and the interfering UE ($M_{2,n}$) mutual information for each subcarrier can be calculated as,

$$I_{\text{IAPA}}\left(\gamma_{1,n}^{o}, \lambda_{1,n}, M_{1,n}, M_{2,n}\right) = I(Y_1; X_1 \,|\, |\alpha_{1,n}|, \zeta_{1,n}, N_0). \tag{4.27}$$

Unfortunately there are no closed form analytical expressions of I_{IAPA} for random channels, therefore, the information mapping is performed with the help of pre-computed LUTs. To compute these tables we performed Monte-Carlo simulations of (4.12) over a wide range of noise and channel realizations. For each channel realization a large number of noise realizations were performed and a random set of $\alpha_{1,n}$, $\zeta_{1,n}$ and corresponding mutual information was obtained. Based on $\alpha_{1,n}$ and $\zeta_{1,n}$, we calculated $\gamma_{1,n}^{o}$ and $\lambda_{1,n}$

for each realization. We calculated the table for big enough realizations so that the maximum variability of the channel is captured. As an example, a graph of MI under interference for QPSK-QPSK (constellation of desired and interfering signal respectively) is shown in Figure 4.4 where on the x-axis is the SNR for the desired user, on y-axis is the ISR for desired user and on z-axis is the mutual information. Then using these tables average mutual

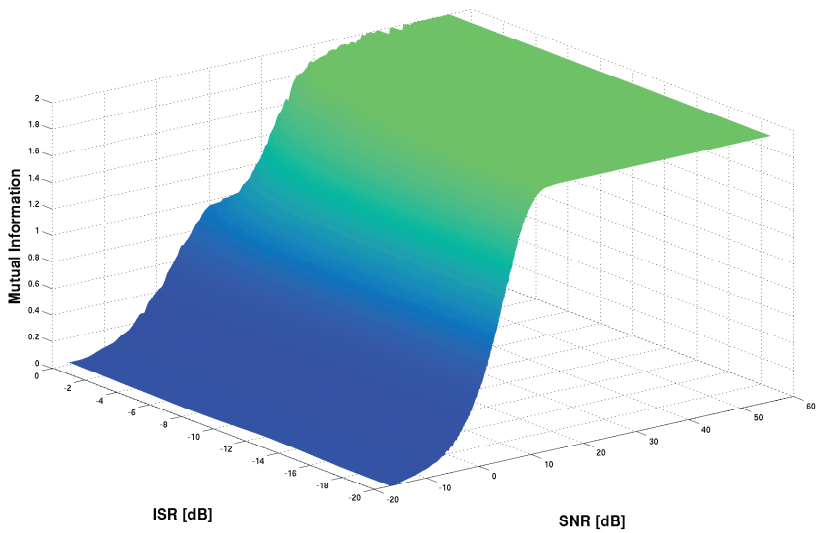

Figure 4.4: Mutual Information of MU MIMO in LTE for Interference Aware Receiver when the desired user and interfering user transmit using QPSK constellation

information per symbol W_{IAPA} for the given codeword is calculated as,

$$W_{\text{IAPA}} = \left[\frac{1}{N} \sum_{n=1}^{N} I_{\text{IAPA}} \left(\gamma_{1,n}^{o}, \frac{\lambda_{1,n}}{\beta}, M_{1,n}, M_{2,n} \right) \right]. \tag{4.28}$$

The important thing to note here is that only the $\lambda_{1,n}$ is adjusted with the help of β. This is because the average mutual information per symbol is affected mainly from interference and to transform a multi-state channel into one-state channel only $\lambda_{1,n}$ is to be adjusted.

To select the reverse information mapping we need to have a function which can provide us with a one-to-one relationship between the W_{IAPA} and γ_{eff}. Since W_{IAPA} has become equivalent to the average mutual information per symbol of one-state channel, we can use I_{MIESM} from equation (4.22) for the reverse mapping function for calculating γ_{eff}.

$$\gamma_{\text{eff}} = \beta I_{\text{MIESM}} \left(W_{\text{IAPA}} \right). \tag{4.29}$$

Finally this γ_{eff} is used to predict the required link quality indicator with the assumption that the γ_{eff} produces the same error rate as it would have produced in the AWGN channel conditions. Such that,

$$BLER(\boldsymbol{\gamma}_1^o, \boldsymbol{\lambda}_1, mcs) \simeq BLER_{\text{AWGN}}(\gamma_{\text{eff}}, mcs), \tag{4.30}$$

where $\boldsymbol{\gamma}_1^o$ and $\boldsymbol{\lambda}_1$ represents the $N \times 1$ vectors of multi-state SNR and ISR for UE-1 across all of the subcarriers of a given codeword. $BLER_{\text{AWGN}}$ is the predicted link quality indicator which is read from the previously calculated and stored AWGN link performance curves for a particular MCS.

4.5 Application to Other Interference-Limited Scenarios

Proposed PHY abstraction model for MU MIMO is also applicable to other interference limited scenarios (e.g. [59]) where the channel of desired user is significantly disturbed by a very strong interferer. This can be scenario for the transmission mode 4 in LTE where the spatial multiplexing is performed with two data streams. In such a case each stream shall see the other stream as an interference of comparable strength and thus can not be assumed Gaussian. If some apriori information is available about the interference then the IA receiver can be used in successive interference cancellation (SIC) [60] manner to remove the interference from each stream.

Other most probable victims of non-Gaussian interference are normally the cell-edge UEs who receive significant interference coming from the neighboring eNodeBs. One example is the case of small cell networks in LTE where there is a possibility that a UE connected to the small cell is affected by the transmission to a neighboring UE by a macro eNodeB. In such a system the eNodeBs can share information about signaling and data over X2 interface [61] (which is over the air interface between eNodeBs). Consider a system with n_r receive antennas and n_t transmit antennas. We assume that $n_t = n_r = R$ and the channel is known perfectly to the UE and a quantized CSIT is present at the eNodeB. In that case the received signal for the n-th resource element at the desired user can be represented as,

$$\mathbf{y}_{1,n} = \mathbf{H}_{1,n}\mathbf{p}_{1,n}x_{1,n} + \mathbf{H}_{2,n}\mathbf{p}_{2,n}x_{2,n} + \mathbf{z}_1, \quad n = 1, 2, \cdots, N$$

where $\mathbf{y}_{1,n} \in \mathbb{C}^{R\times 1}$ is the received signal vector, $\mathbf{H}_{1,n} \in \mathbb{C}^{R\times R}$ is the MIMO channel from the desired eNodeB to the desired UE , $\mathbf{p}_{1,n}$ is the $R\times 1$ precoder vector for desired UE, $x_{1,n}$ is the complex transmit symbol for the desired UE and $\mathbf{z}_{1,n} \in \mathbb{C}^{R\times 1}$ is the circularly symmetric complex white Gaussian noise of double-sided power spectral density $N0/R$ at R receive antennas of the desired UE. Similarly $\mathbf{H}_{2,n} \in \mathbb{C}^{R\times R}$ is the MIMO channel from the interfering

eNodeB to the desired UE , $\mathbf{p}_{2,n}$ is the $R \times 1$ precoder vector from the interfering eNodeB, $x_{2,n}$ is the complex transmit symbol from the interfering eNodeB. In LTE with the help of x2 interface it is possible to share some information between the neighboring eNodeBs and if the required values from the interfering eNodeB can be estimated at the desired UE, then the effective channel at the desired UE can be represented as $\boldsymbol{\alpha}_{1,n} = \mathbf{H}_{1,n}\mathbf{p}_{1,n}$, $\boldsymbol{\delta}_{1,n} = \mathbf{H}_{2,n}\mathbf{p}_{2,n}$. So, after applying the maximum ratio combining (MRC) at the desired UE, the received signal at the desired UE can be rewritten as,

$$\mathbf{y}_{1,n} = \boldsymbol{\alpha}_{1,n}x_{1,n} + \boldsymbol{\delta}_{1,n}x_{2,n} + \mathbf{z}_1, \tag{4.31}$$

$$\begin{aligned} y'_{1,n} &= \frac{\boldsymbol{\alpha}_{1,n}^{\dagger}}{\|\boldsymbol{\alpha}_{1,n}\|}\mathbf{y}_{1,n} \\ &= \|\boldsymbol{\alpha}_{1,n}\|\, x_{1,n} + \underbrace{\frac{\boldsymbol{\alpha}_{1,n}^{\dagger}\boldsymbol{\delta}_{1,n}}{\|\boldsymbol{\alpha}_{1,n}\|}}_{\zeta_{1,n}} x_{2,n} + \underbrace{\frac{\boldsymbol{\alpha}_{1,n}^{\dagger}}{\|\boldsymbol{\alpha}_{1,n}\|}\mathbf{z}_1}_{z'_1} \end{aligned} \tag{4.32}$$

where $\|\boldsymbol{\alpha}_{1,n}\|$ is the gain of desired channel, $\zeta_{1,n}$ is the interference for the desired user after matched filtering and note that the variance of z'_1 is N_0. Note that the equation (4.31)-(4.32) have become similar to the equation numbers (4.3)-(4.5). We can use similar approach as in equation (4.12) for finding the mutual information of finite constellation at the desired UE under this new interference. The new expression will look the same as equation (4.12) as the channel and precoders are no longer random but known at the desired UE.

To use these new mutual information expressions in our proposed PHY abstraction scheme, we need to generate new look-up tables with this expression using Monte-Carlo method with huge number of noise realizations and channel realizations in which the channels and precoders are selected randomly. After generating these tables one can use our proposed PHY abstraction model of section 4.4 for interference limited systems with interference aware receivers.

4.6 Link Level Results

In order to train and test the proposed MU-MIMO PHY abstraction model for interference aware receivers, we used Eurecom's OpenAirInterface[1] (OAI) link level simulator which implements 3GPP LTE Release 8.6 physical layer [8,9,62]. We consider the baseline configuration in LTE for MU MIMO, i.e., a dual antenna eNodeB communicates with two single antenna UEs during same time and frequency resources. We consider ideal PMI feedback from

[1] http://www.openairinterface.org/

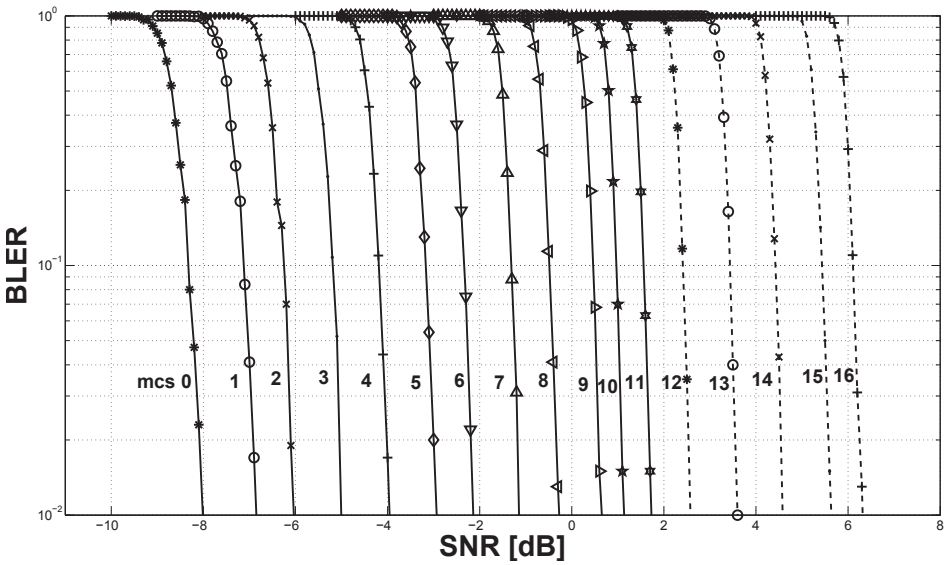

Figure 4.5: AWGN Link Performance Curves in LTE with 5 MHz Bandwidth with ideal channel estimation

the desired UE and the scheduler always serves the second UE with the PMI orthogonal to that of the desired UE. The eNodeB can choose from available MCS 0-28 for both of the scheduled users and we consider the case when both of the UEs are scheduled with the same MCS. In LTE MCS 0-9 corresponds to QPSK modulation, MCS 10-16 corresponds to 16-QAM and MCS 17-28 correspond to the 64-QAM modulation. Depending on the quality of instantaneous channel, different MCS can be used for each new codeword transmission. Before training and testing we performed AWGN link level simulations for all MCS of LTE and stored these AWGN SNR-BLER performance curves to be used for the prediction of BLER during the optimization of adjustment factor β. For ideal channel estimation these are shown in Figure 4.5.

To perform PHY abstraction of MU-MIMO (LTE transmission mode 5) we chose 8-tap Rayleigh channel with exponentially decaying power delay profile and delay spread of 1μs, and spatial channel model (SCM-C) [63] defined by 3GPP with ideal channel estimation. For each MCS we performed link level simulation for at least 100 different channel realizations and during each of the channel realization we simulated the system for 1000 packets or 500 erroneous packets. We saved the BLER and other required parameters necessary for the optimization of β. The other parameters include the PMI choice and frequency response of the channel of both users for each noise variance of each channel realization. With these values and the proposed

Table 4.1: Optimum Adjustment Factor for Proposed IA-PHY abstraction (IAPA), EESM and MIESM with Rayleigh8 Channel Model

MCS	EESM		IAPA		MIESM	
	β	MSE	β	MSE	β	MSE
0	0.03848	1.8341	0.86074	0.0119	0.02139	1.9504
1	0.04951	1.4313	0.83740	0.0204	0.02764	1.5691
2	0.06016	2.1970	0.84277	0.0132	0.03379	2.2876
3	0.07920	1.7999	0.82715	0.0211	0.04424	1.9462
4	0.11436	1.3322	0.82305	0.0477	0.06553	1.4761
5	0.12734	2.2127	0.80137	0.0391	0.07129	2.3181
6	0.15713	3.0461	0.78174	0.0272	0.08643	3.1748
8	0.23994	1.5500	0.74756	0.0606	0.13242	1.7050
9	0.29121	2.1796	0.73008	0.0675	0.16357	2.3413
10	0.37617	3.8321	0.56680	0.0703	0.20684	4.0761
11	0.43877	3.6632	0.55615	0.0920	0.24443	3.8987
12	0.51533	2.7203	0.56719	0.1457	0.30322	2.8469
14	0.80303	0.9866	0.57852	0.2406	0.45889	1.0935
16	2.19121	1.0701	0.56865	0.6383	1.31016	1.1305

PHY abstraction for IA receivers of Section 4.4 we optimized β such that the error in predicted BLER and measured BLER is minimum. We performed this process for the different MCS and just for the comparison we performed PHY abstraction using EESM and MIESM as well. The results of optimization on adjustment factor and resulting minimum mean squared error values (in dB) for both channel models are given in Tables 4.1 and 4.2. Further the Figures 4.6 and 4.7 show the obtained MSE after optimization of adjustment factors using three abstraction models. It is very clear from the tables that our proposed PHY abstraction model can achieve lower MSE from the other two standard models.

Figures 4.8 and 4.9 show the adjustment factors for both of the channel models and for all the three abstraction models. It can be seen that the adjustment factors are not much different for the two channel models but differ greatly for each of the abstraction models. We further applied the optimized adjustment factor β for the PHY abstraction of a random channel realization from link level simulator and the results for that are shown in the Figure 4.10 and 4.11 for both channel models. It can be seen in Figures 4.10 and 4.11 that our approach is very well able to model the link performance of instantaneous channel realizations for the case of MU MIMO in LTE when interference aware receiver is used.

Table 4.2: Optimum Adjustment Factor for Proposed IA-PHY abstraction (IAPA), EESM and MIESM with SCM-C Channel Model

MCS	EESM		IAPA		MIESM	
	β	MSE	β	MSE	β	MSE
0	0.04961	3.3405	0.60127	0.0938	0.00603	3.8158
1	0.06621	4.6060	0.59580	0.0909	0.00806	5.2005
2	0.08092	3.7155	0.57637	0.0554	0.00947	4.2507
3	0.10585	3.6542	0.56104	0.1177	0.01216	4.0918
4	0.12418	3.7941	0.55449	0.0692	0.01475	4.4151
5	0.15537	4.1740	0.53281	0.1268	0.01922	4.8997
6	0.18938	3.9669	0.53008	0.0862	0.02202	4.5980
7	0.24346	3.5132	0.51582	0.1734	0.02828	4.0398
8	0.26670	2.9021	0.51211	0.1967	0.03257	3.5648
9	0.33174	2.2297	0.51670	0.5066	0.04131	2.8009
10	0.35762	1.9734	0.54961	0.1030	0.04319	2.4685
11	0.42637	1.1665	0.53057	0.1123	0.05166	1.4775
12	0.54053	0.4647	0.54961	0.0615	0.06211	0.5887
14	1.19229	0.9616	0.53379	0.4411	0.14502	1.1358
16	2.35596	1.0314	0.52666	0.7720	0.29824	1.1985

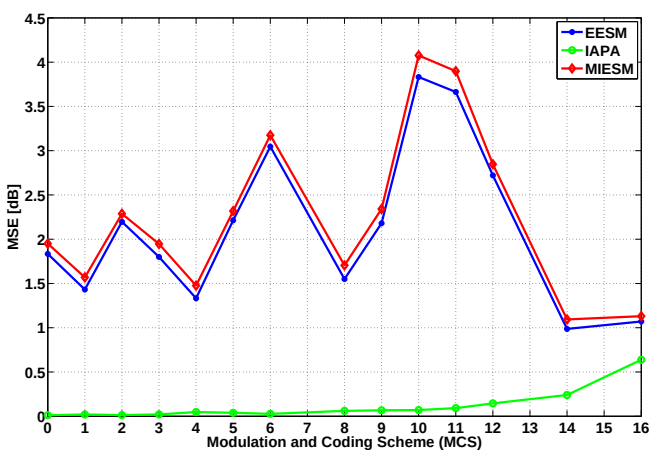

Figure 4.6: MSE for Rayleigh channel model using different PHY abstraction models for MU MIMO in LTE

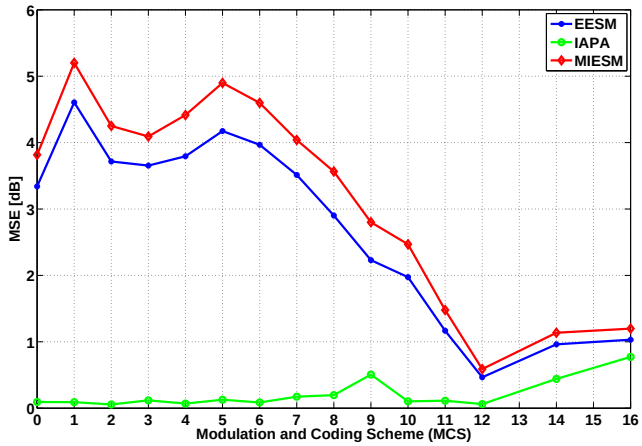

Figure 4.7: MSE for SCM-C channel model using different PHY abstraction models for MU MIMO in LTE

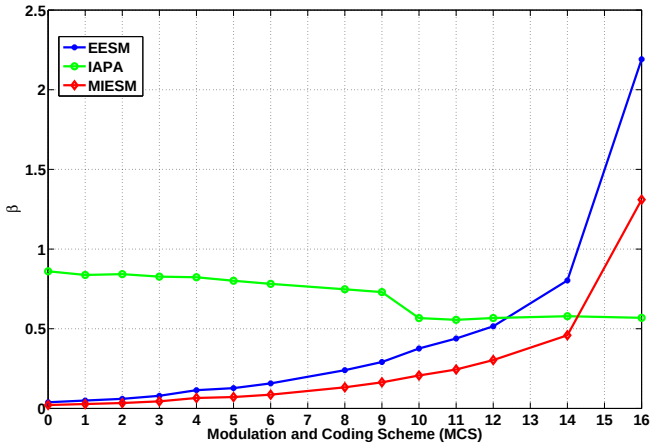

Figure 4.8: Adjustment factor for Rayleigh channel model using different PHY abstraction models for MU MIMO in LTE

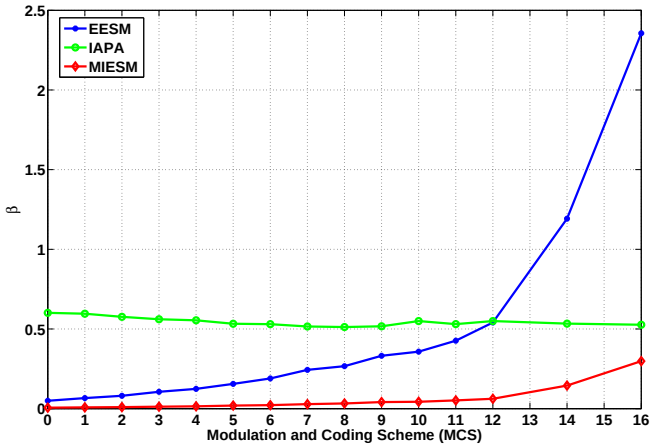

Figure 4.9: Adjustment factor for SCM-C channel model using different PHY abstraction models for MU MIMO in LTE

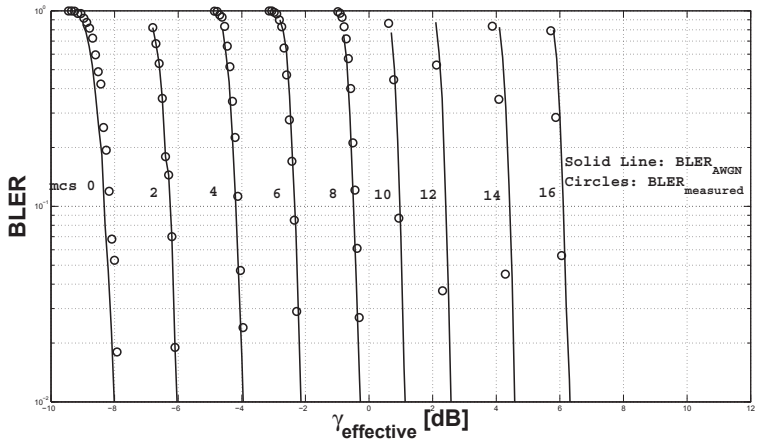

Figure 4.10: Result for Rayleigh8 channel model: IA-PHY abstraction of different MCS for MU MIMO in LTE

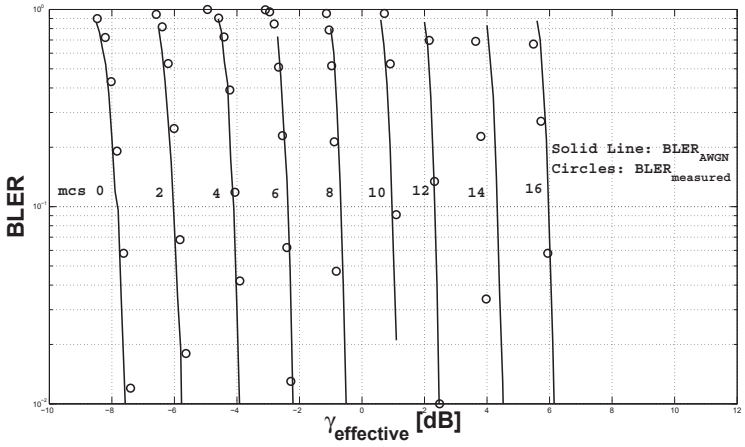

Figure 4.11: Result for SCM-C channel model: IA-PHY abstraction of different MCS for MU MIMO in LTE

4.7 Summary

In this chapter we presented a novel model for incorporating the knowledge of interference along with the desired signal strength to predict the link performance for the MU MIMO system level simulations in LTE when interference aware receivers are used. We showed with the results with the link level simulator that our proposed method is capable of predicting the link performance accurately and outperforms other techniques. We performed simulations for the LTE physical layer for a wide variety of MCS and also preformed optimization of adjustment factor for each MCS. We further showed how this model can be used for the prediction of link performance in interference limited scenarios other than MU MIMO in recent cellular systems.

Chapter 5

LTE Incremental Redundancy HARQ

5.1 Introduction

Incremental redundancy hybrid automatic repeat request (IR-HARQ) scheme [64–68] used in recent wireless communication standards such as 3GPP LTE provides higher benefits in terms of system capacity and robustness. To map these benefits into system level evaluations is of critical importance. Traditional PHY abstraction techniques are usually designed for a fixed bandwidth and do not present a generic solution for the variable bandwidth assignment to the users. Therefore, in this chapter we propose two semi-analytical methodologies for modeling IR-HARQ link performance in LTE for the system level simulators. The proposed schemes allow the arbitrary bandwidth assignments while at the same time reduce the storage requirement for the complex operations of IR-HARQ PHY abstraction.

5.1.1 Related Work

Modeling the performance of hybrid automatic repeat request (HARQ) for the PHY abstraction has gained quite an attention from the research community for its use in the system level simulators to reduce the simulation time and the computational complexity of the physical layer. However modeling the information combining from several HARQ rounds can be complex in the case of incremental redundancy (IR) HARQ where new additional redundancy bits are transmitted along with some of the previously transmitted bits in each HARQ round. In [42] the authors have presented method

of simple HARQ (i.e. no IR-HARQ) modeling in the OFDM systems using exponential effective SINR mapping (EESM) and mutual-information based effective SINR mapping (MIESM). In [69] the authors have presented a recursive method using EESM for HARQ modeling of an OFDM-based system. An interesting work was presented in [70] where the authors showed that a reduced set of reference curves can be used for modeling the link performance of HARQ in general. But their requirement of placing the mutual information of the received bits in to the virtual circular buffer (replicating the process of rate-matching) is a computational overhead for the PHY abstraction. The concept of accumulated mutual information (AMI) for the HARQ PHY abstraction is presented in [71]. In [72] the authors have used the concept of AMI from [71] for the HARQ PHY abstraction in LTE systems with a fixed bandwidth assignment.

5.1.2 Contributions

The limiting points in most of these approaches are that first of all they do not provide detailed analytical insight into the problem of modeling IR-HARQ at system level then they do not address the case of a variable bandwidth (PRBs in LTE) assignment to the users. In this respect the presented techniques are only implementable for some specific bandwidth assignment and for limited scope. Further these techniques (except [70]) require a very large number of reference curves for modeling the performance of HARQ which increases the storage requirement for PHY abstraction. However this chapter presents simple, robust and effective methodologies for modeling the performance of IR-HARQ in the case of an arbitrary bandwidth assignment and also it uses a very reduced set of reference curves. The further discussions in this chapter are in the context of LTE but the methodology can be applied to other cellular standards as well.

5.1.3 Organization

In the rest of the chapter Section 5.2 presents the system model, IR-HARQ and the objective of PHY abstraction in the framework of LTE. Section 5.3 introduces the proposed bit level PHY abstraction approach and Section 5.4 presents the symbol level approach for incorporating IR-HARQ at system level in LTE. Section 5.5 explains how the number of reference performance curves can be reduced. Section 5.6 presents the overall summary of the proposed PHY abstraction in bullet points and Section 5.7 presents the link level validation results of proposed symbol level methodology and Section 5.8 concludes the chapter.

5.2 System Model

In this chapter we consider the baseline configuration of LTE, i.e., transmission mode 1, for the case of possible HARQ retransmissions. The received signal at the UE on n-th resource element and the t-th HARQ round is given as;

$$y_{n,t} = h_{n,t}x_{n,t} + z_{n,t} \quad n = 1, 2, \cdots, N, \quad t = 1, 2, \cdots, T \tag{5.1}$$

where N is the number of resource elements in a subframe, T represents the maximum allowed HARQ rounds, $h_{n,t} \in \mathbb{C}^{1\times 1}$ symbolize the flat Rayleigh fading SISO channel of n-th resource element from the eNodeB to the UE in the t-th HARQ round. It can be modeled as independent identically distributed (i.i.d) ZMCSCG random variable with the variance of 0.5 per dimension. $z_{n,t} \in \mathcal{CN}(0, N_0)$ and $x_{n,t} \in \chi$ with variance $\sigma_u^2 = 1$ is complex symbol for the n-th resource element and t-th HARQ round. χ is the set of the QAM constellation with $|\chi| = \mathrm{M}$ points where $\mathrm{M} \in \{4, 16, 64\}$. The received SNR at n-th resource element for t-th HARQ round is given by,

$$\gamma_{n,t} = \frac{|h_{n,t}|^2.\sigma_u^2}{N_0} = \frac{|h_{n,t}|^2}{N_0} \tag{5.2}$$

IR-HARQ in LTE The received signal is demodulated and decoded at the UE. If the signal is not decoded correctly then UE sends a not-acknowledgment (NACK) signal to the eNodeB using physical uplink control channel (PUCCH). On receiving the NACK from the UE, eNodeB retransmits the packet using the next redundancy version. LTE has four different redundancy versions (RV) already introduced in Chapter 2 which are created by reading out the bits from a different starting point in the virtual circular buffer. Upon receiving the retransmission, the receiver combines the signals from both of the rounds (i.e., adds log-likelihood ratios (LLR) of the bits which are repeated in both rounds and updates the LLRs of the newly received bits) and tries to decode again. If the packet is still not decoded correctly then another NACK signal is transmitted and the eNodeB retransmits the packet using next RV. This can go on until all of the four RVs have been transmitted.

5.3 Bit Level Modeling

For incorporating the IR-HARQ into system level evaluations, the main objective of PHY abstraction is to cast a multi-state frequency selective channel on to an equivalent single-state frequency flat channel by accurately and efficiently modeling the gains achieved by employing IR-HARQ in LTE systems. The abstraction should be able to model the coding gain achieved by transmitting new parity bits in each HARQ round and the received SNR gain

because of the repeated bits. Lets assume that after T HARQ rounds the total number of received coded bits are C out of which the uniquely received bits are represented by C^u and the repeated bits are represented by C_T^r, then we are interested in finding an averaged mutual information for all of the bits, i.e.,

$$I^{\dagger} = \frac{1}{C^u}\sum_{c=1}^{C^u} I\left(\gamma_c\right) + \frac{1}{C_T^r}\sum_{c=1}^{C_T^r}\left[I\left(\sum_{t=1}^{T}\gamma_{c,t}\right)\right], \tag{5.3}$$

where γ_c is the received SNR on c-th unique bit with $c = 1, 2, \cdots, C^u$ and $\gamma_{c,t}$ is the received SNR on the c-th bit and t-th round with $t = 1, 2, \cdots, T$ and $c = 1, 2, \cdots, C_T^r$. The next step shall be to find γ_{eff} such that

$$\gamma_{\text{eff}} = I^{-1}\left(I^{\dagger}\right), \tag{5.4}$$

$$\gamma_{\text{eff}} \rightarrow \text{BLER}_{\text{A}}\left(\text{MCS}(r_{\text{eff}})\right), \tag{5.5}$$

where I in (5.3) and I^{-1} in (5.4) is the normalized BICM mutual information introduced in Chapter 3. An important point to note here is that before the γ_{eff} obtained from (5.4) is used for reading equivalent BLER, we first have to obtain the AWGN performance curve corresponding to the certain MCS and the effective code rate r_{eff} after T HARQ rounds ($\text{BLER}_{\text{A}}\left(\text{MCS}(r_{\text{eff}})\right)$). It is only after obtaining the AWGN performance curves for the effective code rate that we can map γ_{eff} on to an equivalent AWGN BLER.

But for an arbitrary code rate this requires lots of curves to be obtained before hand for each of the MCS which should be normally avoided for the robust models. In this chapter we also propose a method for mapping the arbitrary effective code rate on to a code rate which is usually referred as mother code rate which corresponds to full circular buffer before applying any rate matching in LTE. This reduces the effort of calculating too many performance curves and reduces the storage requirement for PHY abstraction.

Another important point to note is that for a very low code rate transmission in LTE, a certain bit can be repeated many times even in a single transmission and for HARQ transmissions this number can reach till 15. To account for all the tiny details it is important to calculate these numbers from the rate matching algorithm of LTE for all of the possible MCS and four HARQ rounds. And then this information is utilized in the calculation of $I^{\dagger}$ in (5.3). The complete details about this method are given in the Appendix of this chapter.

5.4 Symbol Level Modeling

Our primary goal of the HARQ modeling was to make it so simple and accurate that it can be easily implemented in system level simulators. Therefore in addition to the bit level approach we propose another approach which works at the symbol level rather than bit level and incorporates the IR-HARQ in LTE system level modeling. Symbol level modeling is a simple approach of calculating the γ_{eff} in a suboptimal way and then adjusting the effective code rate for taking into account the effects of the bit repetitions between different HARQ rounds.

This approach targets to model the IR-HARQ based on the available channel symbols and it takes a rather sub-optimal approach at the calculation of γ_{eff}. Due to the random interleaving in LTE it becomes extremely difficult to track down the channel symbols or subcarriers on which a certain bit has traveled in each of the HARQ round and then to keep track of the repeated bits is only possible with the help of turbo decoder. Since in PHY abstraction we want to avoid the complexity of turbo decoding itself therefore we shall simply stack up the channel symbols received in each of the HARQ round and calculate the γ_{eff} averaged over all rounds, i.e.,

$$\gamma_{\text{eff}} = \mathrm{I}^{-1}\left[\frac{1}{N \times T}\sum_{n=1}^{N}\sum_{t=1}^{T}\mathrm{I}\left(\gamma_{n,t}\right)\right], \tag{5.6}$$

where I is the normalized BICM mutual information given in chapter 3. This γ_{eff} is calculated in a way where the repetition for the bits is completely ignored. But we propose to accommodate for the overlapped regions or repeated bits in the calculation of effective code rate based on which an equivalent BLER has to be obtained. This is explained in the next section.

5.4.1 Effective Channel Code Rate

The effective channel code rate after certain HARQ rounds must be calculated very carefully because it should be able to reflect the effect of the repeated bits and the new bits after each HARQ round. But again to keep track of all the bits for each MCS and each HARQ round is not a trivial task. Therefore, for the sake of simplicity of the PHY abstraction we propose to calculate the effective code rate as if there was no bit repetition in the consecutive HARQ rounds and then we adjust it for the repeated bits. The total code rate with assumption of no bit repetitions after T HARQ rounds can be calculated as,

$$r_{c,T} = \frac{\prod_{t=1}^{T} r_t}{\sum_{t=1}^{T}\prod_{s=1,s\neq t}^{T} r_s}. \tag{5.7}$$

where r_t represents the channel code rate used in t-th round. For example after the third HARQ round, we can obtain $r_{c,3}$ using equation (5.7) as

$$r_{c,3} = \frac{r_1.r_2.r_3}{r_2.r_3 + r_1.r_3 + r_1.r_2} \tag{5.8}$$

It is important to note that $r_{c,T}$ does not consider the bits which are repeated in the consecutive HARQ rounds thus can not be used for the PHY abstraction. The reason is that it will over estimate the resulting BLER obtained using γ_{eff}. This problem arises due to the increased diversity of the HARQ rounds over a new channel in each HARQ round and because the ratio of total bits transmitted over the total bits received shall be different due to the partial overlapping. Therefore we need to adjust the effective channel code rate considering the number of repeated coded bits in each of the HARQ round. This can be accomplished by counting the number of new and repeated bits in each of the consecutive HARQ round for each of the MCS. This information can be obtained from the rate matching algorithm of LTE and then stored in the PHY abstraction module for the 29 different MCS and 4 HARQ rounds in each of the MCS. For a fixed number of resource block allocation to the users this approach does not pose a huge burden on the PHY abstraction module. However for the variable resource block assignments, the transport block size changes in LTE and thus this information about the repeated and new bits changes as well. Which means that adjusting the $r_{c,T}$ for an arbitrary resource block assignment requires a huge effort during the pre-processing of the PHY abstraction and also makes the abstraction more complex in practice.

To avoid this problem we propose rather a simple approach of not using the number of repeated and new bits for the correction of $r_{c,T}$ but the percentage of the overlapping region. The difference in using the percentage and the actual numbers is that in LTE the proportion of the overlapped region is independent of the size of the TBS and is always relevant to the size of the circular buffer used in the rate matching. This observation in LTE rate matching makes the portions of overlapped regions in the adjacent RVs independent of the TBS which is the function of PRB assignment in LTE. These proportions of the overlapping regions in adjacent RVs can be calculated as,

$$\xi(\text{MCS}, T) = \frac{\left(\sum_{t=1}^{T}(N_t) - N_Q\right)}{\sum_{t=1}^{T}(N_t)}, \tag{5.9}$$

where $N_t \quad t = 1, 2, \cdots, T$ are the number of bits received in each HARQ round and N_Q is the total number of received bits in the turbo decoder after T HARQ rounds. For example consider the Figure 5.1 where the case for two HARQ rounds is depicted. In Figure 5.1 N_1, N_2, N_Q represent the number of transmitted bits in the first round, in the second round and total number of

received bits in the buffer after 2 rounds respectively. Then the overlapped region after two rounds can be calulated as,

$$\xi(\mathrm{MCS}, 2) = \frac{((N_1 + N_2) - N_Q)}{(N_1 + N_2)}, \tag{5.10}$$

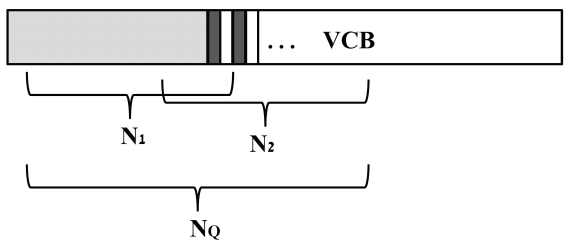

Figure 5.1: Overlapping of bits in consucetive rounds

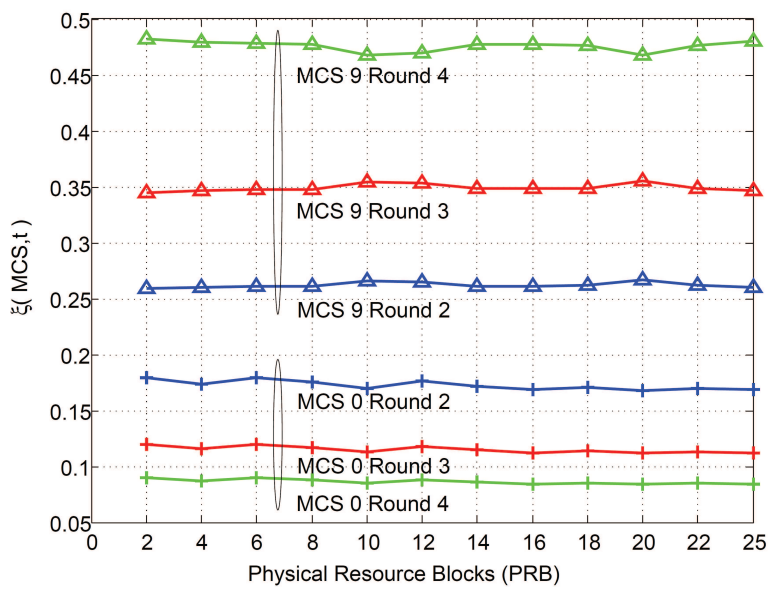

Figure 5.2: $\xi(MCS, t)$ in the second, third and fourth HARQ round for MCS 0 and 9 for different PRB Assignment - It is clear that for different bandwidth assignment the value of $\xi(MCS, t)$ does not changes significantly.

To show that $\xi(\mathrm{MCS}, T)$ is independent of PRB assignment, we calculated $\xi(\mathrm{MCS}, T)$ over a wide range of PRB assignment for MCS 0 to 27 with the help of LTE rate matching using OAI link level simulator. Table 5.1 shows the mean and variance of $\xi(MCS, T)$ for the second, third and the

fourth HARQ rounds for MCS 0 to 27 over PRB assignment from zero to twenty five with the step size of two PRBs[1]. It can be observed that the variance of $\xi(\text{MCS}, T)$ after each HARQ round is extremely small and it is always (almost) equal to its mean value. In Figure 5.2 we plot the value of $\xi(\text{MCS}, T)$ for the different PRB assignments and for two different MCS. Along the x-axis is the size of PRBs assigned to the UE and along y-axis is the $\xi(\text{MCS}, T)$ for all four HARQ rounds. It can be seen that $\xi(\text{MCS}, T)$ does not changes for different PRB assignments and remains almost constant over different PRB assignment. Since it is observed from Table 5.1 that the variance of $\xi(\text{MCS}, T)$ is negligibly small for all HARQ rounds therefore the mean value of $\xi(\text{MCS}, T)$ can be used for all PRB assignments in LTE. For incorporating the repeated bits in the calculation of the effective channel code rate $\xi(\text{MCS}, T)$ can be utilized as,

$$r_{\text{eff}} = r_{c,T} + \xi(\text{MCS}, T).r_{c,T} \tag{5.11}$$

and this r_{eff} is appropriate to be used for the PHY abstraction as it incorporates the repeated bits for each HARQ round. This was a very important step in PHY abstraction as it has to decide about the decodability of the packet therefore it needs to be adjusted accordingly after each HARQ round.

5.5 Reference Performance Curves

The second step in the PHY abstraction is to map the effective SINR value on to a pre-computed additive white Gaussian noise (AWGN) performance curves for each type of MCS. These AWGN performance curves reflect mainly the turbo codes performance which is highly dependent on the code block size (known as transport block size TBS in LTE). In LTE the TBS is a function of the bandwidth assigned to a specific user which is assigned in terms of PRBs where each PRB consists of 180 KHz of bandwidth. LTE has the operating bandwidth from 1.4 MHz to 20 MHz i.e. from 6 PRBs to 100 PRBs and there are 29 different MCS available in the LTE. A user can be assigned minimum of 1 PRB and maximum of 100 PRBs which means that for the PHY abstraction it is required to have 100x29=2900 different AWGN performance curves for all possible combinations of PRB assignments and MCS. For the IR-HARQ retransmissions this requirement is further increased to accommodate the possible 4 HARQ rounds, i.e., the number of required performance curves becomes 4x2900=11600. Please note, this number corresponds to the case when the same MCS is used for all of the IR-HARQ rounds. And this number will be even higher when a different MCS is allowed to be used for the retransmissions. Clearly this requirement is quite impractical and should

[1]We show results till 25 PRBs as 5MHz is the maximum allowed bandwidth in our LTE link level simulator.

Table 5.1: Mean and Variance of $\xi(\text{MCS}, T)$ for IR-HARQ rounds using variable bandwidth (PRBs 2-25)

MCS	Round 2		Round 3		Round 4	
	Mean	Var	Mean	Var	Mean	Var
0	0.173	0.00002	0.115	0.00001	0.086	0.00000
1	0.227	0.00019	0.151	0.00008	0.113	0.00005
2	0.275	0.00017	0.184	0.00007	0.138	0.00004
3	0.354	0.00017	0.236	0.00007	0.177	0.00004
4	0.432	0.00002	0.288	0.00001	0.216	0.00001
5	0.473	0.00004	0.351	0.00002	0.264	0.00001
6	0.374	0.00006	0.417	0.00003	0.313	0.00002
7	0.315	0.00001	0.420	0.00001	0.370	0.00002
8	0.290	0.00000	0.387	0.00000	0.420	0.00001
9	0.262	0.00001	0.349	0.00001	0.476	0.00002
10	0.476	0.00002	0.317	0.00001	0.238	0.00001
11	0.474	0.00001	0.351	0.00000	0.263	0.00000
12	0.397	0.00002	0.402	0.00001	0.301	0.00001
13	0.328	0.00000	0.438	0.00000	0.343	0.00001
14	0.307	0.00000	0.409	0.00001	0.386	0.00001
15	0.285	0.00000	0.379	0.00001	0.431	0.00001
16	0.269	0.00001	0.358	0.00001	0.462	0.00003
17	0.384	0.00005	0.411	0.00002	0.308	0.00001
18	0.349	0.00004	0.434	0.00002	0.325	0.00001
19	0.319	0.00000	0.425	0.00001	0.362	0.00001
20	0.302	0.00001	0.403	0.00001	0.396	0.00002
21	0.284	0.00001	0.379	0.00001	0.431	0.00002
22	0.268	0.00001	0.358	0.00001	0.463	0.00002
23	0.249	0.00001	0.333	0.00001	0.497	0.00001
24	0.232	0.00000	0.309	0.00001	0.463	0.00002
25	0.213	0.00001	0.285	0.00001	0.427	0.00002
26	0.195	0.00001	0.261	0.00002	0.391	0.00005
27	0.183	0.00001	0.245	0.00002	0.367	0.00005

be avoided in order to generalize the PHY abstraction for the variable PRB assignment.

In our observation of the performance curves we found that for the variable PRB assignment, the slope of the AWGN reference curve becomes different, but for the case of same PRB assignment the slope of the performance curve remains constant for all of the MCS. In other words, the reference curves are shifted versions of each other. We exploit this feature to reduce the number of required reference curves. In LTE three different modulations are used; QPSK (MCS 0-9), 16-QAM (MCS 10-16) and 64-QAM (17-29). We calculate the performance curve for each of the mentioned modulation type for the code rate 1/3 (which is referred as the mother code rate r_m). Then it is required to calculate the accurate shift for the performance curve with respect to the current MCS.

We propose to calculate the proper shift R in the reference curves with the help of effective channel code rate (r_{eff}) and the mother code rate (r_m). This facilitates the PHY abstraction process as it does not require any additional knowledge. The shift in the performance curves translates to the gain/loss in mutual information for the specific modulation scheme. Since LTE air interface is based on BICM, therefore we use already available normalized BICM mutual information for calculating the shift R in dBs as shown in Figure 5.3.

$$R[dB] = {I_M}^{-1}(r_m) - {I_M}^{-1}(r_{\text{eff}}). \tag{5.12}$$

We use the fact that for the capacity achieving channel codes with long enough code block size, the normalized mutual information and channel code rate can be used interchangeably, therefore, using r_{eff} and r_m we calculate the difference (or shift) in the performance of both code rates. Then using this difference one can be directly mapped on to another. In our approach we calculate R and apply this to shift the reference curve corresponding to the mother code rate to obtain shifted performance curve which we represent by $\text{BLER}_{\text{A,R}}$. Then this $\text{BLER}_{\text{A,R}}$ is used for the mapping of γ_{eff} on to equivalent AWGN BLER, i.e.,

$$\gamma_{\text{eff}} \rightarrow \text{BLER}_{\text{A,R}}(\text{M}), \tag{5.13}$$

where M represents the modulation of that specific MCS.

So far we have reduced the number of required reference curves from 29 to only three for a fixed bandwidth assignment and now we shall extend this for arbitrary RB assignment. The performance of turbo code for an arbitrary TBS (which is a function of assigned RBs) is measured with an SNR-BLER

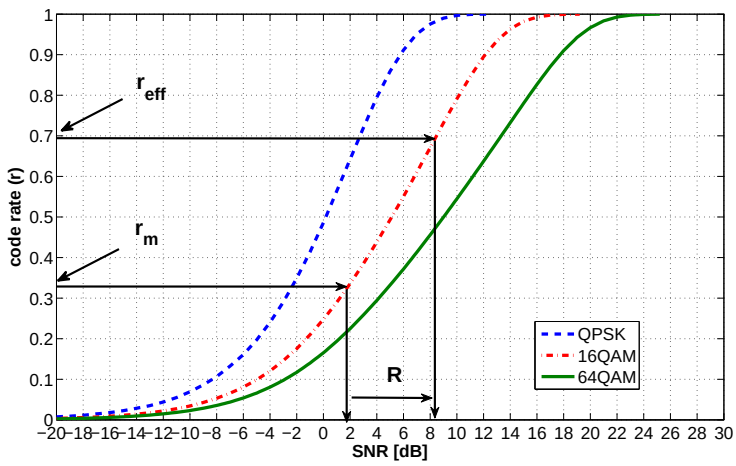

Figure 5.3: Normalized BICM Mutual Information and calculation of Shift with respect to the mother code rate

based AWGN performance curve. For an arbitrary bandwidth/RB assignment the SNR-BLER AWGN reference curve has variable slope. Ideally (for a large TBS) the BLER curve looks like waterfall but for smaller transport block sizes it is not an immediate waterfall. To account for this factor we propose to use an offset Δ (in dB) at the 10% of the BLER for each type of bandwidth assignment with respect to the maximum bandwidth assignment as shown in Figure 5.4. Unfortunately for the different possible combinations of code block size and coding rate Δ need to be calculated numerically from the link level simulator and there is no analytical expression available to calculate it. But the good point is that Δ has to be calculated only once and only for the code rate 1/3. Once it is calculated then the mother code rate for specific bandwidth assignment can be adjusted with respect to the stored (maximum bandwidth assignment) reference curve, such as,

$$r_m = r_{mm} + \Delta\left(NB_{RB}\right) \tag{5.14}$$

where r_{mm} represents the reference curve for the mother code rate corresponding to the maximum number of assigned resource blocks and $\Delta\left(NB_{RB}\right)$ represents the offset for the NB_{RB} assigned resource blocks. It is clear that by using our proposed approach the required number of AWGN performance curves is reduced from the count of 11600 (corresponding to all possible combinations of PRB assignment and MCS) to just three which is a significant improvement in state-of-the-art methodologies. This reduces the storage requirement for the PHY abstraction. Moreover our proposed method can also be used for the scenarios when the retransmission for HARQ rounds is done

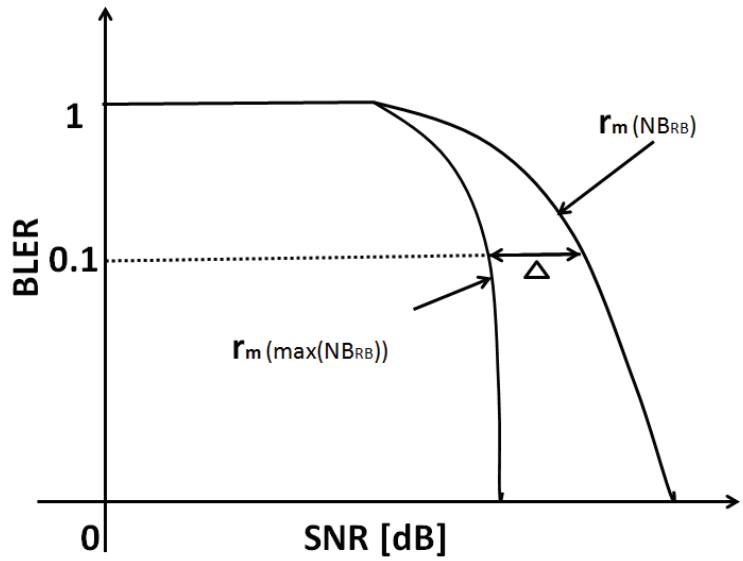

Figure 5.4: Calculation of bandwidth dependent performance offset

using a different coding rate.

5.6 Summary

For the PHY abstraction of IR-HARQ for variable bandwidth assignment it is required to have

- 3 AWGN mother code reference curves corresponding to the maximum bandwidth assignment,
- Table 5.1 which has $\xi(MCS, t)$ values for all HARQ rounds,
- A table of $\Delta\,(NB_{RB})$ for different number of PRB assignment.

Then the following steps,

- Generate the frequency selective channel for assigned bandwidth (for each HARQ round)
- Determine the received SINR across each of the resource element and across each of HARQ round
- Use (5.6) to calculate γ_{eff} using the received SINR from all HARQ rounds
- Calculate r_{eff} using (5.11)

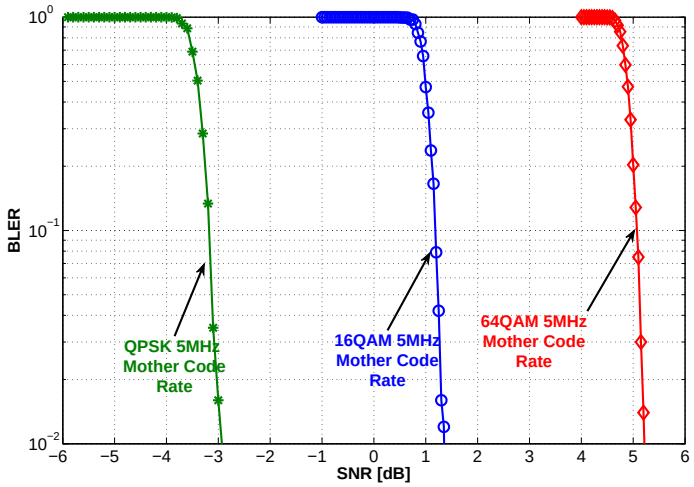

Figure 5.5: Reference AWGN curves for LTE Systems using QPSK, 16QAM and 64QAM Modulations

- if the NB_{RB} is different than $\max(NB_{RB})$ then apply $\Delta(NB_{RB})$ to r_m
- Calculate R using (5.12) and add it to r_m
- Determine BLER corresponding to γ_{eff} from modified r_m reference curve

5.7 Results

For the validation of our proposed scheme, we used Eurecom's OpenAirInterface[2] link level simulator which implements 3GPP LTE Release 8.6 physical layer [8,9,62]. We show the results for a highly frequency selective Rayleigh channel model with 8-taps and for the bandwidth assignment of 5 MHz. The simulations are performed for a very large number of different channel realizations and for a very large number of noise realizations during each of the channel realization. For HARQ we calculate the BLER based on all of the previous transmissions and for each retransmission we generate a new channel to provide the channel diversity. The reference curves corresponding to the mother code rate are shown in Figure 5.5. These curves correspond to the case when all of the 25 available PRBs are assigned to a user. Then we apply the PHY abstraction as summarized in Section 5.6.

[2]http://www.openairinterface.org/

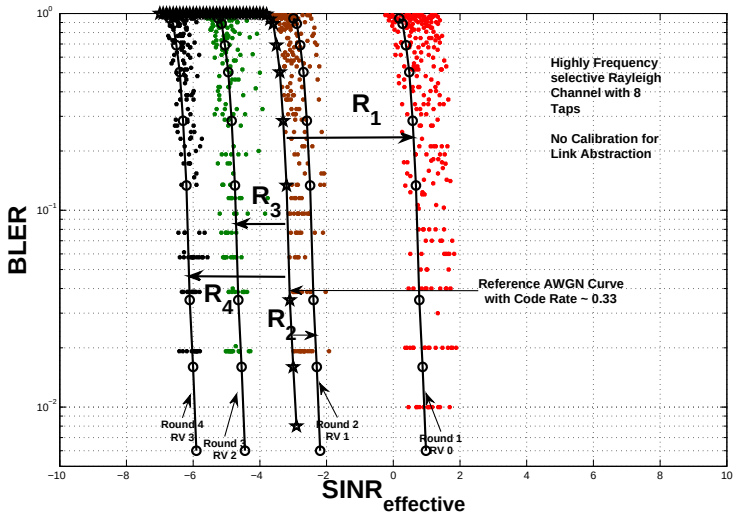

Figure 5.6: LTE MIESM IR HARQ MCS 9 (QPSK) For All Four Retransmissions

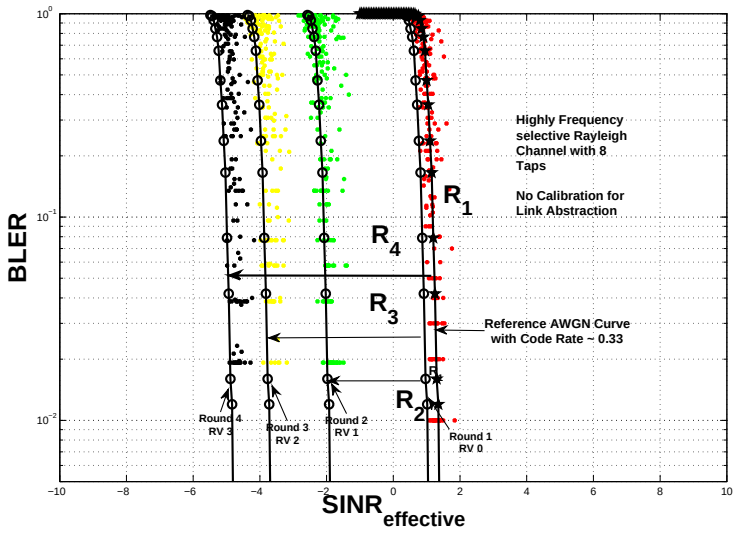

Figure 5.7: LTE MIESM IR HARQ MCS 10 (16 QAM) For All Four Retransmissions

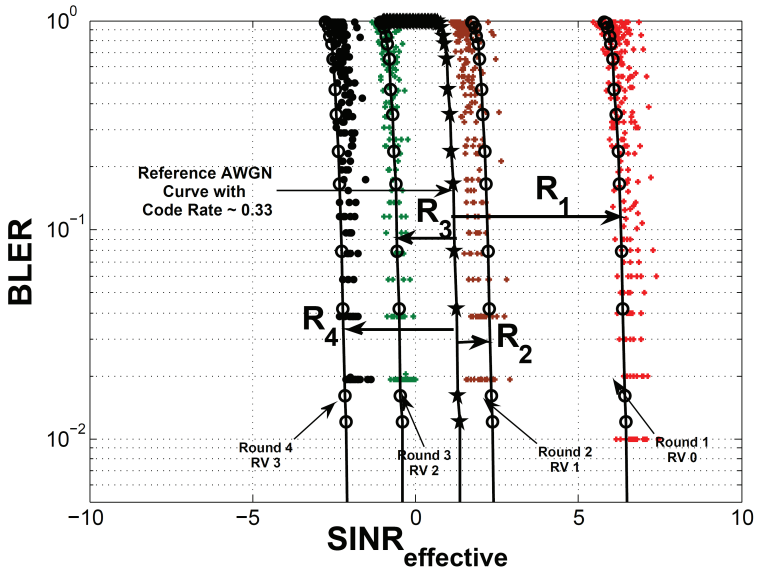

Figure 5.8: LTE MIESM IR HARQ MCS 16 (16 QAM) For All Four Transmissions

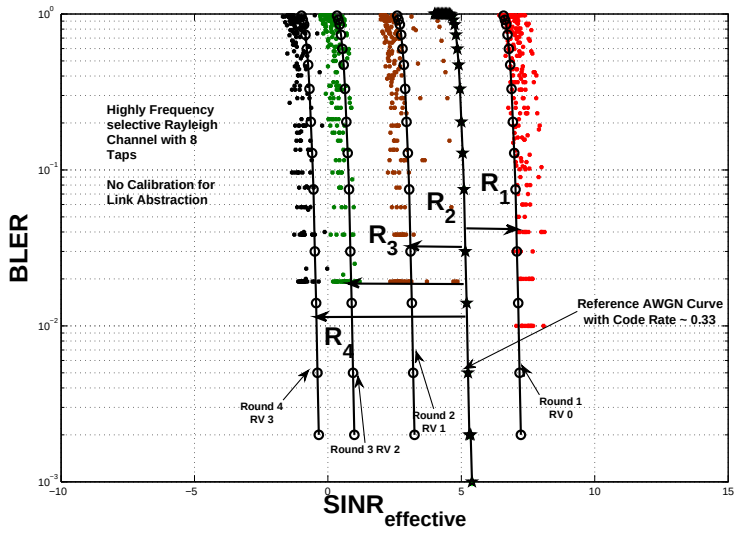

Figure 5.9: LTE MIESM IR HARQ MCS 17 (64 QAM) For All Four Retransmissions

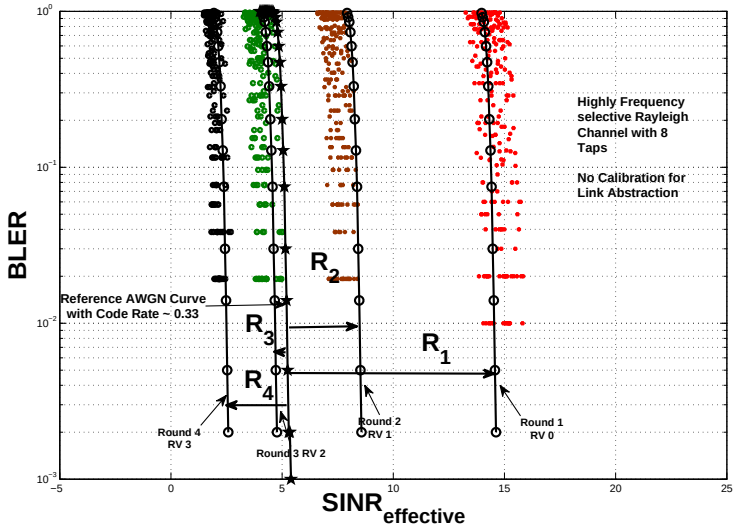

Figure 5.10: LTE MIESM IR HARQ MCS 25 (64 QAM) For All Four Retransmissions

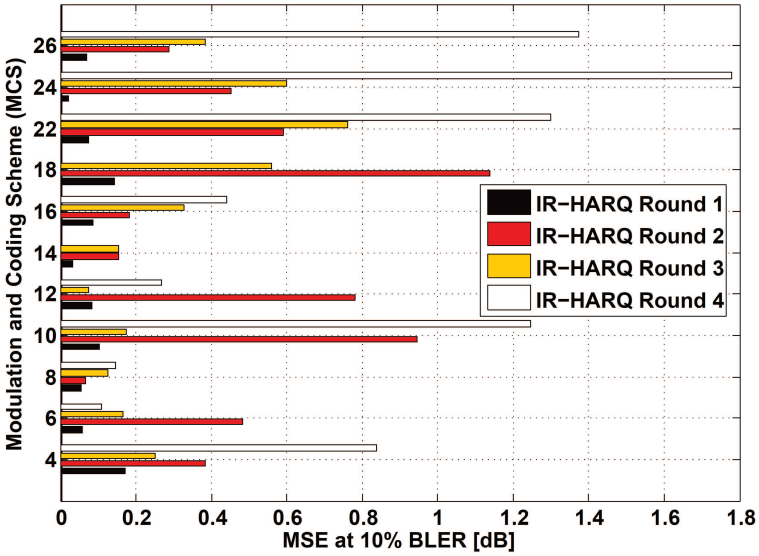

Figure 5.11: Mean Squared Error (MSE) at 10% BLER points of Rayleigh channel model with respect to the shifted AWGN curves for different MCS in LTE after 4 HARQ rounds

Figures 5.6, 5.7, 5.8, 5.9 and 5.10 show the shift of mother code rate reference curve for different HARQ rounds for MCS 9, 10, 16, 17 and 25 respectively. The solid line curve with stars corresponds to the mother code rate r_m and the solid lines with circles are the shifted performance curves for each round. The points around the solid lines are the abstracted experimental BLER points from the link simulator. We see from the results that the shifts for each round, i.e., $R_t, \quad t = 1, \ldots 4$ are very well calculated. Further in Figure 5.11 we show the mean squared error (MSE) at 10% BLER points of Rayleigh channel model with respect to the shifted AWGN curves for a wide variety of MCS. It can be seen that the MSE is generally very small but it is slightly higher for the last round in some of the cases. However if we wish to reduce the MSE further then it is only possible by performing the optimization on the calibration factors of (5.6).

5.8 Conclusion

We have presented two novel IR-HARQ PHY abstraction methodologies for the variable bandwidth assignment in LTE where the former is simple, robust and requires low storage and the latter takes more systematic approach towards obtaining more accuracy but is also little bit complex. We showed that if our proposed approaches are used then some of the important factors required for the PHY abstraction become independent of the bandwidth assignment. Also we showed how the required number of reference curves for the PHY abstraction can be significantly reduced from 11600 to 3 with a very small extra apriori effort. In other words our proposed models are very robust, accurate and practical. Further we showed with results that both of the proposed methods are very well designed to model the performance of IR-HARQ in LTE and provide very accurate shifts for the performance curves.

5.A Bit Level Approach

The detailed technique has been published in [73] and is attached here for the access of reader.

Part II

Applications

Chapter 6

System Level Simulations

6.1 Introduction

In wireless communications the evaluation of large scale systems with the help of system simulators is of utmost importance. However, these simulations have a high computational complexity and very long evaluation run time due to the physical layer algorithms and the channel model used. Many system level simulators therefore rely on PHY abstraction techniques that predict the performance of the PHY layer based on the current channel state. It was found with the help of profiling in OAI system level simulator that even for a simple system with just one eNodeB and one UE more than 82% of the total simulation time and resources were spent only on the PHY layer. This is a huge overhead in terms of complexity and time duration of large system level evaluations. And for the evaluations of system performance in even a medium scale simulations, i.e., with fewer eNodeBs and fewer UEs, it can take months if simulated with full PHY processing. Therefore, to reduce the complexity and duration of system level evaluations it is required to have a PHY abstraction model.

The use of PHY abstraction in system evaluations should provide four main benefits, 1) low complexity and speed by replacing the complete physical layer processing with a rather simple calculations using table look ups, 2) scalability in system evaluations by making it possible to evaluate huge systems with hundreds of nodes, 3) applicability in diverse use cases and finally 4) the most important is realism of providing the true link quality metric as it would have obtained with full PHY processing. So in this form PHY abstraction is an extremely valuable low complexity tool for the large scale

system evaluations as it provides the system simulator with the necessary link quality indicator without actually having to code and decode the packets. Moreover it can also be used for fast resource scheduling and fast link adaptation.

6.1.1 Related Work

In the open source domain there are some simulators which can be used for the LTE system level evaluations by employing PHY abstraction. We shall like to mention Vienna system level simulator [74] which is implemented on MATLAB and can be used for LTE system level evaluations for different antenna configurations. Another interesting simulator is IMTAphy [75] from Technical University of Munich which is implemented in C++ and also supports multiple antenna transmission with MMSE and ZF receivers. Then there is LTE-SIM [76] from Technical University of Bari which is also based on C++ and finally the Network Simulator (NS) 3 [77] which can be used for LTE system level simulations.

6.1.2 Contributions

The limiting point in most of the open-source LTE system simulators is that their implementation of PHY abstraction is not specialized for MISO/MIMO channels and they do not provide a framework where the performance of system with and without PHY abstraction can be validated with more than one UE. Whereas this chapter presents a method of implementing the PHY abstraction schemes, presented in previous chapters, for different antenna configurations in system level simulators and shows that the expected benefits of low complexity, scalability, applicability and realism from PHY abstraction are achievable. We shall be studying the implementation process by taking Eurecom's OpenAirInterface as a case study and show that it can be used for scalable system level evaluations of LTE with low complexity and greater flexibility. We have implemented both EESM and MIESM PHY abstraction methods in the OAI system level simulator and both of them provide similar results as we have used the adjustment factors which were calibrated in chapter 3. Eurecom's OAI system level simulator is the only open-source simulator which has highly optimized link layer implementation as well so that it can be used in real time demonstrations. In the end we provide results of system simulations with and without PHY abstraction for same scenarios and show that PHY abstraction is a useful tool for system level simulations.

6.2 PHY Abstraction in OpenAirInterface

In OpenAirInterface the required parameters for large scale system simulations are highly dynamic and can be generated either by the specialized tools which are already included in the simulator, i.e., openair traffic generator, openair mobility generator etc., or these parameters can be specified explicitly in great details for the specific scenarios and evaluations in a scenario file which can be given as an input to the simulator. The use of PHY abstraction in OpenAirInterface system simulator is explained in Figure 6.1.

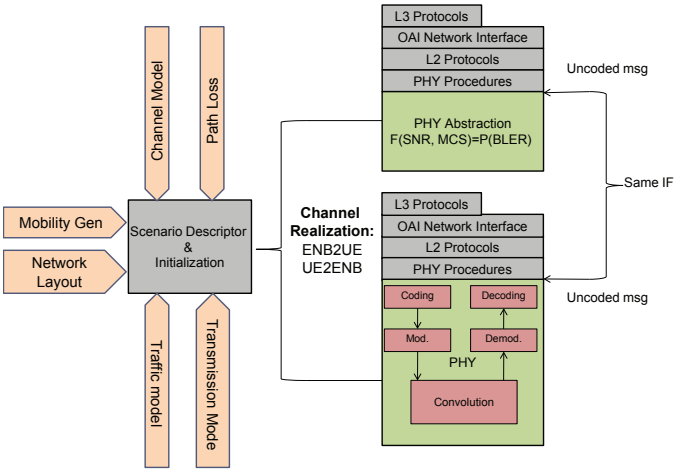

Figure 6.1: PHY Abstraction in System Performance Evaluation in OpenAirInterface

It can be seen from the Figure 6.1 that there are two important steps in any evaluation using OpenAirInterface, parameterization and processing.

6.2.1 Parametrization

As the name suggests parametrization is used to define the parameters for running the simulation for example, the number of UEs and eNodeBs, transmission mode, channel model, mobility, traffic generation, pathloss, seed for random number generation etc. Please note that parameterization is independent of the knowledge about the PHY abstraction. So based on the requirement a scenario file can be generated with all the parameters defined in it. After a scenario file is generated based on the parametrization then the decision of running the simulation either with full PHY or PHY abstraction can be taken by the simulator.

6.2.2 Processing

After the scenario file is created the simulator starts the main processing and during the initialization of OAI environment it generates channel realizations based on the defined scenarios. Then with these channel realizations the rest of the processing continues. It can be seen that in the case of PHY abstraction there is no coding, decoding or other complex operations involved from the transceiver chain at the physical layer (L1) only. The main output of the physical layer is the information on the success or failure of the decoding of the codewords to the higher layers. In full PHY this information is obtained only after performing all the receiver's blocks whereas in the case of PHY abstraction this is achieved by predicting a link quality indicator in terms of block error probability from the instantaneous channel realizations across all of the subcarriers. To complete the decoding in PHY abstraction mode a random number between 0 and 1 is generated to be compared with the obtained link quality indicator for taking the decision on the successful or unsuccessful decoding. Finally the outcome of this probabilistic experiment is passed to the higher layers which perform their tasks independent of the knowledge that whether the decision came from full PHY or PHY abstraction.

6.2.3 Implementation on System Simulator

The purpose of OAI in wireless research is many fold. It can not only just be used for the simulations but emulations and real time demonstrations as well with an implementation of full LTE protocol stack. OAI system simulator has integrated link level simulator which should be bypassed in the case of simulations with PHY abstraction. Therefore, it is important to first identify the blocks which have to be excluded from the simulation chain in the case of PHY abstraction but still be able to obtain the necessary output of the block so that the higher layers are unaware of the fact that the simulation is running with full PHY or with PHY abstraction.

6.3 System level validation for Single User SISO and MISO channels

Link level results presented in previous chapters showed that our approach for the ESM PHY abstraction is very much accurate and any of the two methods can be used in system level simulators. However we have implemented both of the ESM methods with the adjustment factors presented in the previous chapters for the OAI system level simulator. The results presented in this chapter are based on calibrated EESM approach. We wanted to show how the link abstraction can provide us with 1) low complexity and speed 2) scalability 3) applicability and most importantly 4) accuracy. To show all

these we performed system level simulations for different transmission modes both with full PHY and PHY abstraction with the same scenario file.

6.3.1 System Model

The underlying scenario consists of a single cell scenario with one eNodeB and 4 UEs. The UEs are placed around eNodeB in a random manner as shown in the Figure 6.2. The UEs are at different distances from the eNodeB and there is no mobility for the UEs. The information on the channel model can be configured in the scenario files and in general we assume that small scale fading between each UE and eNodeB is based on tapped delay line Rayleigh channel model with 8 taps and the large scale fading is log normal. There is traffic only on the downlink and it is generated with the OAI traffic generator with full buffer assumption. LTE DLSCH transmission mode can be configured in the scenario file and it can be chosen as 1, 2, 5 or 6. The eNodeB transmits with total power of 43dBm and the pathloss exponent is selected as 3.67. The other important factors for the system level simulations are,

- Abstraction is only implemented for the downlink shared channel and there is no abstraction for uplink and Control channels.
- Scheduler gives most of the resources to the user with better CQI.
- Full Buffer traffic is produced and the eNodeB performs link adaptation based on the CQI and can select between mcs 0-22 for the downlink communication.

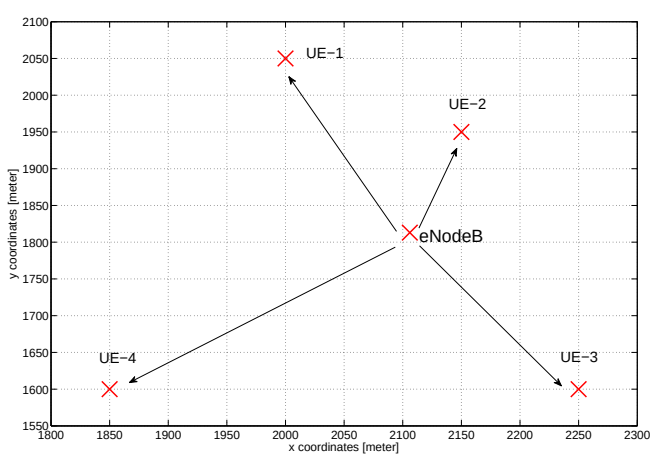

Figure 6.2: System model with 4 randomly placed UEs

Our main motivation was to show that the PHY abstraction can provide all the mentioned benefits in system level simulations and we did not want the implementation conflicts of protocol stack to temper the results for our simulations so in the beginning we restrict the eNodeB to schedule just one UE from the four available UEs. Then we ran the simulations for each transmission mode using PHY abstraction and full PHY for the same scenario file. We performed the system level simulations for 1000 LTE frames and for each simulation we calculated both the accumulated averaged throughput of system over given number of frames and the execution time for each simulation.

6.3.2 Speed

To show that using PHY abstraction is less complex and speeds up the evaluation process, we stored the execution time for system simulations with and without PHY abstraction. We stored these times under Linux operating systems when there was no other application running but the simulation only. We found out that simulations with PHY abstraction took extremely shorter time than those with full PHY processing. The results are shown in Figure 6.3 for transmission mode 1, 2 and 6 for both cases; with PHY abstraction and with Full PHY. The transmission modes are marked along x-axis and the simulation times are represented along y-axis. The blue bar represents the total simulation time whereas the interesting part is the green bar (in the middle) which represents the actual time spent for the simulation.

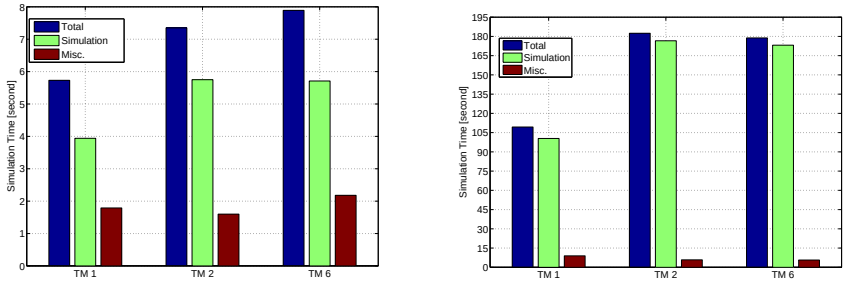

(a) Simulation Time with PHY Abstraction

(b) Simulation Time with Full PHY

Figure 6.3: Comparison of simulation times for the transmission mode 1, 2 and 6 using PHY abstraction and full PHY

The calculated speedup factors for the PHY abstraction are presented in Table 6.1 for all of the transmission modes. It is important to mention here that the scheme which we present here is actually fast enough to be used for system evaluations in real time systems. We simulated 1000 LTE frames

which is exactly 10s in time domain but if we see the time it took for the transmission mode 1 with full PHY then the real time testing of protocol stack is not possible even with a highly optimized PHY implementation in OAI simulator. On the other hand the simulation time for PHY abstraction in transmission mode 1 is around 3.9 seconds, which is feasible for the real time system evaluations. An important point is that even in PHY abstraction case, still most of the time is spent on the initialization of the simulation variables and on the generation of channel realization for each frame. This is the reason that for the case of transmission mode 2 and 6 the increase in the simulation time is observed in PHY abstraction. This is because, for multi-antenna transmission, the system has to generate the channel realizations for each transmit and receive antenna pairs which is more time consuming. However, the time for all transmission modes is, in any case, less than 10 seconds which means that the presented PHY abstraction models are good enough to be used in real time system evaluations.

Table 6.1: Simulation times for different transmission modes and speed up factors

	Time in seconds		Speed Up
TM	Full PHY	PHY Abstraction	Factor
1	101	3.9	26
2	177	5.75	31
6	174	5.71	31

The speed up factors in the case of OAI simulator are quite significant but still not as high as the ones reported recently in [78]. The main reason is that the PHY implementation in simulator used in [78] is not optimized and further their simulator is coded in MATLAB which is good for prototyping but not good for real time demonstrations. Whereas the PHY implementation in OAI simulator is extremely optimized, coded in C language and it utilizes many low-level processor instructions especially for the turbo decoder implementation. But still the impact of the speed up by PHY abstraction is significant as the time reduction is huge. The results show that if a simulation running with full PHY shall take around 30 days to finish then PHY abstraction can finish that simulation in just one day. This is a significant speed up of simulation.

6.3.3 Realims and Accuracy

The next important thing to demonstrate is the realism of abstraction in system level simulations. By realism we mean that the simulations with PHY abstraction should produce the results similar to the simulations with full PHY when the random number generators are initialized using the same

seed and same parameterization is used. This is shown by plotting the accumulated average throughput of the system over a given number of frames in Figure 6.4 for transmission mode 1, 2 and 6 respectively. It is very clear that performance of both full PHY and PHY abstraction is very much close to each other and provide the same system throughput. This is an amazing result as not only the presented PHY abstraction schemes are able to provide a significant speed in simulations but also they provide the same system performance which would have been obtained using the full PHY processing.

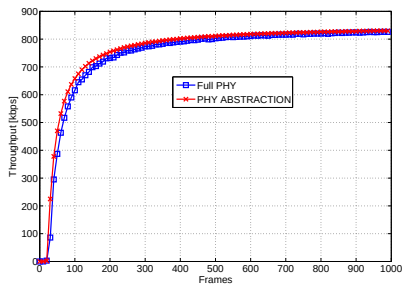

(a) Transmission Mode 1 with highly Frequency Selective Channel

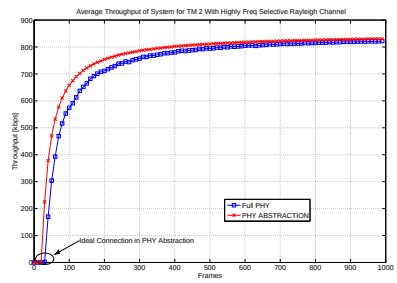

(b) Transmission Mode 2 with highly Frequency Selective Channel

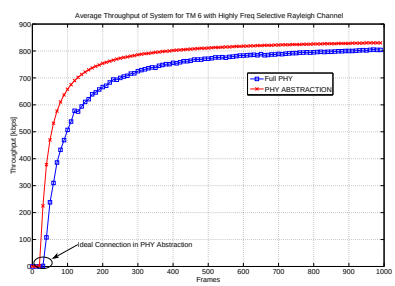

(c) Transmission Mode 6 with highly Frequency Selective Channel

Figure 6.4: Comparison of accumulated average system throughput over given number of frames for full PHY and PHY abstraction with transmission mode 1, 2 and 6

6.3.4 Applicability

To show that the proposed schemes have wide applicability we decided to perform new simulations by scheduling 2 UEs and by running simulations with different kind of available channel models in OAI. Although we calibrated the adjustment factors in chapter 3 with Rayleigh channel model but to show that the same adjustment factors are applicable to wide range of

channel models we performed the simulations with different channel models. The results from these simulations of TM 1 with 8-tap Ricean channel, TM 2 with 8-tap Rayleigh channel and TM 6 with single tap Ricean channel are shown in Figure 6.5. It is clear that the calibrated factors for Rayleigh channel are also applicable to the other channel models, giving rise to its applicability. The main reason for the applicability is that in Chapter 3 the calibration was performed over a very large number of channel and noise realization so that the adjustment factors can capture maximum variations of the channels.

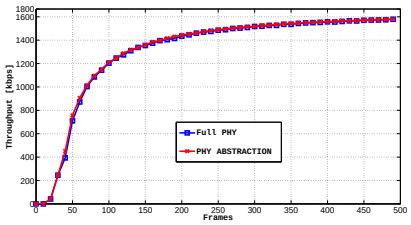

(a) Transmission Mode 1 with tapped-delay line Ricean Channel of 8-taps

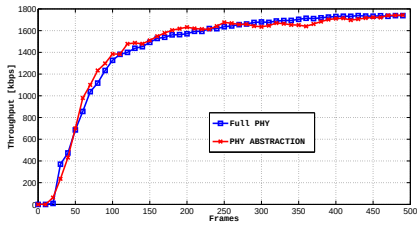

(b) Transmission Mode 2 with tapped-delay line Rayleigh Channel of 8-taps

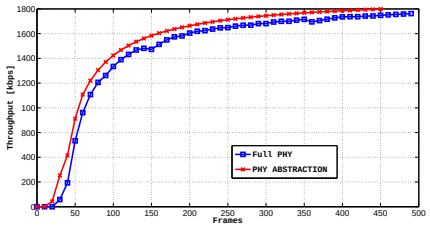

(c) Transmission Mode 6 with single tapped-delay line Ricean Channel

Figure 6.5: For 2 UEs, Comparison of accumulated average system throughput over given number of frames for full PHY and PHY abstraction with transmission mode 1, 2 and 6

6.3.5 Scalability

In the end we shall like to discuss that although we performed these simulations with small number of users but still it shows the significant advantages of using PHY abstraction over full PHY. To show that the scalability of the simulations can be enhanced greatly, we finally performed simulations by scheduling all 4 UEs in the system for transmission mode 1. We present the result in Figure 6.6 where it can be seen that the throughput of the system is scaling quite linearly as with the number of UEs in the abstraction. This can be observed that the throughput obtained in this case is almost double

than the throughput which was obtained with the 2 UEs. As expected this simulation also took a small fraction of time and resources to generate these results. In this respect it can be concluded that PHY abstraction is an extremely valuable tool for large scale system evaluations. Further, it can be easily inferred that in the case of more UEs in the system, the gains achieved from PHY abstraction will be even significant while maintaining the realism of evaluations.

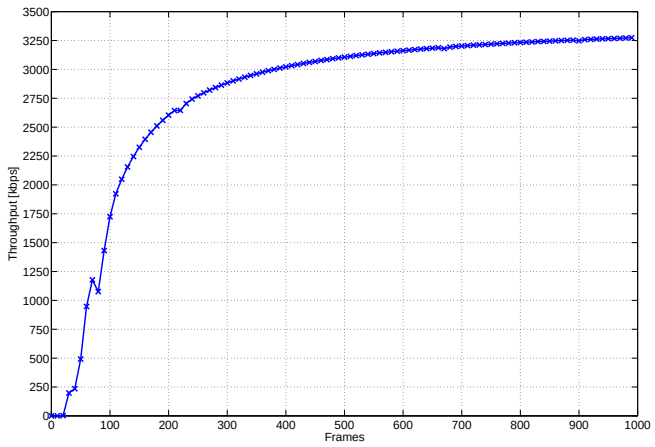

Figure 6.6: For 4 UEs, accumulated average system throughput over given number of frames with PHY abstraction for transmission mode 1

6.4 System level validation for Multi-User MIMO

The case for MU MIMO is special as in this scenario more than one users are assigned for the same time and frequency resources therefore we shall present its results separately. After validating our proposed scheme on the link level simulator we implemented it in the OAI system level simulator. We performed the simulations for MU MIMO with two users which have orthogonal spatial signature with respect to each other from the system model presented in previous section. The channel between eNodeB and each UE is a Ricean channel, i.e. there exist a direct line of sight between each UE and eNodeB which is not a problem for MU MIMO but an advantage indeed.

In case of more users in the system, the scheduler on the eNodeB selects those two UEs to be served in the MU MIMO mode who have requested orthogonal precoders, otherwise it schedules only one UE and performs transmit beamforming towards the scheduled UE [79]. We performed the test for 400 frames and calculated both the throughput and execution time for the simu-

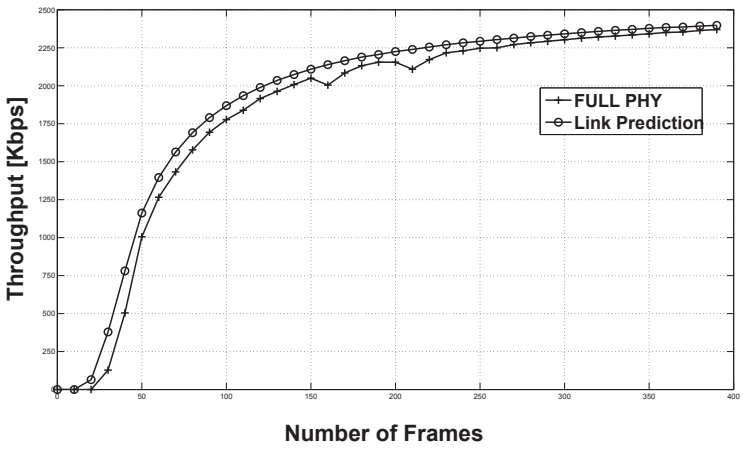

Figure 6.7: Average System Throughput for the Given MU MIMO Scenarion in LTE

lation. The results for instantaneous throughput on both UEs are shown in Figure 6.8 and 6.9 whereas an accumulated average system throughput over the given number of frames is shown in Figure 6.7. It is very clear from the figures that our link prediction model is very much accurate and matches the full physical layer implementation very closely. The minor differences in the throughput results are due to the fact that in the full physical layer implementation, HARQ is performed for the packets which are not received correctly during the first round. Whereas the link prediction model does not take this into account and it always treats the retransmission as a new transmission. The speedup factor for the case of MU MIMO was found to be 27 times and it is quite clear that using PHY abstraction we can accurately and efficiently perform system level simulations.

6.5 Conclusion

In this chapter we have presented a complete methodology of implementing PHY abstraction in a system level simulator and showed that the PHY abstraction is an extremely valuable tool for large scale system simulations. We further showed that using PHY abstraction can provide a huge amount of speed in the simulation and thus can be used for an efficient real time performance evaluations without the loss of real transceiver performance.

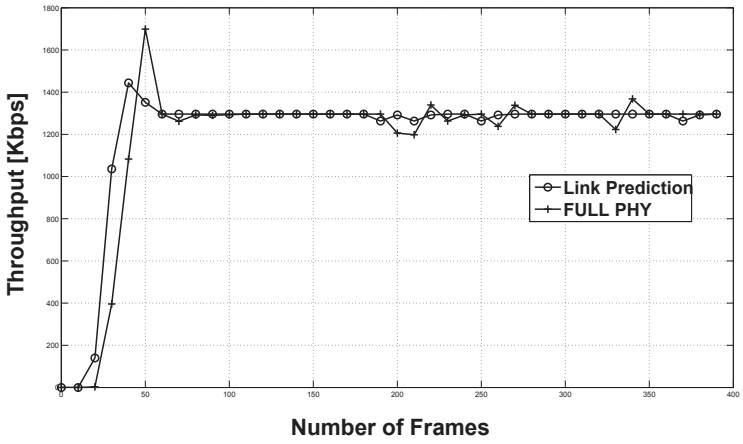

Figure 6.8: Instantaneous Throughput for the first UE in the Given MU MIMO Scenario in LTE

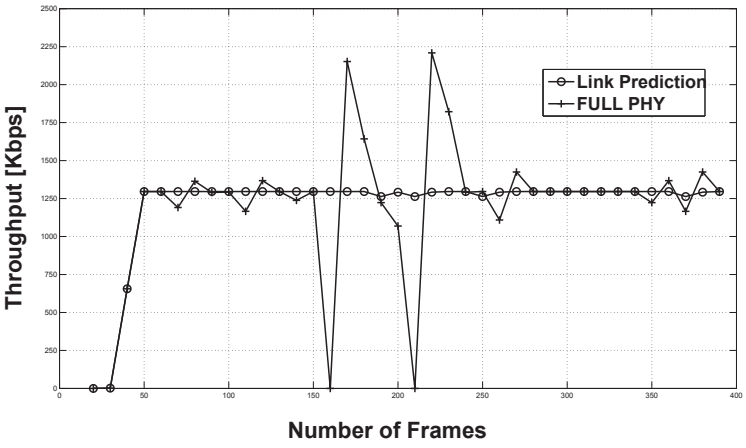

Figure 6.9: Instantaneous Throughput for the second UE in the Given MU MIMO Scenario in LTE

Chapter 7

Comparison of LTE TMs using Channel Measurements at 800 MHz

7.1 Introduction

This chapter presents another applicable scenario in which the concept of PHY abstraction can provide an insight to the problem at hand. The main focus in this chapter is to show that how the PHY abstraction can be used to compare the different transmission modes in rural areas at 800MHz. To compare the performance we used the channel measurements which were stored during a measurement campaign in the south of France for three different sites. Using these real life MIMO channels we not only calculated the performance metrics of the transmission modes for which the measurement campaign was performed but also extrapolated the results to the transmission modes which were not validated during the measurement campaign. The measurement campaign was conducted with Eurecom's OAI testbed which implemented LTE PHY based on [8, 9, 62].

This testbed was based on LTE release 8 PHY layer and implemented transmission modes 1 (single antenna - SISO), 2 (transmit diversity), and 6 (single-user MIMO - closed loop rank-1 precoding) in real time. In addition to the throughput recorded from the real modem, the raw channel estimates were stored and used for extrapolating the performance to transmission mode 5 (multi-user MIMO). This extrapolation was done by means of a mutual-information based PHY abstraction model that abstracts the performance of

MU MIMO for an interference aware receiver proposed by Ghaffar et al and then the results are compared with the performance of abstraction to transmission mode 2 and 6. The superior performance of MU MIMO mode (with interference aware receiver) over other transmission modes is illustrated and it is shown that if the channel admits then even for lower spectral efficiency, MU MIMO is the preferred option.

7.1.1 Contributions

This chapter presents the OAI testbed, LTE channel measurements along with the corresponding results in 800 MHz band and then the complete methodology for comparing the results for different transmission modes in LTE. The main goal of the measurement campaign was to estimate the best throughput achievable by an LTE release 8 nomadic terminal in a rural 5 MHz LTE deployment at 850 MHZ. However, another interest was to compare the effectiveness of different LTE transmission modes in rural deployments. This provides the fundamental guidelines for LTE deployment in the rural areas. The OAI testbed had a 3 sector, dual RF high-power eNodeB (LTE acronym for the base station) and one user equipment (UE) operating at a center frequency of 859.5MHz. In addition to the throughput measurements, raw channel estimates were stored for further post processing. These measurements were taken in the TARN department in south-west France in collaboration with the French space agency (CNES).

7.1.2 Organization

Rest of the chapter is organized as follows: in section 7.2 we present OpenAirInterface testbed with its hardware, software components and some important parameters of LTE release 8. In section 7.3 we present the measurements description. Then the methodology of using PHY abstraction for different TMs is presented in section 7.4 and comparison of different LTE TMs along with results is presented in 7.5. In the end section 7.6 presents the conclusions.

7.2 The OpenAirInterface testbed

7.2.1 Hardware

The testbed equipment was based on the CardBus MIMO I (CBMIMO1)[1] platform developed by EURECOM, complemented with additional RF equipment to operate in the desired frequency band.

[1]currently this card is not being used but new versions of it with enhanced MIMO capabilities are being used.

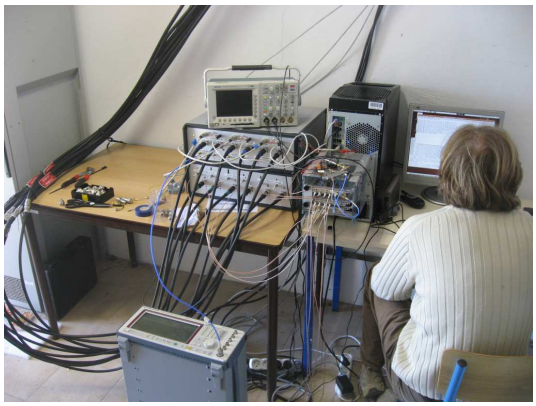

Figure 7.1: Base Station Control Room

CardbusMIMO1

CBMIMO1 was a real-time two-way software-defined radio platform for dual-antenna 5MHz channels which was connected to a standard PC (Desktop or Laptop) host through a PCI bus. Both TX and RX chains were handled on the same card. CBMIMO1 was capable of generating and receiving arbitrary 5 MHz RF signals at 1.9 GHz, which in this context should be seen as an intermediate frequency.

Base Station

The 3-sector eNodeB testbed equipment was built up of a host PC with three CBMIMO1 cards, the RF conversion subsystem, the power amplifiers (PA) and the low noise amplifiers (LNA) subsystem. The CBMIMO1 were temporally synchronized via a logical interconnection. The RF conversion subsystem converted the intermediate frequency of 1.9 GHz to the carrier frequency of 859.6 MHz. For conducting the campaign this equipment was installed in the control room beneath the mast (see Figure 7.1) whereas PAs and LNAs were contained in hermetically sealed enclosures and were co-located with the antenna on the mast (see Figure 7.2). The RF subsystems were connected with the PA/LNA subsystem through 30m long cables. The total transmission power of eNodeB was 43 dBm per sector and the eNodeB antennas were typical tri-sector antennas with dual (cross) polarized ports per sector from Kathrein Scala (ref 840 21000).

User Equipment

The UE testbed equipment was also based on the CBMIMO1 cards, complemented with an additional RF equipment to operate in the desired frequency band. For the UE, the CBMIMO1 card was configured for single-antenna transmission and dual-antenna reception, in line with the first roll-out of

Figure 7.2: Antennas with PAs on mast

Figure 7.3: UE with its antenna and GPS receiver

commercial LTE equipment. The transmission power was 23 dBm. The UE antennas were the 800 MHz TETRA (from Panorama Antennas) vehicular antenna fixed to the vehicle's body. Two such antennas were used for reception and one for the transmission. Another antenna for a nomadic scenario (Laptop outdoors) was the Panorama dual-band antenna.

7.2.2 Implemented LTE subset

At the time of the measurement campaign OAI testbed implemented a subset of the 3GPP LTE release 8.6 with extended cyclic prefix and fewer control channels.

Characteristics The main characteristics of testbed were,

- Total bandwidth of 5 MHz Bandwidth with 25 Resource Blocks
- TDD UL/DL Frame Configuration 3

- Special subframe configuration 0 (longest guard interval)
- Extended cyclic prefix
- OFDMA Downlink
- OFDMA or SC-FDMA Uplink
- 2 TX antenna ports at eNodeB, 1 at UE
- TM 1, 2, 6
- Aperiodic wideband feedback
- Link adaptation
- HARQ

DL Physical Channels The testbed implemented following downlink physical channels,

- Primary Synchronization Signal (PSS)
- Reference Signals (RS) (Pilots)
- Physical Broadcast Channel (PBCH)
- Physical Control Format Indicator (PCFICH)
- Physical Downlink Control Channel (PDCCH)
- Physical Downlink Shared Channel (PDSCH)

UL Physical Channels And the following uplink physical channels were implemented,

- Physical Random Access Channel (PRACH)
- Dedicated Reference Symbols (DRS)
- Sounding Reference Symbols (SRS)
- Physical Uplink Shared Channel (PUSCH)

Current OAI implementation is almost completely LTE compliant and whole LTE protocol stack is implemented. Also from the hardware point of view there has been two more new cards designed which have the capability to perform 4x4 MIMO as well. These are called ExpressMIMO1 and ExpressMIMO2.

7.2.3 Achievable PHY (coded) Throughput

In the LTE specification of 5MHz there are 25 Physical Resource Blocks (PRB). In the extended cyclic prefix configuration each PRB consists of 144 resource elements (RE), giving a total of 3600 REs for 25 PRBs. On the downlink, out of the 144 REs of one PRB 32 are used for control signals (PDCCH) and another 16 are used as cell specific reference signals (in the two transmit antenna configuration) so the effective REs for data transmission in one PRB are 144-32-16 = 96. Since there are 25 PRBs so the total number of available downlink REs for DLSCH in one subframe become 25 * 96 = 2400. This results in a maximum downlink throughput of 2.88 Mbps using QPSK, 5.76 Mbps using 16Qam and 8.64 Mbps using 64Qam. Similarly each uplink subframe has 3600 RE, out of which 600 are used for pilots and 300 for the SRS, leaving 2700 REs for the ULSCH. This results in maximum uplink throughput of 1.62 Mbps using QPSK, 3.24 Mbps using 16Qam and 4.86 Mbps using 64Qam.

7.3 Measurements description

The complete details of the measurement campaign are not relevant for this thesis work but we shall try to provide the basic and necessary information which is required to understand the purpose of this work. For the measurement campaign, three cell-site locations were chosen in the TARN department in south-west France: *Cordes-sur-Ciel, Penne,* and *Ambialet*. The measurements covered the entire road network for each of the sites using a vehicle equipped with the test UE. The real-time throughput of the test UE was measured with the OAI modem. Further the MIMO channel estimates with a complete LTE frame information were stored at the UE and the eNodeB for the realistic offline processing in order to infer the achievable results with higher performance MODEMs.

We conducted measurements for both uplink and downlink transmission between the eNodeB and the UE. But our focus in this chapter shall be on the downlink transmission. Further the measurement campaign did last for months and large amount of the raw channel estimates were stored from this campaign. For this chapter we decided to choose a very small subset of the measurements from the database of channel measurements in such a way that it allowed us to compare the performance of even MU MIMO along with other transmission modes. We took channel estimates from the stored measurements for two different traces and treated them as the channels belonging to two independent and different UEs. These UEs were assumed to be simultaneously present in the same cell area and could be served either using same time/frequency resources in the case of MU MIMO or in multiple access manner for other transmission strategies. The two different traces are

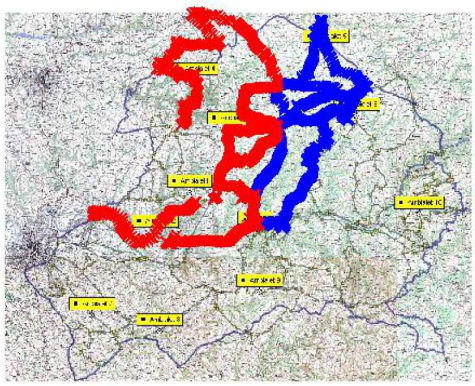

Figure 7.4: Traces used for the multi-user MIMO comparison

shown in figure 7.4 as blue and red points on the map. Important point to mention is that we used only those channel measurements for the DL where the synchronization with the eNB could be established.

7.4 BICM Throughput Calculation using PHY Abstraction

The calculation of the BICM throughput using PHY abstraction uses a modified version of the MIESM methodology presented in [14] and [19]. This is a two step methodology as shown in Figure 7.5 which consists of the modulation model and coding model. Modulation model provides us with the ideal throughput from the real channel estimates based on the BICM constrained capacity calculation whereas the coding model accounts for the implementation losses which include some other factors mentioned later in this section.

7.4.1 Modulation Model

Modulation model provides us with the maximum BICM channel capacity for the particular symbol and is receiver dependent. Consider that the whole bandwidth is allocated to only one UE or both of the UEs are simultaneously scheduled in subframe for MU MIMO. Denote with $h_{j,i}$ the channel measurement of one resource element (RE) for one transmit-receive antenna pair (j, i). To calculate the BICM throughput for such a subframe modulation model applies the following 3 steps,

1. Calculate the SNR for each RE based on the transmission mode and the feedback for each channel estimate in a subframe

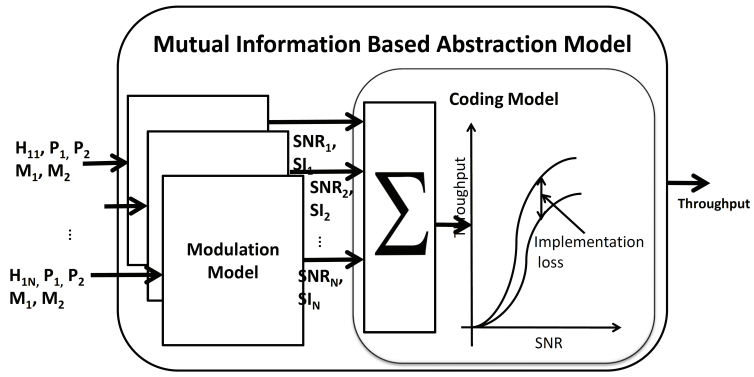

Figure 7.5: PHY abstraction model for BICM Throughput Calculation

2. Calculate the best supported modulation scheme for this subframe
3. Calculate the BICM channel capacity under constraints of the supported modulation scheme

Step 1: Calculation of the SNR The SNR for each of the RE is calculated as,

TM 1 For transmission mode 1 it was calculated as,

$$\gamma = \sum_{i=1}^{n_{\mathrm{Rx}}} \frac{\| h_{1i} + h_{2i} \|^2}{N_{0i}}, \tag{7.1}$$

where N_{0i} is the noise variance of receive antenna i and n_{Rx} is the number of RX antennas. Since antenna configuration during measurement campaign is 2x2 on downlink and in transmission mode 1 the signal is replicated on both of the transmit antennas so superposition of both channels is considered at the each receive antenna and then Maximal Ratio Combining (MRC) is applied at receiver to achieve (7.1).

TM 2 For transmission mode 2 it was calculated as,

$$\gamma = \sum_{i=1}^{n_{\mathrm{Rx}}} \frac{\| h_{1i} \|^2 + \| h_{2i} \|^2}{N_{0i}}. \tag{7.2}$$

In transmission mode 2 , two complex symbols (i.e. s_1 and s_2) are transmitted over two symbol times from two Tx antennas. In first symbol time s_1 and s_2 are transmitted through antenna 1 and antenna 2 respectively whereas in second symbol time $-s_2^*$ and s_1^* is transmitted through antenna 1 and antenna 2 respectively. This gives diversity order of 2 at each of the receive antenna where both of the received channels are considered distinctively thus giving rise in received SNR.

TM 6 For the case of transmission mode 6 it was calculated as,

$$\gamma = \sum_{i=1}^{n_{\mathrm{Rx}}} \frac{\| \ h_{1i} + q * h_{2i} \|^2}{N_{0i}}. \tag{7.3}$$

In transmission mode 6 high SNR is obtained by using precoder q which focuses the transmit energy in specific direction only, so the joint precoded channel is considered in (7.3). In ideal capacity calculation for transmission mode 6, two methods of precoder calculation are considered. In first method the feedback from UE is utilized and sum capacity is calculated, where as in the second method the optimal q which maximizes the overall sum capacity is calculated. Please note that q is selected on subband basis in each subframe.

An important point to note here is that during the measurement campaign the power of the transmit antennas was not divided for the case of MISO transmission and same power was used for both of the transmission antennas that is why we do not see a power scaling factor in the denominator of expressions (7.2) and (7.3).

TM 5 For the case of transmission mode 5 we decided to use the interference aware channel and for the performance comparison of it we need not only the γ but also the ISR (λ). The reasons for this are already explained in Chapter 4 and the expressions for calculating the γ and λ are given as,

$$\gamma = \sum_{i=1}^{n_{\mathrm{Rx}}} \frac{\| \ h_{1i} + q * h_{2i} \|^2}{N_{0i}} \tag{7.4}$$

and

$$\lambda = \sum_{i=1}^{n_{\mathrm{Rx}}} \frac{\| \ h_{1i} - q * h_{2i} \|^2}{\| \ h_{1i} + q * h_{2i} \|^2} \tag{7.5}$$

Step 2: Calculation of the supported modulation scheme After calculating SNR for each of the transmission mode, Shannon capacity for each RE is calculated using the Shannon Capacity formula

$$C = \log_2(1 + \mathrm{SNR})$$

and average it over all the REs. We then chose the next possible modulation order (out of QPSK, 16QAM, and 64QAM) above that value to see what modulation scheme be supported. This step can also be thought of as ideal link adaptation.

Step 3: Constrained capacity calculation. For each channel estimate and each of the transmission mode, the BICM channel capacity is calculated using the constrained capacity mutual information expressions presented in Chapter 4 for MU MIMO and in Chapter 3 for other transmission modes. These are available as look-up tables and can be used to read the BICM channel capacity for each RE. Now using these LUTs and the SNRs we can obtain the γ_{eff} such that,

$$\gamma_{\text{eff}} = I^{-1}\left(\sum_i I(\gamma_i)\right) \tag{7.6}$$

7.4.2 Coding Model

The mutual information curves are an upper bound that most advanced implementation of an LTE modem can achieve. In the above formulas the following effects are completely neglected:

- Channel estimation and interpolation in time and frequency.
- Decoding performance.
- All effects of the RF front end.
- The formulas assume a perfect rate adaptation and a perfect feedback loop.

In order to compensate for some of these effects we have carried out simulations with our modem implementation in an AWGN channel and calculated throughput as a function of block error rate (BLER) and SNR. In order to obtain the throughput as a function of the SNR, we first calculate the throughput per MCS as a function of SNR with the help of BLER and transport block size (TBS),

$$T_{\text{MCS}}(\text{SNR}) = (1 - \text{BLER}_{\text{MCS}}(\text{SNR}))\text{TBS}_{\text{MCS}}. \tag{7.7}$$

Assuming ideal link adaptation, the total throughput is given by chosing the maximum throughput from all the MCS

$$T(\text{SNR}) = \max_{\text{MCS}} \{T_{\text{MCS}}(\text{SNR})\}. \tag{7.8}$$

Figure 7.6 shows the ideal throughput in transmission mode 1 based on the BICM mutual information (MI) and the throughput based on the simulation results in equation 7.8. The difference between abstracted and simulated throughput is what we call the implementation loss. This implementation loss has to be incorporated in the system throughput which we shall calculate and this can be done with the help of γ_{eff} obtained in previous section.

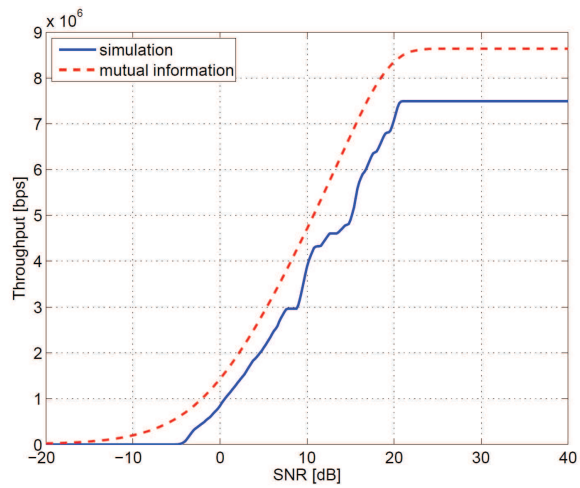

Figure 7.6: Throughput based in mutual information (MI) as well as on simulation results for different SNR values in an AWGN channel. The difference between the MI and the simulated results is called the implementation loss.

Using this γ_{eff} the implementation loss can be very easily calculated from the difference of mutual information and the simulated mutual information in Figure 7.6 to obtain more realistic throughput. The loss in throughput can be attributed to the effects of channel estimation, decoding performance as well as other implementation factors such as limited accuracy due to the use of fixed point representations. Please note that coding model still assumes perfect link adaption and neglects effects of the RF frontend.

7.5 LTE Transmission Modes Performance Comparison

We will be comparing the performance of the LTE TMs 1, 2, 5 and 6. To compare the performance of these TMs we estimate the sum throughput of the cell which consists of two users, based on the raw channel measurements and the methodology outlined in this section. Since there are only two users in the cell so when eNodeB will be in TM 1, 2 and 6, the sum throughput of the cell will be equal to the throughput of the best user in terms of a certain quality metric whereas during TM 5 the sum throughput will be the sum of the throughput of both the UEs.

7.5.1 Feedback calculation

In LTE the feedback consists of a channel quality indicator (CQI), a precoding matrix indicator (PMI) and the rank indicator (RI). Two different feed-

back reporting modes exist: periodic, which is transported over the PUCCH and aperiodic, which is encoded together with the PUSCH. Further, the feedback is classified as wideband feedback, eNodeB-configured sub-band feedback (only in aperiodic reporting mode) or UE-selected sub-band feedback. In our implementation we choose to always use the aperiodic reporting mode with wideband CQI feedback and sub-band PMI feedback. In the LTE 5MHz configuration, the resource blocks (RB) are grouped into 6 subbands of 4 RBs and one sub-band of 1 RB.

In LTE release 8 with two transmit antenna ports at the eNodeB, the PMI consists of two bits that allow to choose one of the following precoders $\mathbf{p} = [1 \quad q]^T, \quad q \in \{\pm 1, \pm j\}$. Each user calculates a PMI for each subband and each receive antenna according to [50]. Further, for every subband, the receive antenna with the stronger RX signal is determined and this information is stored at the UE. When a subband PMI feedback is requested by the eNodeB, the UE reports the PMI of the strongest RX antenna for each subband.

CQI calculation The CQI calculation is based on the SINR measurements at the eNodeB and indicates the highest MCS that the UE can decode with block error probability not exceeding 10%.

7.5.2 Scheduling and sum throughput

The scheduling process depends on the selected TM. In modes 1, 2, and 6, the eNodeB serves only the UE with best channel (in terms of SNR) whereas for TM 5, the eNodeB schedules both UEs jointly only if both of the UEs have asked for the orthogonal PMIs in that particular subband via feedback otherwise it selects the UE with better CQI and enables the TM 6 for the selected UE i.e. it performs *opportunistic MU MIMO* along with single layer precoding. This way we can see that how much gain we get by opportunistic MU MIMO in system throughput and we can conduct a fair comparison between this mixed approach and pure transmission of TMs 1,2 and 6.

7.5.3 Link level abstraction

In order to evaluate the performance of TMs we follow abstraction methodology described in 7.4. For transmission modes 1, 2, and 6, the throughput is calculated as a function of SNR whereas for transmission mode 5, the throughput becomes the function of desired signal strength and interference strength.

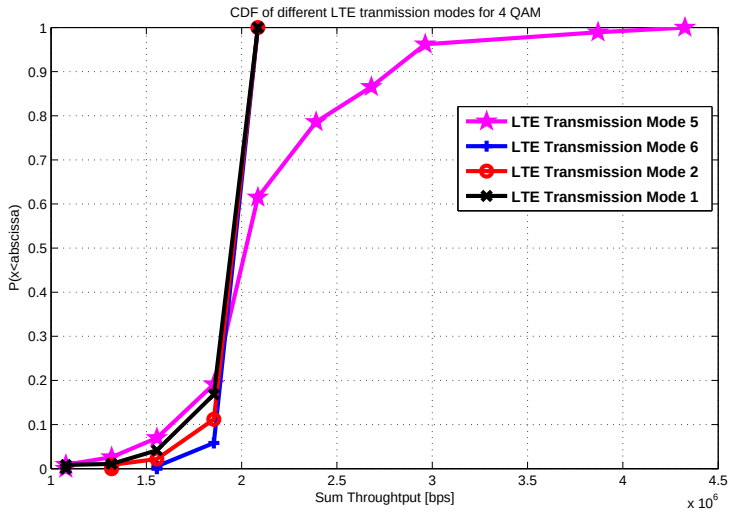

Figure 7.7: CDF comparison of sum throughput of the system with 2 single antenna UEs and an eNodeB equipped with two antennas for different LTE transmission modes using 4QAM

7.5.4 Results

We applied the proposed mutual information based abstraction on measurement data from traces shown in figure 7.4 for LTE TM 1, 2, 6 and opportunistic MU MIMO under the 16-QAM constellation. Figures 7.7 and 7.8 show the cdf comparison of sum throughput of the LTE TMs and opportunistic MU MIMO under 4 and 16-QAM constellations with one eNodeB equipped with 2 antenna and 2 single antenna UEs in the system. For opportunistic MU MIMO eNodeB transmits to both UEs with equal power whereas for other TMs the eNodeB serves only one UE with all of the available power. It can be seen that opportunistic MU MIMO transmission is performing better than the rest of the TMs for high outage rates, i.e., the peak throughput. However, for a 10% outage rate, the sum throughput of MU-MIMO is less favorable. In Figure 7.9 we show the cdf comparison of single user throughput using higher order modulation i.e. 64QAM and it can be seen that TM 2 is only slightly better than TM 6 and TM 6 is about 0.5 Mbps better than TM 2 at an outage rate of 10%. Finally in Figure 7.10 we show the cdf comparison of transmission mode 5 throughput for the case of the mixed interference. It can be seen that when the interference is coming from the signal modulated with higher constellation than the desired signal then the throughput of the whole system is affected.

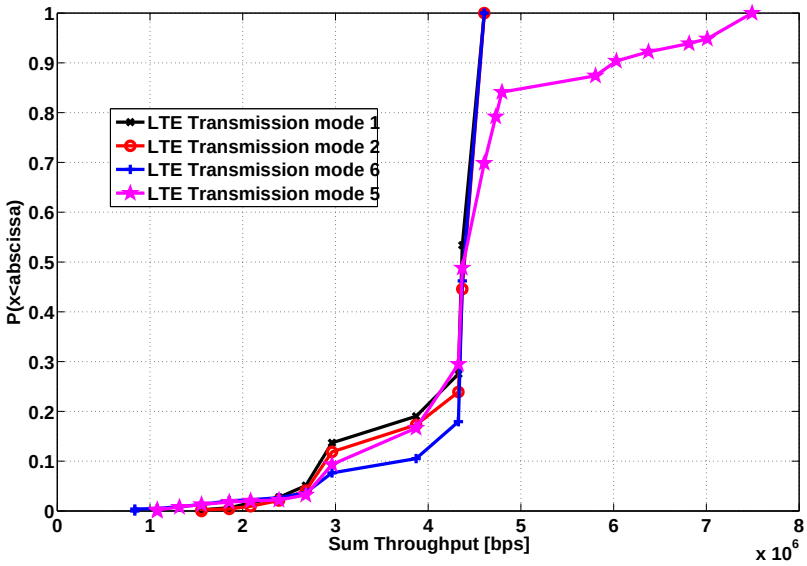

Figure 7.8: CDF comparison of sum throughput of the system with 2 single antenna UEs and an eNodeB equipped with two antennas for different LTE transmission modes using 16-QAM.

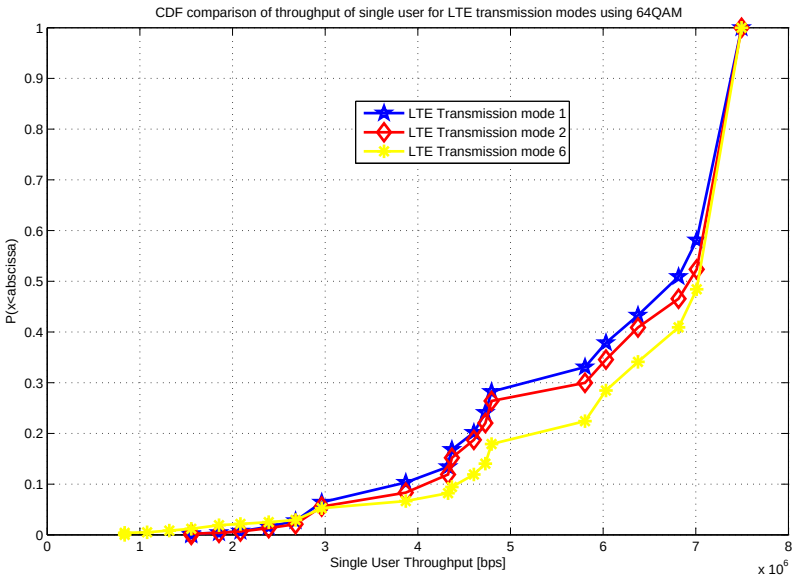

Figure 7.9: CDF comparison of the best selected user throughput of a system with 2 single antenna UEs and an eNodeB equipped with two antennas for different LTE transmission modes when using 64QAM.

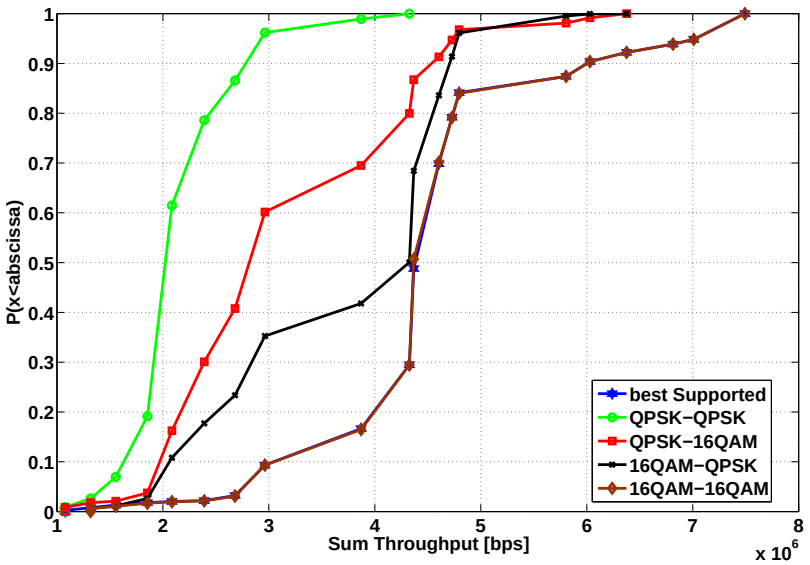

Figure 7.10: CDF comparison of the different interference levels for transmission mode 5 of a system with 2 single antenna UEs and an eNodeB equipped with two antennas.

7.6 Conclusion

We conducted the analysis of different LTE TMs in rural areas in 800MHz frequency band and applied MI-based PHY abstraction to compare their performance in terms of the system throughput. We showed that how the PHY abstraction actually can be utilized in calculating throughput which is accurate for the real systems as well and is also less expensive as compared to the performing full fledged measurement campaigns. Further we showed that it is advantageous to do opportunistic MU MIMO whenever it is possible as it gives overall better throughput even when we restrict our results to only 4-QAM. Important point to note is that we did not see a big difference between the performance of TM 2 and 6 in terms of throughput in rural areas which is mostly because of overall power constraint on the eNodeB side and the mismatch in the feedback. Therefore it is not intelligent to prefer TM 6 over TM 2 in such a scenarios.

Chapter 8

Fast Link Adaptation

8.1 Introduction

This chapter presents a very important application of PHY abstraction for the fast link adaptation and efficient scheduling of UEs in the LTE systems. Based on the current channel state it is possible to select the modulation and coding scheme to meet certain quality of service (QoS) requirements. Lower-order modulation uses small number of bits for each modulated symbol. This can result in low bit rate but it is more robust and can tolerate higher level of noise and interference. Whereas higher order modulations can provide higher data rates but are more prone to the noise and interference levels. Similarly selecting lower code rates for bad channels can improve the decoder performance at the cost of loss in overall throughput and higher code rates can increase the bit rate but at the expense of poor performance of the decoder. This process of selecting a valid combination of modulation and coding scheme based on the current channel state is called adaptive modulation and coding (AMC). Fast link adaptation (FLA) in LTE is based on AMC. FLA is the process of selecting an appropriate MCS for the DL communication based on the channel quality indicator which is sent back to eNodeB from the UE. In LTE there are 29 different possible combinations of MCS and any one of these can be selected for the DL transmission. But the adaptation of these MCS is performed mainly on the feedback from UE to the eNodeB and CQI is one of the key components of this feedback. CQI is based on the received S(I)NR and the receiver design. And in this chapter we shall investigate the calculation of this CQI for the FLA and then scheduling based on this CQI.

8.1.1 Related Work

The concept of FLA is not new in LTE standard as it has been included in WCDMA, HSPA and WiMax. There is plenty of research material on the topic of FLA for WiMax, HSPA and LTE systems. In [80] the authors have presented a suboptimal method of selecting the feedback at the UE using ESM scheme and they have shown that both of the ESM methods (EESM and MIESM) provide almost same kind of performance for the CQI feedback. Further they showed that using their joint RI and PMI feedback scheme, estimation errors have a huge impact on the performance of the system. The reason for this is the joint selection of RI and PMI. If the joint feedback is estimated with errors then the system could take wrong decision on the number of layers and the selection of precoder which can result in the system performance degradation. In [81] the authors have proposed a mean mutual information per coded bit mapping (MMIBM) criterion for MIMO OFDM systems with the help of IEEE 802.11n and showed that it performs slightly better than EESM and MIESM. In their work they also showed that their proposed fast link adaptation provides gains in channels with smaller coherence time and they showed that the feedback delay can have serious impact on the system performance. In [82] the authors have presented a survey on the scheduling issues of LTE and highlighted the fact that the fancy proposed scheduling and link adaptation schemes are in fact either too much complicated to be implemented or take very long time for the optimization of scheduling parameters. Therefore in this chapter we shall provide a robust and practical link adaptation approach which is not only easy to implement but also provides gain in the system performance.

8.1.2 Contributions

In LTE the CRS used for channel estimation are the channel symbols where no data symbols are transmitted. These channel estimates are used for the calculation of CQI at the UE. The CQI calculation is based on the averaged received SINR and the used receiver type. This averaged received SINR can be calculated either with simple arithmetic mean or using ESM approach of PHY abstraction. The latter approach gives more accurate CQI as it is able to capture the frequency selectivity of the channel. However, as it was shown in Chapter 3 that in ESM the adjustment factors are required for accurate mapping and these are MCS dependent. For the channel estimates of CRS there is no MCS used so we can not use any adjustment factors. In this case we can still use the MIESM for SISO transmission (transmission mode 1) but for other antenna configurations MIESM has to be calibrated. However the calibration can be avoided with MIESM using the AWGN curves which have been calculated especially for those specific antenna configurations which are under considerations. This is because the AWGN curves shall already have

had captured the effects of multiple combinations of the received LLRs. For this reason we propose to use AWGN reference curves corresponding to each antenna configuration for the calculation of CQI at the UE.

On the scheduler side, the mapping of CQI to MCS is also generally based on the SISO configuration and in this chapter we propose to adapt it for different antenna configuration as well so that the optimum MCS can be selected for current channel conditions.

8.2 System Model

We consider the transmission modes 1, 2, 5 and 6 in this chapter and the complete system models with received SNR expressions for all of these transmission modes are given in previous chapters.

In LTE the feedback consists of CQI, PMI and the RI. It can be reported either over the physical uplink control channel (PUCCH) in periodic manner or over physical uplink shared channel (PUSCH) in an aperiodic manner. In the latter case the feedback is encoded together with the data. It is further classified in two categories, wideband and subband feedback. In wideband feedback there is only one indicator for the whole bandwidth which results in low overhead on the uplink channel but is unable to cope with the effects of frequency selectivity. On the other hand the subband feedback provide more refine feedback for a group of RBs but poses higher overhead of feedback on the uplink channel. In this chapter we shall only consider the wideband CQI feedback only but the proposed approach can be applied for the subband CQI feedback as well.

8.3 Proposed Link Adaptation

The proposed link adaptation is based on the CQI feedback and on the performance of different transmission modes. We shall provide the reference AWGN curves for the performance mapping of different transmission modes. The proposed link adaptation consists of two steps, 1) selecting an appropriate CQI on the UE side and feeding it back to the eNodeB, 2) selecting an MCS based on the fedback CQI corresponding to the PDSCH transmission mode. Both of these steps shall be discussed in the next sections.

8.3.1 CQI Calculation

The CQI is used to inform the eNodeB about the suitable MCS which should be used for the downlink transmission. This is a 4-bit integer value based on the received SINR at the UE. The CQI estimation process has to take

Table 8.1: LTE CQI Table

CQI	modulation	rate x 1024	efficiency	Code LTE
0		out of range		
1	QPSK	78	0.1523	0.076172
2	QPSK	120	0.2344	0.11720
3	QPSK	193	0.3770	0.18850
4	QPSK	308	0.6016	0.30080
5	QPSK	449	0.8770	0.43850
6	QPSK	602	1.1758	0.58790
7	16QAM	378	1.4766	0.36914
8	16QAM	490	1.9141	0.47852
9	16QAM	616	2.4063	0.60157
10	64QAM	466	2.7305	0.45508
11	64QAM	567	3.3223	0.53717
12	64QAM	666	3.9023	0.65038
13	64QAM	772	4.5234	0.75390
14	64QAM	873	5.1152	0.85253
15	64QAM	948	5.5547	0.92578

into account the transmission mode in which UE is scheduled and the type of receiver which is used for the detection. This is very important as for the same SINR value the MCS supported by different transmission modes can be different and therefore it needs to be taken into account.

The CQI is reported by the UE which measures the averaged received SINR across the entire bandwidth and then chooses the appropriate CQI such that the error probability for decoding at the UE is below 10%. In LTE standard there are 15 useful CQI values for the different combinations of modulation and code rate. These are shown in the Table 8.1 and the reference AWGN performance curves for all MCS with a bar on 10% error rate is shown in Figure 8.1.

The averaged received SINR can be calculated in many ways but the accurate method shall be which is able to capture the effects of frequency selectivity of the channel. If the averaged SINR is calculated using the simple arithmetic mean of received SINRs across the estimated channel symbols then it shall be unable to capture the frequency selectivity across the whole bandwidth. It was shown in the previous chapters that γ_{eff} in PHY abstraction is able to capture the effects of frequency selectivity. Therefore, we propose to use γ_{eff} as the averaged received SINR using the generic ESM

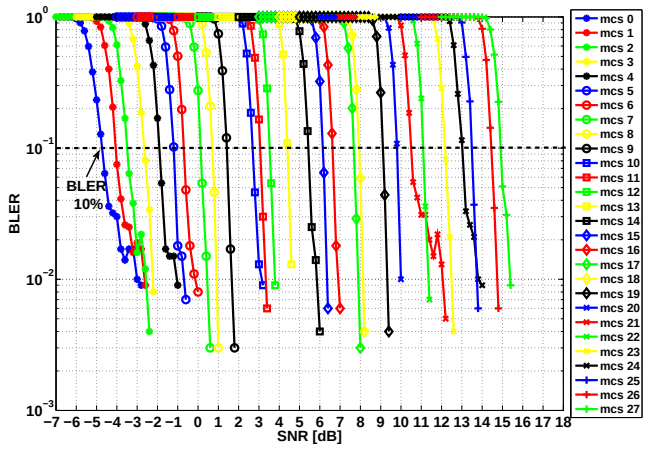

Figure 8.1: Reference AWGN curves for SISO with probability of error below 10%

method, i.e.,

$$\gamma_{\text{eff}}\left(\beta_1, \beta_2\right) = \beta_1 I^{-1}\left[\frac{1}{N}\sum_{n=1}^{N} I\left(\frac{\gamma_n}{\beta_2}\right)\right], \tag{8.1}$$

where the I is given by the BICM channel capacity presented in previous chapters. This γ_{eff} is now an appropriate link quality metric which can be used for the calculation of link quality indicator.

The purpose of the link adaptation is to select the CQI which matches the current channel state and since there is no apriori knowledge available for the adjustment factors to be used for the ESM formulation so we propose to use mutual information based ESM method where the calibration is not a necessary step for transmission mode 1. For other transmission modes we suggest to use the reference AWGN curves which has been calculated for those specific transmission modes so that we do not need the adjustment factors for other transmission modes. Therefore we can assume $\beta_1 = \beta_2 = 1$ in (8.1). Mapping of γ_{eff} to CQI is performed with the help of reference AWGN curves. These reference AWGN curves for transmission mode 2, 5 and 6 are shown in Figures 8.2, 8.3 and 8.4 respectively. The point of interest (we shall refer it as γ_{ref}) in these curves is the 10% of BLER which is marked with a dotted line for all of the MCS. This γ_{ref} can be calculated corresponding to each MCS for all different transmission modes. These γ_{ref} for the discussed transmission modes and all MCS are shown in Figure 8.5.

It can be seen from Figure 8.5 that the performance of different antenna configurations corresponding to the different transmission modes is differ-

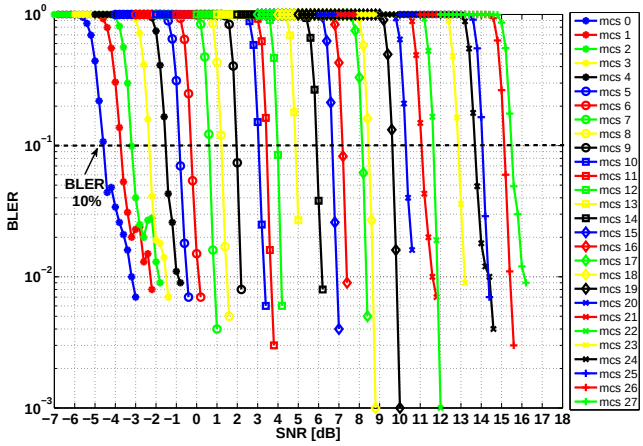

Figure 8.2: Reference AWGN curves for transmission mode 2 with probability of error below 10%

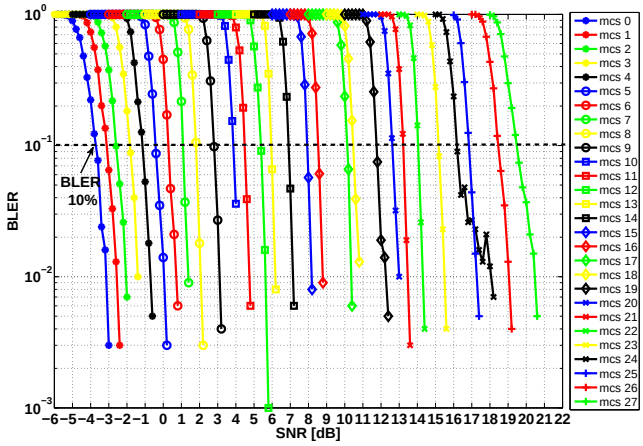

Figure 8.3: Reference AWGN curves for transmission mode 5 with probability of error below 10%

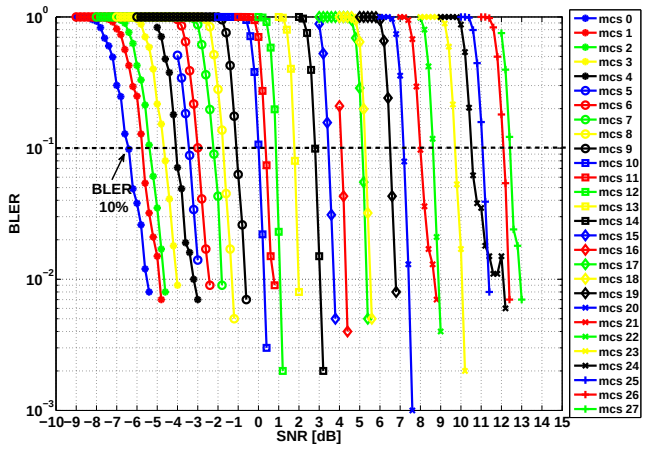

Figure 8.4: Reference AWGN curves for transmission mode 6 with probability of error below 10%

ent. This is not only due to the transmit and receive processing for different transmission strategies but also for the different number of resource elements for PDSCH in the resource element grid in LTE. In addition, the number of PDCCH symbols can also vary from one to three resulting in different number of resources left for the PDSCH. This can result in variation of the code rates and thus the performance for the same MCS when used with different antenna configurations. The variations in the code rates of different MCS in LTE with antenna configurations and different number of PDCCH symbols are given in Tables 8.4 and 8.5 in the Appendix.

It can be observed from the Figure 8.5 that beamforming has almost 3dB of gain for all of the MCS when compared to transmission mode 1, 2 and 5. This means that if the CQI calculation of a UE scheduled in transmission mode 6 is performed with the reference AWGN performance of any other transmission mode then it shall always underestimate the CQI and this shall result in the loss of the achievable system performance.

The γ_{ref} values for all CQI and for the discussed transmission modes are shown in Table 8.2 calculated with the help of OAI link level simulator for LTE 5MHz bandwidth and real channel estimation. Then the selection of CQI is performed such that,

$$\begin{aligned} &\min q \in \mathrm{Q} \\ &\text{s.t. } \gamma_{\text{eff}}(m) \geq \gamma_{\text{ref}}(q, m) \end{aligned} \tag{8.2}$$

where Q is the subset from the possible CQIs where the condition of $\gamma_{\text{eff}}(m) \geq \gamma_{\text{ref}}(q, m)$ is fulfilled and m represents the transmission mode. In (8.2) q

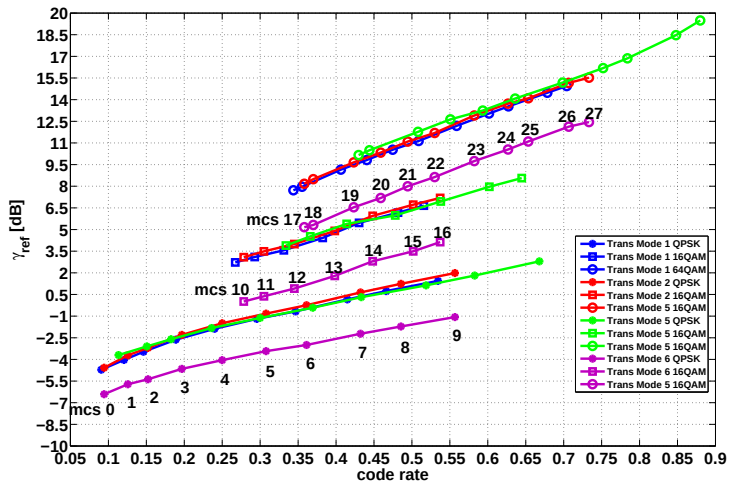

Figure 8.5: Required SNR Vs Code rate for having probability of error below 10%

Table 8.2: γ_{ref} For different transmission modes

CQI	Code	γ_{ref} [dB]			
		TM 1	TM 2	TM 5	TM 6
0		out of range			
1	0.0761	-4.7133	-4.5769	-3.7000	-6.4132
2	0.1172	-4.0384	-3.7114	-3.7000	-5.7243
3	0.1885	-2.6358	-2.3004	-2.6017	-4.6550
4	0.3008	-1.1951	-0.8247	-1.1280	-3.4251
5	0.4385	0.1584	0.6419	0.3147	-2.2187
6	0.5879	1.4385	1.9843	1.8128	-1.0660
7	0.3691	4.4191	3.9921	4.5214	0.9118
8	0.4785	6.1728	6.7209	5.9763	3.4900
9	0.6015	6.6527	7.1902	7.9632	4.1314
10	0.4550	9.8165	10.3291	10.4949	7.1849
11	0.5371	12.1824	11.6899	12.6339	8.6368
12	0.6503	13.5337	14.0954	14.0729	11.0975
13	0.7539	14.9437	15.5193	16.1864	12.4446
14	0.8525	14.9437	15.5193	18.4675	12.4446
15	0.92578	14.9437	15.5193	19.4878	12.4446

Table 8.3: CQI to MCS mapping for different transmission modes at the eNodeB

CQI	MCS			
	TM 1	TM 2	TM 5	TM 6
0	out of range			
1	0	0	0	0
2	1	1	0	1
3	3	3	2	3
4	5	5	4	5
5	7	7	6	7
6	9	9	8	9
7	13	12	11	12
8	15	15	13	15
9	16	16	15	16
10	20	20	18	20
11	23	22	20	22
12	25	25	22	25
13	27	27	24	27
14	27	27	26	27
15	27	27	27	27

represents the minimum channel quality indicator which can be decoded 90% of the times or in other words has outage probability of 10%. This index is sent back to the eNodeB where a decision on the selection of MCS has to be taken so that the requirement of 10% outage probability is fulfilled.

8.3.2 MCS Selection at eNodeB

On the eNodeB side this wideband CQI value is used to determine the optimum MCS and the corresponding PDSCH transport block such that the target block error probability requirements are achieved. The mapping of CQI to MCS is shown in Table 8.3 which is actually based on the code rate of CQI and MCS. It can be seen in the table that at the eNodeB side the mapping of CQI to MCS is almost constant for all of the transmission modes. The reason is that the CQI value has already captured the effects of antenna configuration and the type of received detection used at the UE therefore the mapping on the eNodeB side can be considered independent of the transmission mode.

The target BLER of 10% is normally not considered as the firm choice and this can be changed based on the quality of service requirements. It can vary from one to thirty or even 50 percent as well. If the target BLER is

different than 10% and after the first transmission the target BLER is not achieved then the eNodeB can choose either an aggressive or conservative approach to adjust its MCS in such a way that the target BLER is achieved. For example if the requirements on the BLER are lowered then the eNodeB can select a higher MCS than the one pointed by the CQI and vice versa.

8.4 Results

To show the results of the proposed LA we performed simulations for the transmission mode 6 with OAI system level simulator presented in Chapter 6. We performed the simulations for transmission mode 6 as this was the only transmission mode which was almost 3dB better than the other transmission modes and we were interested in showing the gains which can be achieved by using the proposed link adaptation.

We simulated the system with two UEs randomly placed around the eNodeB and we used the three different channel models for the simulations. These channel models are tapped delay line Rice channel model with 1 tap, with 2 taps and 3GPP Extended Vehicular A (EVA) channel model. To compare the performance with our proposed link adaptation we ran the simulations where CQI calculation is based on an averaged wideband measurement of the signal energy on the estimated channels and the case when our proposed link adaptation is used. Other required parameters of the simulations are already similar to the parameters described in the Chapter 6 and shall not be repeated here. We ran the simulations with same scenario files with both of the link adaptation schemes and scheduled the two UEs. The UEs calculated their CQIs based on our proposed link adaptation and averaged energy measurement. We ran the simulations for 1000 LTE frames and calculated the accumulated throughput of the system. The results are shown in the Figures 8.6, 8.7 and 8.8.

The curves with red diamond show the accumulated average throughput of the system for the given number of frames when proposed link adaptation is used. Whereas the line with blue boxes represents the throughput for the system when an averaged wideband measurement is used. It is very clear that for all of the channel models the proposed link adaptation performs much better and provides a reasonable gain in the overall throughput of the system. Further it was observed that for the case of proposed link adaptation there were less number of HARQ retransmission as compared to the other link adaptation which clearly indicates that using proposed link adaptation is beneficial.

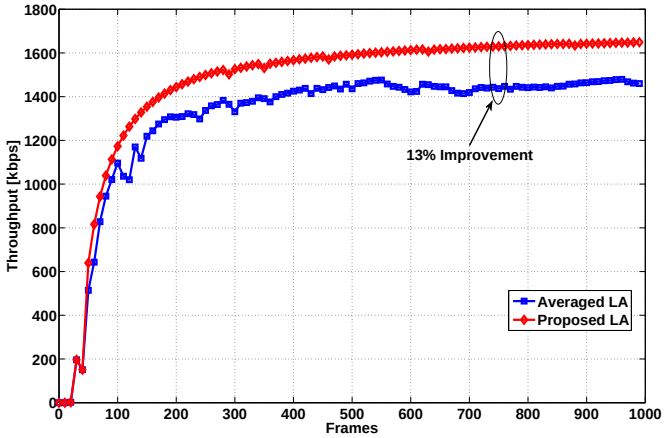

Figure 8.6: Accumulated average throughput of the system with and without proposed link adaptation for transmission mode 6 and tapped delay line Rice channel model having 8 taps

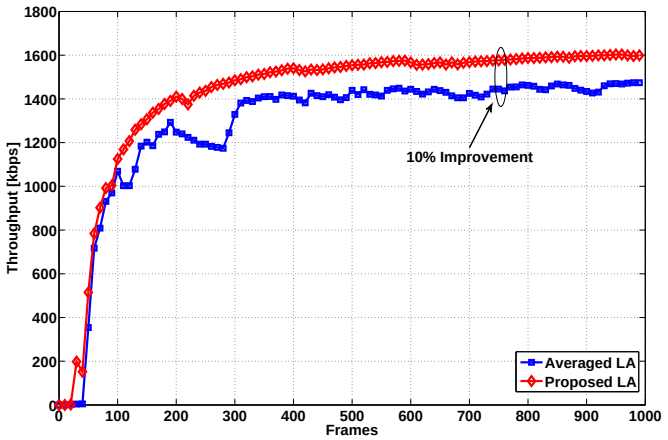

Figure 8.7: Accumulated average throughput of the system with and without proposed link adaptation for transmission mode 6 and tapped delay line Rice channel model having 1 taps

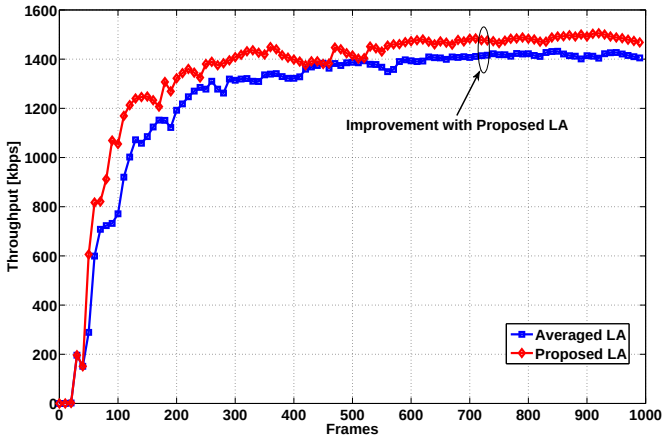

Figure 8.8: Accumulated average throughput of the system with and without proposed link adaptation for transmission mode 6 and EVA channel model

8.5 Summary

In this chapter we have presented a novel, robust and simple link adaptation scheme which can be used in LTE systems. This proposed link adaptation scheme makes used of the PHY abstraction and about the knowledge of the transmission mode in which the user is being served. The detailed tables for the effective SINR to CQI mapping are given and the procedure for optimal CQI calculation with the help of PHY abstraction is presented. Furthermore, the results are provided using OAI system level simulator and it was shown that proposed link adaptation can provide gain in the system throughput. However, further investigations are required to refine this model and provide detailed analysis with more results.

Table 8.4: LTE Resource Table for 1 PDCCH Symbol

I_{MCS}	Q_m	N_C	I_{TBS}	TBS(25 RB)	NP 1Tx	NP 2Tx
0	2	1	0	680	0,09	0,09
1	2	1	1	904	0,12	0,13
2	2	1	2	1096	0,15	0,15
3	2	1	3	1416	0,19	0,20
4	2	1	4	1800	0,24	0,25
5	2	1	5	2216	0,30	0,31
6	2	1	6	2600	0,35	0,36
7	2	1	7	3112	0,41	0,43
8	2	1	8	3496	0,47	0,49
9	2	1	9	4008	0,53	0,56
10	4	1	9	4008	0,27	0,28
11	4	1	10	4392	0,29	0,31
12	4	1	11	4968	0,33	0,35
13	4	1	12	5736	0,38	0,40
14	4	2	13	6456	0,43	0,45
15	4	2	14	7224	0,48	0,50
16	4	2	15	7736	0,52	0,54
17	6	2	15	7736	0,34	0,36
18	6	2	16	7992	0,36	0,37
19	6	2	17	9144	0,41	0,42
20	6	2	18	9912	0,44	0,46
21	6	2	19	10680	0,47	0,49
22	6	2	20	11448	0,51	0,53
23	6	3	21	12576	0,56	0,58
24	6	3	22	13536	0,60	0,63
25	6	3	23	14112	0,63	0,65
26	6	3	24	15264	0,68	0,71
27	6	3	25	15840	0,70	0,73
28	6	3	26	18336	0,81	0,85

Table 8.5: LTE Resource Table for 3 PDCCH Symbol

I_{MCS}	Q_m	N_C	I_{TBS}	TBS(25 RB)	NP 1Tx	NP 2Tx
0	2	1	0	680	0,11	0,11
1	2	1	1	904	0,14	0,15
2	2	1	2	1096	0,17	0,18
3	2	1	3	1416	0,22	0,24
4	2	1	4	1800	0,29	0,30
5	2	1	5	2216	0,35	0,37
6	2	1	6	2600	0,41	0,43
7	2	1	7	3112	0,49	0,52
8	2	1	8	3496	0,55	0,58
9	2	1	9	4008	0,64	0,67
10	4	1	9	4008	0,32	0,33
11	4	1	10	4392	0,35	0,37
12	4	1	11	4968	0,39	0,41
13	4	1	12	5736	0,46	0,48
14	4	2	13	6456	0,51	0,54
15	4	2	14	7224	0,57	0,60
16	4	2	15	7736	0,61	0,64
17	6	2	15	7736	0,41	0,43
18	6	2	16	7992	0,42	0,44
19	6	2	17	9144	0,48	0,51
20	6	2	18	9912	0,52	0,55
21	6	2	19	10680	0,57	0,59
22	6	2	20	11448	0,61	0,64
23	6	3	21	12576	0,67	0,70
24	6	3	22	13536	0,72	0,75
25	6	3	23	14112	0,75	0,78
26	6	3	24	15264	0,81	0,85
27	6	3	25	15840	0,84	0,88
28	6	3	26	18336	0,97	1,02

Chapter 9

Conclusion & Future Work

9.1 Conclusions

In this thesis we have been able to highlight the importance of PHY abstraction for the system level simulations. The thesis was divided in two main parts. In the first part we have investigated and proposed new PHY abstraction models for different antenna configurations in LTE. We have provided a detailed process of the validation of the PHY abstraction methods with the help of link level simulator. The main stress of the thesis was to provide pragmatic approaches toward the inclusion of PHY abstraction in system level simulators so that these abstraction models have higher level of applicability, accuracy and realism. This section also handled the problem of IR-HARQ in LTE and proposed two approaches which are very easy to implement and their validation through link level simulators show that these can provide required link quality indicator with a very good accuracy. The main achievements presented in this section are,

- **PHY Abstraction for SU SISO & MISO systems in LTE**
  In this chapter we have presented the solution for the problem of PHY abstraction for different transmission modes of LTE which correspond to SU SISO and MISO systems. These include LTE transmission mode 1 (SISO), 2 (STBC) and 6 (Transmit Precoding). We showed the complete methodology with which the two popular variants of ESM method can be applied for these different transmission modes and we provided the complete information about the important steps for their validation. We showed that the calibration of adjustment factors is a necessary and important step for the case of MISO channel even with the use of mutual information based PHY abstraction. In this chapter

we have presented results for a wide variety of available MCS in LTE with both ideal and real channel estimation. The results are presented in detailed tables as well which can be used right away in the system level simulators.

- **PHY Abstraction for MU MIMO using IA Receiver**
  In this chapter we have extended the topic of PHY abstraction for the IA receivers and MU MIMO where the MU interference is a major problem and it deviates greatly from it usual Gaussian assumption. The IA receivers utilize the knowledge about the structure of the interference for the decoding purposes therefore we proposed a novelty of including the interference strength as an important parameter in the process of PHY abstraction for MU MIMO and compared the results with the standard ESM methods. It was verified that our proposed model did outperform other two methods during the validation process using the link level simulator. Further in this chapter we extended this model for the case of SU MIMO where spatial multiplexing is used. We provided a framework in which this proposed model can also be used for SU MIMO scheme emplying IA receiver.

- **PHY Abstraction for IR-HARQ in LTE**
  In this chapter we dealt with the problem of the inclusion of IR-HARQ in LTE for system level simulations. The main focus of this chapter was to provide a rather simple and accurate PHY abstraction approach which can be easily implemented on the system level simulators for the LTE systems. Thus we proposed two novel approaches for modeling the IR-HARQ at the system level simulators out of which one was was very simple to implement whereas the other was very accurate. We also reduced the storage requirements for the reference AWGN curves. The important point to highlight is that simplified proposed model used the information which is already available in the control information of LTE frames so no extra signaling is needed for the presented approach. We have provided results for wide range of MCS up till the fourth HARQ round and showed that both methodologies are very accurately validated with the help of link level simulators.

The second part of the thesis covers the applications of the PHY abstractions. It is shown in this part that the PHY abstraction can provide huge benefits for the system level simulations without any significant loss in the realism of the system performance. It can provide significant speed up in the system level simulations because of which it becomes possible to simulate large scale system simulations.

- **System Level Simulations in LTE**
  In this chapter we presented a complete methodology of implementing

the presented PHY abstraction schemes in to system level simulations. We took Eurecom's OAI system level simulator as a case study and showed that the inclusion of PHY abstraction solves the problem of running the simulations for extremely long duration and provide accurate results as compared to the ones which are obtained by running the simulations with full PHY processing. It was also shown that using PHY abstraction can provide not only a huge factor in the speed of simulations but accuracy, applicability and scalability. To highlight the importance of PHY abstraction in system simulators we showed the results for different transmission modes of LTE with and without PHY abstraction and showed that PHY abstraction is indeed an extremely valuable low complexity tool for large scale system simulations.

- **Comparison of LTE Transmission Modes at 800 MHz**
  In this chapter we present another useful application of PHY abstraction where we performed the comparison of different LTE transmission modes based on the real channel estimates which were collected during a measurement campaign. We presented the complete methodology about the use of PHY abstraction in calculating the performance of different transmission modes of LTE and we also showed that how the raw channel estimated can be used to extrapolate the performance evaluation of other transmission modes. As an example we showed the results for the MU MIMO which was not implemented at the time of measurement campaign but using the channel estimates we calculated the throughput of the system as if it would have been implemented using IA receivers.

- **Fast Link Adaptation**
  In this chapter we have presented a novel, robust and simple link adaptation scheme which can be used in LTE systems. This proposed link adaptation scheme makes used of the PHY abstraction and about the knowledge of the transmission mode in which the user is being served. The detailed tables for the effective SINR to CQI mapping are given and the procedure for optimal CQI calculation with the help of PHY abstraction is presented. Furthermore, the results are provided using OAI system level simulator and it was shown that proposed link adaptation can provide gain in the system throughput.

The work in this thesis has provided the fundamental basis in the improvement for the system level simulators for complex and large scale system level simulations. Also it did provide detailed results in the form of tables which can be readily used in the scenario of LTE.

9.2 Future Work

This thesis has tried to cover all the major areas in scope of LTE system level evaluations but still there are some possible directions in which this thesis can be easily extended. These are described below,

- The main focus of PHY abstraction has been on the downlink in this thesis and uplink has not been discussed. Although we have progressed on general framework for the inclusion of abstraction for the uplink in system level simulator but this still requires validated using UL link level simulator. The schemes for the UL PHY abstraction has been already investigated and a framework for its inclusion in the system level simulator has also been defined and implemented. Therefore, the work presented in this work can be easily extended for UL PHY abstraction and further investigations for different antenna configurations in UL communication can be investigated.

- Another important direction it can be extended is for the case of inclusion of relays in the system simulators. Since there are number of relaying strategies which are proposed in literature so first it has to be decided that what type of relay channel is to be considered. Then the link between transmitter and receiver can be modeled using the approach presented in [25] where the relay link can be thought of providing either an additional diversity branch (like in LTE transmission mode 2) or both relay and transmitter can do beamforming (like in transmission mode 6) towards receiver.

- Further the IR-HARQ approach can be extended to the case of MIMO transmission and the problem of adjustment factors can be investigated for this scenario. It has still to be implemented in the OAI system level simulator. Further the results with variable bandwidths and resource allocations can also be studied.

- The proposed link adaptation can be used for the design of an improved scheduler, which can take advantage of the antenna configurations and do the arbitrary resource allocation in order to increase the system throughput.

Chapter 10

Summary

10.1 Motivation

La communication mobile a véritablement révolutionné la façon dont nous communiquons. Elle a conduit à un changement radical dans le domaine de la télécommunication avec le passage du fil au sans fil, ce qui a permis de courir des régions où le déployement d'infrastructure basée sur les câbles était douteux. De plus, selon l'Union internationale de Télécommunication (UIT), le nombre de personnes souscrits à la téléphonie mobile a atteint 6.8 milliards, soit 96% de la population de la planète [1]. Une comparaison entre l'évolution de l'abonnement au réseau mobile et celle d'autres types d'abonnements, comme présenté dans la Figure 10.1, démontre clairement le désir des hommmes à vouloir communiquer entre euse même durant leurs déplacement. De même, l'Internet apparait comme une autre technologie qui q contribué à la transformation de la planète en un village mondial. En effet, avec le dernier concept de cloud computing, l'Internet est devenu un réseau mondial indispensable utilisé dans presque tout les aspects de la vie quotidienne telle la médicine, défense, business et surtout les médias sociause. La Figure 10.2 supporte cette ideé et montre qu'environ 80% des ménages dans les pays développés ainsi que 43% des mondiause ont accès à l'Internet. Une tendance similaire peut être observée chez les particuliers à travers le monde. L'augmentation du nombre d'abonnés au réseau mobile ainsi ainsi que celle du nombre d'utilisateurs de l'Internet démontrent une demande de plus en plus croissante sur les services basés sur l'Internet et la connection mobile.

Au cours des 10 dernières années la communication mobile est passée du réseau purement circuit à un réseau tout IP. Cette évolution a permis de

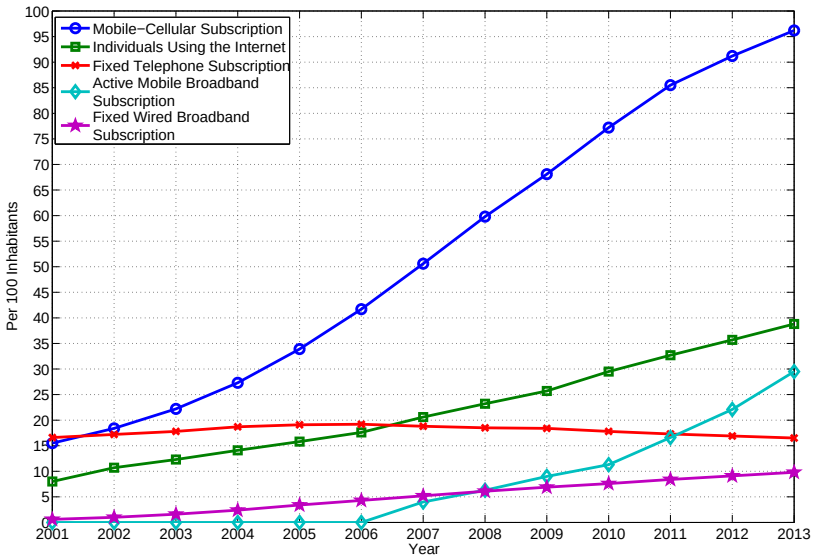

Figure 10.1: Global ICT development 2001-2013 [1]

fournir des débits élevés sur les appareils mobiles, débit qui n'étaient que possible sur les réseaux fixes il ya a 10 ans. Aujourd'hui, les réseaux cellulaires basés sur le Long Term Evolution (LTE) du partenariat de troisième génération (3GPP) [3] a déjà été déployés dans certaines régions du monde et il assure un débit d'environ 100 Mbps en downlink et de 50 Mbps en uplink. De plus, les statistiques de ITU montrent que non seulement le nombre d'abonnés aux services mobiles de large bande. Ceci peut être observé dans la Figure 10.1 qui présente le Global Information Technology Communication (ICT) tendances et on peut voir que, avant 2006, les abonnements au large bande mobile sont nuls et depuis lors, il a atteint le niveau de 30 % de la population mondiale. Il s'agit d'une indication claire qu'il y aura une augmentation significative de la demande de débits plus élevés pour les services de données mobiles à l'avenir.

Cependant, pour répondre à la demande croissante des débits plus élevés, il est nécessaire d'étudier les techniques plus efficaces et innovantes qui peuvent non seulement fournir le débit de données requis en étant plus efficace du spectre, mais sont aussi respectueux de l'environnement en termes de consommation d'énergie. Un exemple de tels efforts est la normalisation du système 3GPP LTE. Il déploie non seulement les réseaux de grande envergure où plusieurs antennes sont utilisées à la station mobile et à la station de base, mais aussi les réseaux de petite échelle utilisent les stations de base à une puissance d'émission très faible i.e., les réseaux des cellules femto, pour aug-

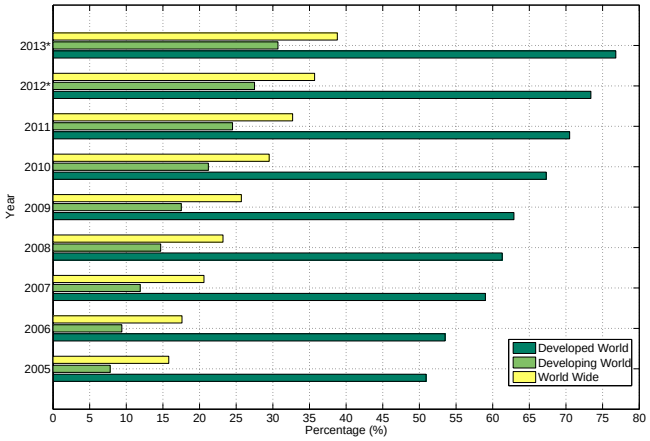

(a) Évolution dans l'utilisation d'Internet par les individus dans la vie quotidienne

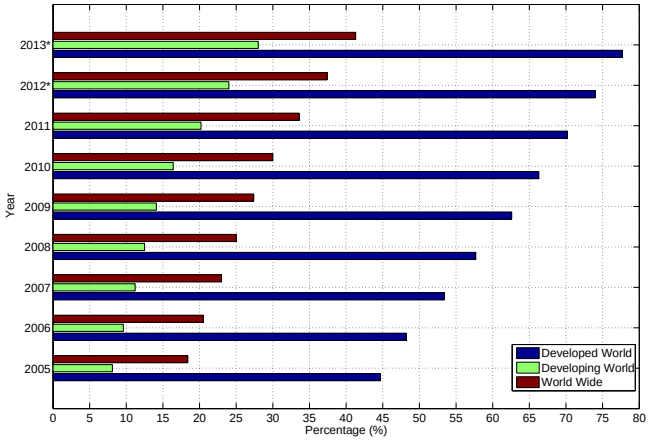

(b) Ménages avec Internet accès à la maison

Figure 10.2: Utilisation croissante d'Internet dans la vie quotidienne [1]

menter l'efficacité spectrale. En outre, il prend en charge la communication coopérative où les stations de base des cellules voisines peuvent partager des données et des signaux de commande afin d'éviter les interférences et augmenter la puissance du signal vers l'utilisateur mobile souhaité. Il prend également en charge des concepts avancés comme virtuelle MIMO et le relais.

Les gains offerts par ces techniques sur le lien de communication unique ne représentent pas nécessairement les mêmes gains lorsqu'il est déployé dans un système énorme. Par conséquent, les simulations au niveau système sont

les besoin absolue pour les évaluations de rendement avant le déploiement de ces systèmes. Et c'est là que l'on prend conscience de l'importance des simulations au niveau système. Dans les simulations au niveau système, la véritable performance des techniques proposées est évaluée par la mise en oeuvre du système à l'échelle complète et la compatibilité de ces régimes avec ceux déjà existants est également validée.

Les simulations au niveau système exigent normalement les calculs lourds pour très longue durée de temps en raison de la caractérisation des liaisons radio entre chaque utilisateur et de la station de base. Les simulations au niveau lien de chacune de ces liaisons est le goulet d'étranglement dans ces simulations. Pour trouver l'impact des calculs de simulation au niveau lien, nous avons effectué une petite simulation avec un eNodeB LTE et un UE à l'aide de simulateur OpenAirInterface (OAI) d'Eurecom qui est un simulateur au niveau système et comporte un simulateur au niveau lien intégrée aussi.

Pour en savoir plus sur les ressources consacrées à la couche physique nous avons réalisé le profilage sur les différents blocs du simulateur. Pendant la simulation, nous avons calculé le temps qui a été passé sur chaque bloc dans le simulateur et aussi la fréquence d'appeler un certain bloc a été calculé. Ceci est illustré dans la Figure 10.5 où les boîtes en vert correspond aux principales tâches liées au simulateur au niveau lien en sens descendante [1]. On peut voir que la majeure partie du temps et des ressources sont consacrés aux blocs qui correspondent au simulateur au niveau lien.

Une version plutôt simplifiée du profilage est représenté dans la Figure 10.3 où le pourcentage de la durée de temps passé pour les simulations au niveau lien et le reste des tâches lié au niveau système lié est affiché. Bien qu'il était un système extrêmement trivial, mais encore plus de 82 % du temps de simulation a été consacré à la simulation au niveau lien alors que seule une petite fraction du temps a été consacré à la pile de protocole et d'autres tâches liées au système.

Par conséquent, afin de réduire la complexité et la durée des simulations au niveau système, il est absolument nécessaire d'avoir un modèle d' abstraction précis de couche physique précise (PHY) qui remplace les calculs réels du niveau lien et fournit les couches supérieures avec une mesure de qualité de lien nécessaire et précis, i.e., taux d'erreur de bloc (BLER) ou

[1] S'il vous plaît noter que le profilage a été réalisée en utilisant *gprof* sous système d'exploitation Linux et gprof a la capacité limitée du profilage et ne peut pas le profiler pour les instructions spécifiques de matériel. En OAI simulateur, Turbo décodeur est mis en oeuvre avec une grande précision et très faible complexité en utilisant le jeu d'instructions Intel et les appels à décodeur Turbo ne sont pas visibles dans la Figure de profilage.

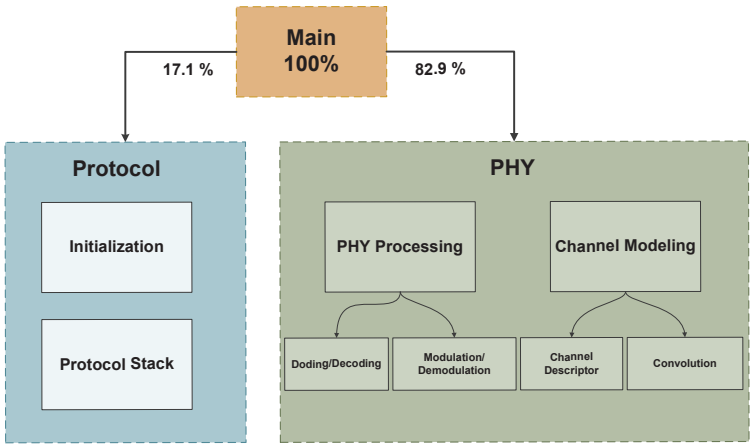

Figure 10.3: Schéma simplifié de profilage au niveau système de simulations

taux d'erreur de paquet (PER). Un modèle d'abstraction de lien est utilisée pour déterminer l'indicateur de qualité au niveau système requis à l'aide d'adaptation du lien idéal sans avoir à simuler n'importe quel traitement de couche physique i.e. , le codage , la modulation, la convolution du canal avec le signal, la démodulation et le décodage. Ceci est illustré dans la Figure 10.4 où il peut être vu que PHY abstraction fournit aux couches supérieures la décision nécessaire sur le décodage du paquet sous les conditions de canal instantanées tandis que dans le traitement complète de PHY, cette décision peut être obtenue seule à partir du décodeur lui-même. Dans cette forme, il est un outil de faible complexité extrêmement précieux pour simulations efficace au niveau système à grande échelle. En outre, il peut également être utilisé pour l'ordonnancement des ressources rapide, l'adaptation du lien rapide en utilisant la commande de puissance adaptative et la modulation et le codage adaptatifs.

La motivation principale de cette thèse était donc d'étudier et de proposer des nouveaux modèles d'abstraction PHY pour les configurations d'antennes différentes en LTE et fournir une approche pragmatique afin que ces modèles d'abstraction aient plus haut niveau d'applicabilité, de précision et de réalisme. Ce ne doit pas seulement fournir la base fondamentale de l'amélioration pour les simulateurs au niveau système, avec lesquelles il sera possible de tester différents protocoles de couche supérieure et des politiques d'ordonnancement, mais aussi ces régimes d'abstraction PHY peuvent être utilisés dans les évaluations en temps réel des stations de base.

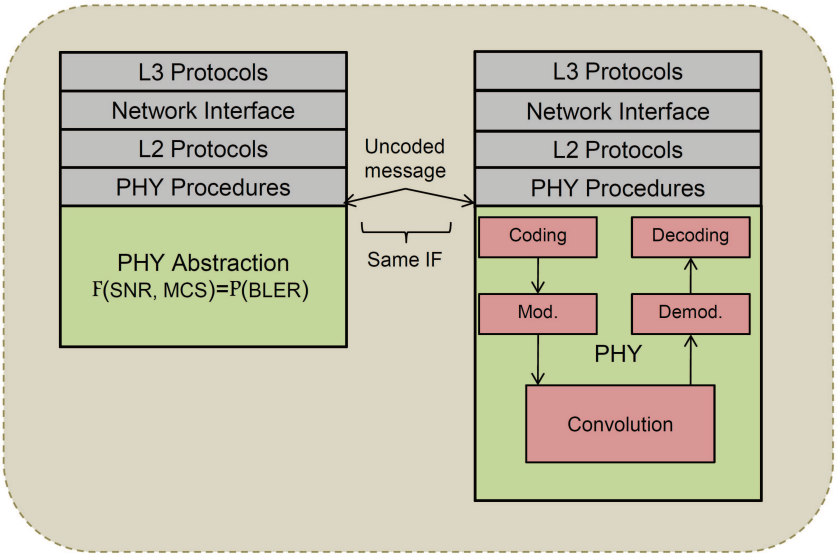

Figure 10.4: Comparaison de la pile de protocole avec et sans PHY abstraction

En outre, cette thèse fournit des paramètres fondamentaux pour l'abstraction PHY des différents modes de transmission de LTE et fournit une analyse en profondeur sur les différents aspects de l'abstraction PHY. Le problème d'avoir une solution analytique pour l'inclusion de redondance incrémentale - requête automatique de répétition hybride (IR-HARQ) est également traité dans cette thèse et deux approches semi-analytiques ont été proposée pour cartographier les avantages de IR-HARQ avec un haut niveau de précision et l'efficacité.

Un autre objectif de cette thèse est de montrer que les techniques d'abstraction PHY ont beaucoup de potentiel et peuvent être utilisés dans plusieurs scénarios et objectifs. Nous montrons que l'abstraction PHY, mis en oeuvre dans le simulateur au niveau système, augment la vitesse de la simulation au moins 30 fois par rapport au système dans le quel PHY est complètement traité. Nous avons également montré en fournissant un débit agrégé sur un nombre donné des trames que PHY abstraction fournit exactement le même genre de performance comme un système de traitement complet de PHY. Ceci fourni un résultat positif et très encourageant en faveur de l'utilisation de l'abstraction PHY dans les simulations système. Aussi, nous avons montré que ce peut améliorer le feed-back de l'indicateur de qualité de canal (CQI) pour le choix approprié de la modulation et de codage (MCS) en lien descendant et avec une légère modification, il peut également être utilisée pour les estimations réelles de canal pour prouver les concepts fondamentaux

de communication dans divers environnements.

10.2 Outline and Contributions

Cette thèse est principalement divisée en deux parties, méthodologies et applications. Certains concepts de base liés à la technologie LTE et les sujets abordés dans cette thèse sont présentés comme des connaissances de base dans le chapitre 2. Part - I décrit les régimes d'abstraction PHY différents pour les différents modes de transmission LTE et leur validation par les simulateurs au niveau lien. Au début, cette partie donne une vue globale sur la méthodologie de l'abstraction PHY et répond à certaines questions très importantes sur la validation de ces régimes à l'aide de simulateurs au niveau lien. Puis il étend les régimes d'abstraction pour le cas de multi-utilisateurs (MU) MIMO communication où l'interférence est non gaussienne et sa structure est exploitée lors du décodage donc l'abstraction PHY doit également être capable d'exploiter les connaissances sur les interférences pour une modélisation précise. L'inclusion de l'IR-HARQ pour le LTE est ensuite discuté en détail et deux nouvelles procédures semi-analytiques sont proposées qui font usage de seulement trois références courbes de bruit blanc additif gaussien (AWGN) de et fourni une solution simple pour le largeur de bande variable.

Partie II présente quelques-unes des applications possibles de l'abstraction PHY à partir de sa mise en oeuvre pour des simulations au niveau système, puis compare les différents aspects de l'abstraction PHY où elle est bénéfique. Il peut également être utilisé pour l'adaptation de lien rapide du LTE où un CQI efficace peut être calculée en utilisant l'abstraction PHY et une modulation et codage (MCS) appropriée peut être sélectionné pour le lien descendant. Une autre application très importante de l'abstraction PHY est la validation de différents aspects de la communication à l'aide des estimations de canal mesurées. Un bref aperçu de chaque chapitre est présenté ci-dessous.

10.2.1 Fondamentaux

Ce chapitre couvre les concepts de base liés à la norme LTE en général et plus particulièrement sur la couche physique. Il est destiné à fournir une référence rapide aux différents concepts de système LTE qui sera fréquemment utilisé dans le reste de la thèse. Il commence par un bref historique de l'évolution des normes cellulaires et discute le protocole LTE, structure de trame LTE et le traitement du lien descendant, e.g., le codage de canal, modulation etc, et la correction d'erreurs en avant dans LTE en utilisant la technologie IR-HARQ. Ensuite, il fournit une courte introduction à un concept important de bits entrelacés modulation codée (BICM) et présente

la capacité de BICM pour la modulation d'amplitude en quadrature (QAM) alphabets. Enfin, ce chapitre se termine par une introduction formelle de l'abstraction PHY pour les systèmes basés sur multiplexage par répartition orthogonale de fréquence (OFDM). Ce chapitre présente également une introduction formelle de la plate-forme OpenAirInterface qui est largement utilisé pour produire les résultats de cette thèse.

OpenAirInterface

OpenAirInterface est une plate-forme open-source pour l'expérimentation dans les systèmes sans fil avec un fort accent sur les technologies cellulaires telles que LTE et LTE-Advanced. La plate-forme comprend du matériel et des composants logiciels et peut être utilisé pour la simulation / émulation de même que l'expérimentation en temps réel. Il comprend de l'ensemble de la pile de protocole à partir de la physique à la couche réseau. L'objectif de cette plateforme est de combler l'écart entre la simulation et l'expérimentation en temps réel en fournissant les données de référence pour la validation du protocole, évaluation de la performance et test du système de pré-déploiement. Les principales caractéristiques sont

- Conformité extensif de LTE Release 8.6 avec certaines caractéristiques de LTE-Advanced
- Pile complète de protocoles pour les implémentations d'UE et d'eNB
- Fournit une interface de réseau Linux pour exécuter n'importe quelle application sur le dessus
- Possibilité de Carrier aggregation
- Met en oeuvre plusieurs modes de transmission (TM) importants de LTE
    - LTE TM 1 (SISO)
    - LTE TM 2 (STBC - Alamouti Codes)
    - LTE TM 5 (MU MIMO)
    - LTE TM 6 (Transmit Precoding)

OpenAirInterface comprend une implémentation en C hautement optimisé, y compris tous les éléments de la 3GPP LTE Rel 8.6 pile de protocole pour l'UE et l'eNB (PHY , MAC , RLC , RRC , PPPC , NAS driver). A part de fonctionnement en temps réel du modem logiciel sur une cible matérielle, la pile de protocole complet peut être exécutée en émulation. L'environnement d'émulation d'OpenAirInterface permet la virtualisation de noeuds de réseau dans les machines physiques et déploiement distribué sur les réseaux Ethernet câblés. Les noeuds du réseau communiquent par virement direct à la

mémoire quand ils font partie de la même machine physique et par multidiffusion IP sur Ethernet quand ils sont dans des machines différentes. Dans le premier cas, l'émulateur peut soit être exécuté avec la couche PHY compète ou avec l'abstraction PHY tandis que dans le dernier cas, les noeuds interface au niveau de la couche 2. Le reste de la pile de protocole (MAC et RLC) pour chaque instance de noeud utilise la même implémentation, de même que l'ensemble du système. Chaque noeud dispose de sa propre interface IP qui peut être reliée soit à une application ou un générateur de trafic. L'émulateur comprend également un modèle de mobilité simple et modèle de canaux, y compris l'affaiblissement de propagation, l'effet de masque et stochastique évanouissements rapides.

Il est destiné à fournir une référence rapide aux différents concepts de système LTE qui sera fréquemment utilisé dans le reste de la thèse. Il commence par un bref historique de l'évolution des normes cellulaires et discute le protocole LTE, structure de trame LTE et le traitement du lien descendant, par exemple, le codage de canal, modulation, etc , et la correction d'erreurs en avant en utilisant la technologie LTE IR- HARQ. Ensuite, il fournit une courte introduction à un concept important de bits entrelacés modulation codée (BICM) et présente la capacité de BICM pour la modulation d'amplitude en quadrature (QAM) alphabets. Enfin, ce chapitre se termine par une introduction formelle de l'abstraction PHY pour les systèmes basés sur multiplexage par répartition orthogonale de fréquence (OFDM).

10.2.2 Part I - Méthodologies

LTE Single-User (SU) SISO & MISO Systèmes

Au cours de la dernière décennie, le besoin d'une modélisation PHY d'abstraction plus sophistiqué a gagné beaucoup d'attention non seulement au sein de la communauté de recherche, mais aussi dans l'industrie à cause de son importance pour des évaluations précises au niveau système. Ce chapitre présente un aperçu de la littérature et de l'état de l'art des méthodes d'abstraction PHY pour les systèmes de communication LTE mono-utilisateur (SU). Il propose ensuite les schèmes qui permettent d'étendre les méthodes simples pour des systèmes plus complexes en utilisant la diversité de transmission et la formation de faisceau.

Dans ce chapitre, les techniques d'abstraction PHY les plus populaires sont présentés en accentuant sur leur mise en oeuvre point à point pragmatique et ceci pour les différents types de schèmes de transmission et de réception des systèmes LTE. Les deux régimes d'abstraction PHY les plus utilisés sont EESM et MIESM. Ces deux régimes sont basés sur le concept de correspondence du SINR effective qui représente une moyenne du SINR subie par

un canal. Un paramètre important pour ces deux schèmes est le facteur d'ajustement(s) pour les différents types de stratégies de transmission et de modèles de canal. Dans ce chapitre, nous avons fourni uen compréhension claire de ces facteurs d'ajustement et sur leur exigence pour l'exactitude du modèle. Nous montrons que les facteurs d'ajustement doivent être calibré et validé pour s'assurer que l'abstraction PHY fournit une information réaliste en imitant la pleine pérformance de PHY.

La plupart des travaux dans la littérature présente des résultats pour des systèmes très limitées alors que dans ce chapitre, nous présentons une compréhension générique sur différents aspects de l'abstraction PHY avec l'aide de différentes configurations d'antennes dont un canal SISO, un canal MISO avec diversité de transmission [26–31] et les techniques de beamforming à la transmission [32–41]. Ces régimes sont appelés, respectivement, les mode de transmission 1 , 2 et 6 dans les systèmes LTE. Ce chapitre fournit une méthodologie complète de calibration et validation des systèmes d'abstraction PHY mentionnés et présente les résultats à l'aide du simulateur OAI de niveau liaison .

Elle répond aux différentes questions fondamentales sur la conception et la validation de systèmes d'abstraction PHY avec l'aide de résultats très exhaustives et détaillées. Il fournit les courbes de rendement de référence AWGN utilisés pour l'indication de la qualité de la liaison et montre que la calibration des facteurs d'ajustement dans les régimes d'abstraction PHY populaires, est une étape nécessaire en particulier pour le cas d' abstraction PHY et de configurations multi-antennes basés sur l'information mutuelle. La méthodologie est présentée pour les canaux SISO et MISO, en utilisant les codes en blocs espace-temps comme par exemple les codes Alamouti et le précodage à la transmettre. Ce chapitre fournit les connaissances fondamentales de l'abstraction PHY et montre que la façon dont l'abstraction PHY peut être formé et validé pour n'importe quelle configuration de système LTE .

Il a été montré qu'avec un calibrage correct, EESM et MIESM auront des pérformances équivalente et donc n'importe lequel pourraient être utilisés pour les évaluations du système. En fin de compte il a été montré que les facteurs d'ajustement calibrés sont globalement optimals et donnent les valeurs MSE minimales pour l'ensemble des MCS. Il est très clair d'après les résultats que cette méthodologie est très précise et même peut être directement utilisée pour les évaluations au niveau système. En outre, dans l' annexe A, nous présentons les facteurs d'ajustement calibrés pour les modes de transmission déjà mentionnés qui peuvent être utilisées dans les simulateurs de niveau système. Certains des résultats de ce chapitre ont été déjà publiés dans les conférences mondiales renommées de l'IEEE.

LTE Multiutilisateur MIMO avec Le Récepteur Conscient de L'interférence

Dans ce chapitre, nous étudions l'abstraction PHY pour les systèmes limités par les interférences et les algorithmes de réception avancées. Cette tâche est assez difficile surtout pour les systèmes MIMO. La communication MIMO offre un gain linéaire dans la capacité du système proportionnellement au minimum du nombre d'antennes à l'émetteur et au récepteur sans avoir besoin d'augmenter la bande passante ou la puissance [43] [44]. Les systèmes MIMO se répartissent généralement en deux catégories, SU MIMO et MU MIMO [45]. MU MIMO a plusieurs avantages par rapport à SU MIMO et résout de nombreux problèmes principaux du SU MIMO [46] [47]. Le principe de base de la communication MU MIMO est que plus d'un utilisateur peut être servi en utilisant les même ressources de temps et de fréquence augmentant ainsi directement l'efficacité spectrale et la capacité du système.

Bien que les gains offerts par MU MIMO avec une meilleure conception de livre de codes et le récepteur IA sont significatifs sur le lien de communication unique [51] le vrai potentiel de ces récepteurs est testé au niveau système. Toutefois, les évaluations au niveau système exigent normalement des calculs lourds pour de très longues durées de temps en raison de la caractérisation des liaisons radio entre chaque utilisateur et la station de base. Les simulations au niveau de lien de chacune de ces liaisons est la charge la plus lourde dans ces évaluations. Par conséquent, pour réduire la complexité et la durée des simulations au niveau système nous avons besoin d'un modèle d'abstraction PHY précis.

La caractéristique la plus importante des modèles d'abstraction PHY est de pouvoir non seulement capturer les caractéristiques de l'émetteur-récepteur de manière très précise, mais aussi être en mesure de fournir un niveau élevé de précision pour le simulateur de niveau système. Dans ce chapitre, nous étudions l' abstraction PHY, avec l'aide du MU MIMO en détail, et améliorons la méthodologie présentée dans [55] en termes de complexité et de précision. Nous proposons un nouveau modèle d'abstraction PHY (IAPA) basé sur l'information mutuelle et le niveau d'intérference pour le MU MIMO LTE et quand les récepteurs IA à faible complexité sont utilisés. Nous montrons que le modèle d'abstraction PHY proposé est capable d'exploiter les interférences pour fournir un indicateur de la qualité de la liaison précis. Pour la comparaison, nous montrons comment les modèles d'abstraction PHY standards peuvent être utilisés pour les récepteurs LTE qui prennent en compte les interférences et nous comparons leurs résultats avec notre modèle d'abstraction PHY proposé. En outre, dans ce chapitre, nous généralisons le modèle d'abstraction PHY proposé pour des scénarios limitées par l'interférence autres que le MU MIMO LTE .

Ce chapitre présente un nouveau modèle d'abstraction PHY pour intégrer la connaissance des interférences avec la puissance du signal désiré pour prédire la performance de liaison pour les systèmes MU MIMO. Un aspect important de cette méthode est qu'elle peut être utilisée non seulement pour des systèmes MU MIMO mais aussi pour les autres systèmes MIMO limitées par l'interférence mais ainsi lorsque l'interférence est non gaussienne. Un exemple particulier d'un tel scénario est la transmission basée sur le multiplexage spatial en LTE avec deux flux de données indépendants. Pour ce cas, l'interférence reçue sur les deux flux n'est pas gaussienne et appartient à un alphabet de modulation QAM finie dont la structure peut être exploité au cours du décodage. L'abstraction PHY proposé est en mesure d'exploiter ces informations pour l'abstraction PHY. Ce chapitre présente les résultats de la validation de schéma proposé avec deux méthodes à la pointe de l'art et sa supériorité est prouvée en utilisant un simulateur de niveau liaison. Les résultats de ce chapitre sont publiés dans des conférences IEEE.

Redondance Incrémental HARQ de LTE

le schéme (IR-HARQ) [64–68] utilisé dans les normes de communication sans fil récentes tels que 3GPP LTE offre des prestations plus élevées en termes de capacité du système et de robustesse. Mapper ces avantages dans les évaluations au niveau système est d'une importance critique. Les techniques traditionnelles d'abstraction PHY sont généralement conçus pour une bande passante fixe et ne présentent pas une solution générique pour l'affectation variable de bande passante pour les utilisateurs. Par conséquence, dans ce chapitre, nous proposons deux méthodes semi-analytiques pour modéliser les performances IR-HARQ au niveau liaison en LTE pour les simulateurs de niveau système. Les systèmes proposés permettent l'attribution arbitraires de bande passante alors que dans le même temps ils réduisent les besoins de stockage pour les opérations complexes de l'abstraction IR-HARQ PHY.

la modélisation des performances des (HARQ) pour l'abstraction PHY a acquis toute une attention de la part de la communauté de recherche pour son utilisation dans les simulateurs de niveau système pour réduire le temps des simulations et la complexité du calcul de la couche physique. Cependant la modélisation de la combinaison des informations de plusieurs séries HARQ peut être complexe dans le cas de redondance incrémentale HARQ où de nouveaux bits de redondance supplémentaires sont transmis avec certains des bits transmis précédemment à chaque tour HARQ. Dans [42], les auteurs ont présenté une simple modélisation HARQ (pas IR- HARQ) dans les systèmes OFDM utilisant application exponentielle efficace SINR (EESM) et mutuel d'information sur la base de la cartographie SINR efficace (MIESM). Dans [69] les auteurs ont présenté une méthode récursive en utilisant EESM pour la modélisation HARQ d'un système OFDM. Un travail intéressant a

été présenté dans [70] où les auteurs ont montré qu'un ensemble réduit de courbes de référence peut être utilisé pour la modélisation de la qualité de la liaison de HARQ en général. Mais leur exigence de placer l'information mutuelle des bits reçus dans la mémoire tampon circulaire virtuelle (reproduire le processus de taux de correspondance) est une charge de calcul pour l'abstraction PHY. Le concept d'information mutuelle accumulé (AMI) pour l'abstraction HARQ PHY est présenté dans [71]. Dans [72] les auteurs ont utilisé le concept de l'AMI de [71] pour l'abstraction HARQ PHY dans les systèmes LTE avec une affectation de bande passante fixe .

Les points limitants dans la plupart de ces approches sont, tout d'abord, qu'ils ne fournissent pas un aperçu analytique détaillée sur le problème de la modélisation IR-HARQ au niveau système en plus ils ne traitent pas le cas d'une largeur de bande variable (PRB en LTE) assignée aux utilisateurs. À cet égard, les techniques présentées ne sont réalisables que pour des affectations de bande passante spécifiques et pour des portées limitées. En plus, ces techniques (sauf [70]) nécessitent un très grand nombre de courbes de référence pour la modélisation de la performance HARQ ce qui augmente les besoins de stockage pour l'abstraction PHY . Toutefois, ce chapitre présente des méthodes simples, robustes et efficaces pour la modélisation des performances de l'IR-HARQ dans le cas d'affectation arbitraire de la bande passante et aussi il utilise un ensemble très réduit de courbes de référence. Les autres discussions dans ce chapitre sont dans le contexte de la technologie LTE, mais la méthode peut être appliquée à d'autres normes cellulaires.

Ce chapitre présente deux nouveaux modèles d'abstraction PHY semi-analytiques qui permettent de prédire la performance au niveau liaison des systèmes LTE avec IR- HARQ et attribution variable de bande passante . Ces modèles proposés utilisent une conception intelligente de l'adaptation du débit en LTE pour faire la modélisation de l'IR- HARQ indépendament de la taille du bloc de transport (TBS) et réduit les besoins de stockage pour l'abstraction PHY en utilisant les courbes de performance de référence correspondant au taux du code initial. Les deux approches proposées sont *la modélisation au niveau de symbole et de la modélisation au niveau binaire*. Comme il est clair à partir des noms que le premier est basé sur la modélisation au niveau de symbole et est donc plus facile à mettre en oeuvre alors que la seconde est basée sur la modélisation au niveau binaire et est plus précis. Les résultats pour les différents cycles de l'IR- HARQ sont présentés dans ce chapitre et il est observé que les modèles proposés fournissent des résultats de validation très précis à partir du simulateur du niveau liaison. Les résultats de ce chapitre sont publiés dans des conférences renommées.

10.2.3 Part II - Applications

Simulations au Niveau Système

Dans les communications sans fil, l'évaluation des systèmes à grande échelle avec l'aide de simulateurs système est d'une importance capitale. Cependant, ces simulations ont une grande complexité de calcul et un temps d'évaluation très long en raison de l'exécution de l'algorithme de couche physique et du modèle de canal utilisé. De nombreux simulateurs au niveau système reposent donc sur les techniques d'abstraction PHY qui prédisent la performance de la couche PHY en fonction de l'état actuel du canal. Il a été constaté à l'aide de profils en simulateur OAI au niveau système que, même pour un système simple avec un seul eNodeB et un seul UE plus de 82 % du temps de simulation total et de ressources ont été consacrées uniquement pour la couche PHY. Il s'agit d'une énorme contrainte en termes de complexité et de la durée de temps de grandes évaluations au niveau système. Et pour les évaluations de la performance du système, même dans un simulations à l'échelle moyen, c'est à dire avec moins de eNodeB et moins UEs, il peut prendre des mois si simulé avec un traitement PHY complet. Par conséquent, pour réduire la complexité et la durée des évaluations au niveau du système, il est nécessaire d'avoir un modèle d'abstraction PHY .

L'utilisation de l'abstraction PHY dans les évaluations du système devrait fournir quatre principaux avantages, 1) faible complexité et rapidité en remplaçant le traitement complet de la couche physique avec des calculs assez simples en utilisant des tables de look up, 2) l'évolutivité dans les évaluations du système en permettant d'évaluer d'énorme systèmes avec des centaines de noeuds, 3) applicabilité en cas d'utilisation diverses et enfin 4) le plus important est le réalisme en fournissant la véritable mesure de qualité de lien comme il aurait obtenu avec un traitement PHY complet . Ainsi, dans cette forme l'abstraction PHY est un outil de faible complexité extrêmement précieux pour les évaluations de système à grande échelle car il fournit au simulateur du système l'indicateur de qualité de liaison nécessaire sans avoir à coder et décoder les paquets. En outre, il peut également être utilisé pour la planification des ressources rapide et l'adaptation rapide de liaison .

Dans ce chapitre, nous avons présenté une méthodologie complète de mise en oeuvre de l'abstraction PHY dans un simulateur de niveau système et nous avons montré que l'abstraction PHY est un outil extrêmement précieux pour les simulations de systèmes à grande échelle. Nous avons en outre montré que l'utilisation de l'abstraction PHY peut énormement accélerer les simulations et peut donc être utilisé pour une évaluation de performance efficace et en temps réel, sans perte de performance réelle de l'émetteur-récepteur.

Comparaison des TMs de LTE en utilisant des mesures de canal à 800 MHz

Ce chapitre présente un autre scénario applicable dans lequel le concept d'abstraction PHY peut donner un aperçu du problème en main. L'objectif principal de ce chapitre est de montrer la façon avec laquelle l'abstraction PHY peut être utilisé pour comparer les différents modes de transmission dans les zones rurales à 800 MHz. Pour comparer les performances, nous avons utilisé les mesures de canal qui ont été stockés au cours d'une campagne de mesure dans le sud de la France pour trois sites différents. L'utilisation de ces canaux MIMO réels a permie non seulement le calcul les indicateurs de performance des modes de transmission pour lesquels la campagne de mesure a été effectuée, mais aussi extrapolé les résultats à des modes de transmission qui n'ont pas été validés au cours de la campagne de mesure. La campagne de mesure a été menée avec le banc d'essai de l'OAI Eurecom qui implémente LTE PHY basé sur [8,9,62].

Ce banc d'essai a été basé sur la technologie de couche PHY LTE version 8 et les modes de transmission 1, 2 et 6 en temps réel. En plus du débit enregistré du modem réel, les estimations de canal brutes ont été stockées et utilisées pour extrapoler la performance en mode de transmission 5 (MIMO multi-utilisateur). Cette extrapolation a été réalisée au moyen d'un modèle d'abstraction PHY basé sur l'information mutuelle qui fait abstraction d'un récepteur pour MU MIMO basé sur la connaissance d'interférence proposé par Ghaffar et al, puis les résultats sont comparés avec les performances de l'abstraction des modes de transmission 2 et 6. la performance supérieure du mode MU MIMO (avec le récepteur basé sur l'interférence) par rapport aux autres modes de transmission est illustré et il est démontré que si le canal admet alors même pour une efficacité spectrale inférieure, MU MIMO est l'option préférée.

Ce chapitre présente le banc d'essai de l'OAI, les mesures de canal LTE ainsi que les résultats correspondants dans la bande 800 MHz, puis la méthodologie complète pour comparer les résultats pour les différents modes de transmission de la technologie LTE. L'objectif principal de la campagne de mesure a consisté à estimer le meilleur débit possible par un terminal LTE version 8 nomade dans un déploiement LTE de 5 MHz à 850 MHz rural. Cependant, un autre intérêt était de comparer l'efficacité des différents modes de transmission de la technologie LTE dans les déploiements rurales. Cela donne les orientations fondamentales pour le déploiement LTE dans les zones rurales. Le banc d'essai de l'OAI a un eNodeB LTE (acronyme de la station de base) à 3 secteur, double RF de haute puissance et un équipement utilisateur (UE) fonctionnant à une fréquence centrale de 859.5MHz. En plus des mesures de débit, des estimations de canal brutes ont été stockées pour un traitement

ultérieur. Ces mesures ont été prises dans le département de Tarn dans le sud-ouest de la France, en collaboration avec l'agence spatiale française (CNES).

Ce chapitre fournit une autre application importante de l'abstraction PHY. Il fournit la comparaison des performances des différents modes de transmission de la technologie LTE dans les zones rurales à 800 MHz avec l'aide d'estimations de canal réels et d'abstraction PHY basée sur l'information mutuelle. Il fournit une méthodologie détaillée pour l'utilisation de l'abstraction PHY dans de telles expériences. Il peut, non seulement, valider certains des concepts bien compris de la communication, mais peut également être utilisé pour une analyse approfondie par l'extrapolation des résultats à d'autres scénarios. Dans ce chapitre, les résultats de MU MIMO sont extrapolés à partir des estimations de canal d'un autre mode de transmission et il est démontré qu'il est avantageux de faire du MU MIMO opportuniste chaque fois qu'il est possible, car il fournit un meilleur débit, même si nous limitons nos résultats aux faibles modulations. Les résultats de ce chapitre sont publiés dans des conférences IEEE.

Adaptation de Lien Rapide (Fast Link Adaptation)

Ce chapitre présente une application très importante de l'abstraction PHY pour l'adaptation rapide de lien et planification efficace des UEs dans les systèmes LTE. Sur la base de l'état actuel du canal, il est possible de sélectionner le schéma de modulation et de codage pour répondre à certaine spécifications de qualité de service (QoS). les modulation de faible ordre utilise un petit nombre de bits pour chaque symbole modulé. Cela peut aboutir à un faible débit binaire, mais il est plus robuste et peut tolérer des niveaux plus élevés de bruit et d'interférence. Cependant les modulations d'ordre supérieur peuvent fournir des débits plus élevés, mais sont plus vulnérable aux niveaux de bruit et d'interférence. De la même façon, sélectioner des taux de codage inférieures pour des mauvais canaux peuvent améliorer la performance du décodeur au prix de la perte de débit global et sélectionner un taux de codage plus élevées peuvent augmenter le débit, mais au détriment de la mauvaise performance du décodeur. Ce processus de sélection d'une combinaison valable de modulation et de codage sur la base de l'état actuel du canal est appelé modulation et le codage adaptatifs (AMC). L'adaptation rapide de lien (FLA) en LTE est basé sur AMC. La FLA est le processus de sélection d'un MCS approprié pour le DL sur la base de l'indicateur de qualité du canal qui est renvoyé à partir de l'équipement utilisateur à l'eNodeB. Dans LTE, il ya 29 différentes combinaisons possibles de MCS et n'importe lequel peut être sélectionnés pour la transmission DL. Mais l'adaptation de ces MCS est basée principalement sur les compte rendus de l'UE à eNodeB et l'CQI est l'un des éléments clés de cette rétroaction. CQI est basé sur le

S(I)NR reçu et la conception du récepteur. Et dans ce chapitre, nous allons étudier le calcul de cette CQI pour la FLA et la planification basé sur ce CQI.

Le concept de FLA n'est pas nouveau dans la norme LTE puisqu'il a été inclus dans WCDMA, HSPA et WiMax. Il ya beaucoup de contribution de recherche sur le thème de la FLA pour les systèmes WiMax, HSPA et LTE. Dans [80] les auteurs ont présenté une méthode sous-optimale de la sélection de la rétroaction à l'UE selon un système ESM et ils ont montré que les deux méthodes d'ESM (EESM et MIESM) fournissent presque le même niveau de performance pour les évaluations de l'CQI. En outre, ils ont montré qu'en utilisant leurs schémes RI et PMI de rétroaction, les erreurs d'estimation ont un impact énorme sur les performances du système. La raison de cela est la sélection conjointe des RI et PMI. Si les évaluations des comptes rendus est estimé avec des erreurs, le système pourrait prendre une mauvaise décision sur le nombre de couches et la sélection de pré-codeur ce qui peut entraîner la dégradation des performances du système. Dans [81] les auteurs ont proposé l'information mutuelle moyenne par cartographie de bits codés (MMIBM) comme critère pour les systèmes MIMO OFDM à l'aide de la norme IEEE 802.11n et a montré qu'il est un peu plus pérformant que EESM et MIESM. Dans leurs travail, ils ont aussi montré que leur FLA proposée permet des gains dans les canaux avec un temps de cohérence plus réduit et ils ont montré que le délai de feedback peut avoir un impact sérieux sur les performances du système. Dans [82] les auteurs ont présenté une étude sur les problèmes de planification dans LTE et ont mis en évidence le fait que les régimes proposé de planification et d'adaptation de lien très sophistiqués sont en fait soit trop compliqué à mettre en oeuvre ou prennent beaucoup de temps pour pouvoir optimiser les paramètres de planification. Par conséquent, dans ce chapitre, nous allons fournir une approche robuste et pratique pour l'adaptation de lien qui est non seulement facile à mettre en oeuvre, mais aussi fournit un gain dans les performances du système.

Dans LTE, les CRS utilisées pour l'estimation de canal sont les symboles de canal où aucun des symboles de données n'est transmis. Ces estimations de canal sont utilisés pour le calcul de CQI à l'équipement UE. Le calcul CQI est basé sur le SINR moyen reçu et le type de récepteur utilisé. Cette SINR reçu moyenné peut être calculée soit avec une simple moyenne arithmétique ou en utilisant l'approche ESM d'abstraction PHY. Cette dernière approche donne un CQI plus précis car il est capable de capter la sélectivité en fréquence du canal. Cependant, comme il a été montré au chapitre 3, dans ESM les facteurs d'ajustement sont nécessaires pour une cartographie précise et ceux ci dépondent des MCS. Pour les estimations de canal de CRS, il n'y a pas de MCS utilisés donc nous ne pouvons pas utiliser les facteurs d'ajustement. Dans ce cas, nous pouvons toujours utiliser le MIESM pour la transmission SISO (mode de transmission 1), mais pour d'autres config-

urations d'antenne MIESM doit être calibré. Cependant le calibrage peut être évité avec MIESM en utilisant les courbes AWGN qui ont été calculées en particulier pour les configurations d'antennes spécifiques qui sont sous considération. Ceci est due au fait que les courbes de AWGN ont déjà capturé les effets de multiples combinaisons des LLR reçues. Pour cette raison, nous proposons d'utiliser des courbes de référence AWGN correspondantes à chaque configuration d'antenne pour le calcul de l'CQI à l'UE .

Du côté de l'ordonnanceur, le mapping de CQI à MCS est aussi généralement basée sur la configuration SISO et dans ce chapitre, nous proposons de l'adapter à des configurations d'antennes différentes, se qui permet au MCS optimal peut être sélectionné pour les conditions courantes du canal.

Ce chapitre présente le problème de l'adaptation rapide de liaison (FLA) en LTE et montre que l'utilisation de la connaissance de la configuration des antennes donnée par les informations de contrôle de canal, une version améliorée de CQI peut être calculé à l'aide de d'une abstraction PHY basé sur l'information mutuelle. Ensuite, en utilisant cette amélioration de CQI le planificateur de l'eNodeB peut sélectionner un MCS plus approprié ce qui peut augmenter le débit global du système. Nous montrons que, quand un équipement utilisateur est programmé en mode d'émission 6, cette adaptation de lien améliorée peut fournir un gain dans le débit du système en sélectionnant un MCS plus fesable sur la liaison descendante.

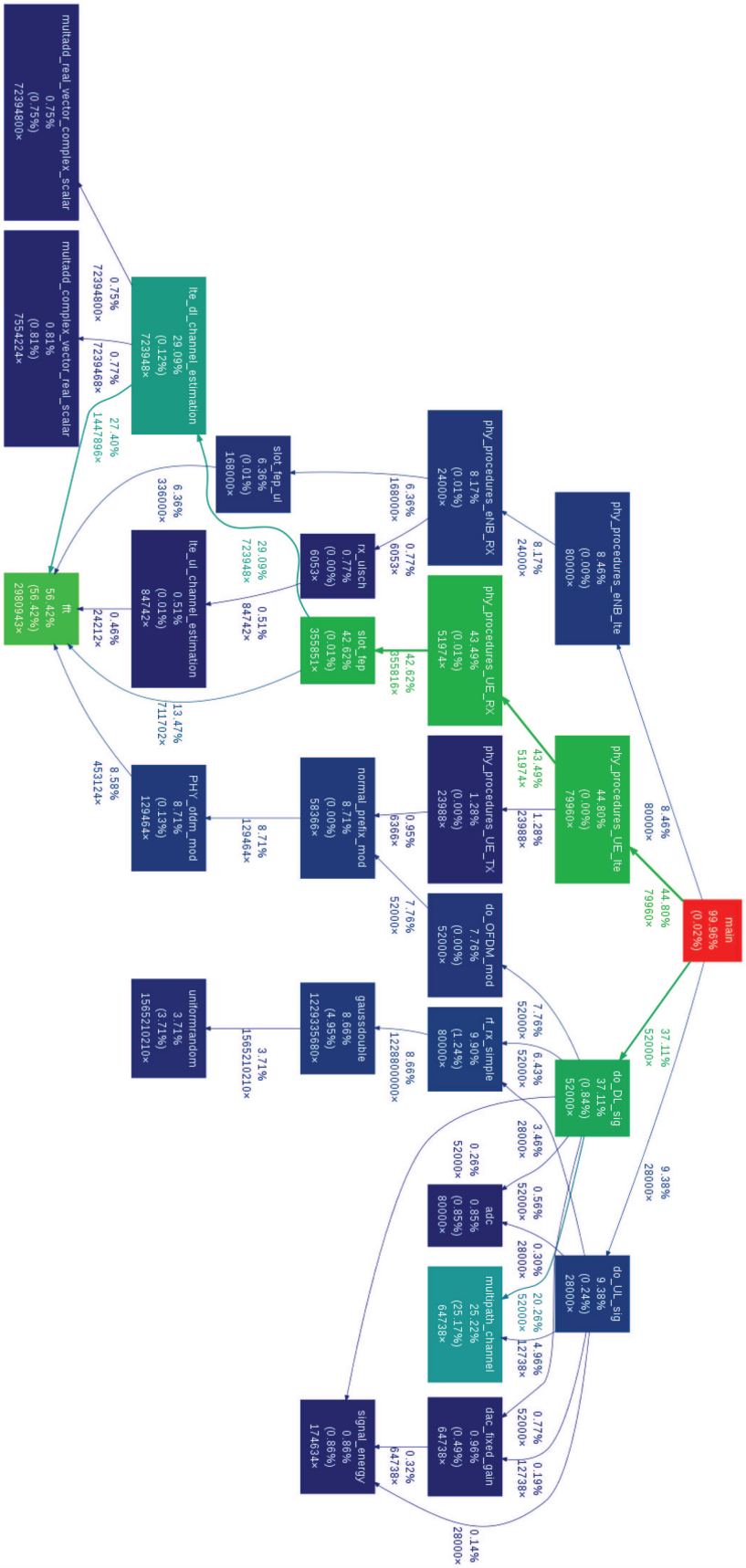

Figure 10.5: Profiling for System Simulation with 1 eNodeB and 1 UE in the context of LTE, SISO channel, frequency selective Rayleigh channel and constant bit rate traffic.

Bibliography

[1] I. T. U. (ITU), "Global ict developments," *http://www.itu.int/en/ITU-D/Statistics/Pages/stat/default.aspx*, 2013.

[2] A. Lucent, "Introduction to Evolved Packet Core (EPC)," *http://www.lte.alcatel-lucent.com/locale/en_us/downloads/wp_evolved_packet_core.pdf*.

[3] 3GPP, "Technical specification group radio access network; requirements for evolved utra (e-utra) and evolved utran (e-utran)," 3GPP, Technical Specification TR 25.913, 2009.

[4] S. Sesia, I. Toufik, and M. Baker, Eds., *UMTS Long Term Evolution: From Theory to Practice*. Wiley and Sons, 2009.

[5] 3GPP, "Technical specification group radio access network; evolved universal terrestrial radio access (e-utra) packet data convergence protocol (pdcp) protocol specification," 3GPP, Technical Specification TS 36.323-V9.0.0, 2009.

[6] ——, "Technical specification group radio access network; evolved universal terrestrial radio access (e-utra) radio link control (rlc) protocol specification," 3GPP, Technical Specification TS 36.322-V9.0.0, 2009.

[7] ——, "Technical specification group radio access network; evolved universal terrestrial radio access (e-utra) medium access control (mac) protocol specification," 3GPP, Technical Specification TS 36.321-V9.0.0, 2009.

[8] ——, "Physical channels and modulation," 3GPP, Technical Specification 36.211-V8.6.0, Sep. 2009.

[9] ——, "Multiplexing and channel coding," 3GPP, Technical Specification 36.212-V8.6.0, Sep. 2009.

[10] J.-F. Cheng, A. Nimbalker, Y. Blankenship, B. Classon, and T. Blankenship, "Analysis of circular buffer rate matching for lte turbo code," in *Vehicular Technology Conference, 2008. VTC 2008-Fall. IEEE 68th*, sept. 2008, pp. 1 –5.

[11] E. Zehavi, "8-psk trellis codes for a rayleigh channel," *Communications, IEEE Transactions on*, vol. 40, no. 5, pp. 873–884, 1992.

[12] G. Caire, G. Taricco, and E. Biglieri, "Bit-interleaved coded modulation," *Information Theory, IEEE Transactions on*, vol. 44, no. 3, pp. 927 –946, may 1998.

[13] M. Döttling, "Assessment of Advanced Beamforming and MIMO Technologies," European Commission, Project Deliverable IST-WINNER (2003-507581), 2005.

[14] R. Srinivasan, J. Zhuang, L. Jalloul, R. Novak, and J. Park, "IEEE 802.16m Evaluation Methodology Document (EMD)," no. IEEE 802.16m-08 004r5, pp. 1–199, 2009. [Online]. Available: http://wirelessman.org/tgm/

[15] H. Olofsson, M. Almgren, C. Johansson, M. Hook, and F. Kronestedt, "Improved interface between link level and system level simulations applied to gsm," in *Universal Personal Communications Record, 1997. Conference Record., 1997 IEEE 6th International Conference on*, 1997, pp. 79–83 vol.1.

[16] Nortel Networks, "OFDM Exponential Effective SIR Mapping Validation, EESM Simulation Results," 3GPP, Tech. Rep. R1-040089, Jan. 2004.

[17] L. T. Tu, R. Robles, A. Silva, C. Nicolae, D. Castelain, V. Bota, M. Varga, M. A. Badiu, M. P. Stef, and Z. Polgar, "Intermediate Version of the System Level Simulator," European Commission, Deliverable FP7-ICT-2007-215477 D5.2, Sep. 2009. [Online]. Available: http://www.ict-codiv.eu/private/docs/deliverables/D5.2.pdf

[18] K. Brueninghaus, D. Astely, T. Salzer, S. Visuri, A. Alexiou, S. Karger, and G. A. Seraji, "Link Performance Models for System Level Simulations of Broadband Radio Access Systems," in *16th Annual IEEE International Symposium on Persoanl, Indoor and Mobile Radio Communications Germany*, 2005, pp. 2306–2311.

[19] L. Wan, S. Tsai, and M. Almgren, "A Fading-Insensitive Performance Metric for a Unified Link Quality Model," in *Wireless Communications and Networking Conference, 2006. WCNC 2006. IEEE*, vol. 4, 2006, pp. 2110 –2114.

[20] R. B. Santos, W. C. Freitas Jr., E. M. G. Stancanelli, and F. R. P. Cavalcanti, "Link-to-System Level Interface Solutions in Multistate Channels for 3GPP LTE Wireless System," *XXV Simposio Brasileiro de Telecomunicacoes*, 2007.

[21] A. Oborina and M. Moisiot, "Speed Up of Effective SINR Mapping Calculations for System Level Simulations," *IET Seminar Digests*, pp. 43–43, 2007.

[22] A. Rodriguez-Herrera, S. McBeath, D. Pinckley, and D. Reed, "Link-to-System Mapping Techniques using a Spatial Channel Model," in *IEEE 62nd Vehicular Technology Conference, 2005. VTC-2005-Fall.*, vol. 3, sept., 2005, pp. 1868 – 1871.

[23] E. Tuomaala and H. Wang, "Effective SINR Approach of Link to System Mapping in OFDM/Multi-Carrier Mobile Network," in *2nd International Conference on Mobile Technology Applications and Systems*, nov. 2005, pp. 5 pp. –5.

[24] J. Olmos, S. Ruiz, M. Garcia-Lozano, and D. Martin-Sacristán, "Link Abstraction Models Based on Mutual Information for LTE Downlink," *COST 2100 TD(10)11052*, pp. 1–18, 2010.

[25] A. A. Dios, "Relay-Assisted Transmission and Radio Resource Menagement for Wireless Networks," Ph.D. dissertation, Technical University of Catalonia, 2008.

[26] S. Alamouti, "A simple transmit diversity technique for wireless communications," *Selected Areas in Communications, IEEE Journal on*, vol. 16, no. 8, pp. 1451–1458, 1998.

[27] V. Tarokh, A. Naguib, N. Seshadri, and A. Calderbank, "Space-time codes for high data rate wireless communication: performance criteria in the presence of channel estimation errors, mobility, and multiple paths," *Communications, IEEE Transactions on*, vol. 47, no. 2, pp. 199–207, 1999.

[28] V. Tarokh, H. Jafarkhani, and A. Calderbank, "Space-time block codes from orthogonal designs," *Information Theory, IEEE Transactions on*, vol. 45, no. 5, pp. 1456–1467, 1999.

[29] A. Wittneben, "Basestation modulation diversity for digital simulcast," in *Vehicular Technology Conference, 1991. Gateway to the Future Technology in Motion., 41st IEEE*, 1991, pp. 848–853.

[30] R. Heath and A. Paulraj, "Transmit diversity using decision-directed antenna hopping," in *Communication Theory Mini-Conference, 1999*, 1999, pp. 141–145.

[31] B. Bjerke and J. Proakis, "Multiple-antenna diversity techniques for transmission over fading channels," in *Wireless Communications and Networking Conference, 1999. WCNC. 1999 IEEE*, 1999, pp. 1038–1042 vol.3.

[32] A. Scaglione, P. Stoica, S. Barbarossa, G. Giannakis, and H. Sampath, "Optimal designs for space-time linear precoders and decoders," *Signal Processing, IEEE Transactions on*, vol. 50, no. 5, pp. 1051–1064, 2002.

[33] H. Sampath, P. Stoica, and A. Paulraj, "Generalized linear precoder and decoder design for mimo channels using the weighted mmse criterion," *Communications, IEEE Transactions on*, vol. 49, no. 12, pp. 2198–2206, 2001.

[34] L. Collin, O. Berder, P. Rostaing, and G. Burel, "Optimal minimum distance-based precoder for mimo spatial multiplexing systems," *Signal Processing, IEEE Transactions on*, vol. 52, no. 3, pp. 617–627, 2004.

[35] E. Visotsky and U. Madhow, "Space-time transmit precoding with imperfect feedback," *Information Theory, IEEE Transactions on*, vol. 47, no. 6, pp. 2632–2639, 2001.

[36] S. Zhou and G. Giannakis, "Optimal transmitter eigen-beamforming and space-time block coding based on channel mean feedback," *Signal Processing, IEEE Transactions on*, vol. 50, no. 10, pp. 2599–2613, 2002.

[37] H. Sampath and A. Paulraj, "Linear precoding for space-time coded systems with known fading correlations," in *Signals, Systems and Computers, 2001. Conference Record of the Thirty-Fifth Asilomar Conference on*, vol. 1, 2001, pp. 246–251 vol.1.

[38] S. Jafar, S. Vishwanath, and A. Goldsmith, "Channel capacity and beamforming for multiple transmit and receive antennas with covariance feedback," in *Communications, 2001. ICC 2001. IEEE International Conference on*, vol. 7, 2001, pp. 2266–2270 vol.7.

[39] S. Zhou and G. Giannakis, "Optimal transmitter eigen-beamforming and space-time block coding based on channel correlations," *Information Theory, IEEE Transactions on*, vol. 49, no. 7, pp. 1673–1690, 2003.

[40] J. Akhtar and D. Gesbert, "Spatial multiplexing over correlated mimo channels with a closed-form precoder," *Wireless Communications, IEEE Transactions on*, vol. 4, no. 5, pp. 2400–2409, 2005.

[41] D. Love and R. Heath, "Multimode precoding for mimo wireless systems," *Signal Processing, IEEE Transactions on*, vol. 53, no. 10, pp. 3674–3687, 2005.

[42] A. M. Cipriano, R. Visoz, and T. Salzer, "Calibration issues of phy layer abstractions for wireless broadband systems," in *VTC Fall.* IEEE, 2008, pp. 1–5.

[43] G. J. Foschini and M. J. Gans, "On limits of wireless communications in a fading environment when using multiple antennas," *Wireless Personal Communications*, vol. 6, pp. 311–335, 1998.

[44] A. Goldsmith, S. Jafar, N. Jindal, and S. Vishwanath, "Capacity limits of mimo channels," *Selected Areas in Communications, IEEE Journal on*, vol. 21, no. 5, pp. 684–702, 2003.

[45] Q. Spencer, C. Peel, A. Swindlehurst, and M. Haardt, "An introduction to the multi-user mimo downlink," *Communications Magazine, IEEE*, vol. 42, no. 10, pp. 60–67, 2004.

[46] Q. H. Spencer, C. B. Peel, A. L. Swindlehurst, and M. Haardt, "An introduction to the multi-user MIMO downlink," *IEEE Commun. Mag.*, vol. 42, no. 10, pp. 60–67, Oct. 2004.

[47] D. Gesbert, M. Kountouris, R. W. Heath, Jr., C. B. Chae, and T. Sälzer, "From single user to multiuser communications: Shifting the MIMO paradigm," *IEEE Signal Process. Mag.*, vol. 24, no. 5, pp. 36–46, Sep. 2007.

[48] J. Duplicy, B. Badic, R. Balraj, R. Ghaffar, P. Horvath, F. Kaltenberger, R. Knopp, I. Z. Kovacs, H. T. Nguyen, D. Tandur, and G. Vivier, "MU-MIMO in LTE systems," *Eurasip Journal on Wireless Communications and Networking, 2011, Article ID 496763, ISSN: 1687-1472*, 2011.

[49] M. Costa, "Writing on dirty paper (corresp.)," *Information Theory, IEEE Transactions on*, vol. 29, no. 3, pp. 439 – 441, may 1983.

[50] R. Ghaffar and R. Knopp, "Making Multiuser MIMO work for LTE," in *IEEE 21-st International Symposium on Personal, Indoor and Mobile Radio Communications (PIMRC 2010)*, Istanbul, September 2010.

[51] R. Ghaffar and R. Knopp, "Interference-Aware Receiver Structure for Multi-User MIMO and LTE," *EURASIP Journal on Wireless Communications and Networking 2011*, 2011.

[52] R. Visoz, A. Berthet, and M. Lalam, "Semi-analytical performance prediction methods for iterative mmse-ic multiuser mimo joint decoding," *Communications, IEEE Transactions on*, vol. 58, no. 9, pp. 2576–2589, 2010.

[53] S.-H. Moon, K.-J. Lee, J. Kim, and I. Lee, "Link performance estimation techniques for mimo-ofdm systems with maximum likelihood receiver," *Wireless Communications, IEEE Transactions on*, vol. 11, no. 5, pp. 1808–1816, 2012.

[54] I. Latif, F. Kaltenberger, R. Ghaffar, R. Knopp, D. Nussbaum, H. Callewaert, and G. Scot, "Performance of LTE in Rural Areas - Benefits of Opportunistic Multi-User MIMO," in *PIMRC 2011, 22nd Annual IEEE International Symposium on Personal, Indoor and Mobile Radio Communications, September 11-14, 2011, Toronto, Canada*, 09 2011.

[55] Imran Latif, Florian Kaltenberger, and Raymond Knopp, "Link abstraction for multi-user MIMO in LTE using interference-aware receiver," in *WCNC 2012, IEEE Wireless Communications and Networking Conference, April 1-4, 2012, Paris, France*, Paris, FRANCE, 04 2012.

[56] 3GPP, "Technical specification group radio access network; evolved universal terrestrial radio access (e-utra); further advancements for e-utra physical layer aspects," 3GPP, Technical Specification TR 36.814-V9.0.0, 2010.

[57] R. Ghaffar and R. Knopp, "Interference sensitivity for multiuser mimo in lte," in *Signal Processing Advances in Wireless Communications (SPAWC), 2011 IEEE 12th International Workshop on*, 2011, pp. 506–510.

[58] Rizwan Ghaffar, "Interference mitigation in multi-antenna systems," Ph.D. dissertation, Thesis, 11 2010. [Online]. Available: http://www.eurecom.fr/publication/3265

[59] H. Dai, A. Molisch, and H. Poor, "Downlink capacity of interference-limited mimo systems with joint detection," *Wireless Communications, IEEE Transactions on*, vol. 3, no. 2, pp. 442–453, 2004.

[60] N. Miridakis and D. Vergados, "A survey on the successive interference cancellation performance for single-antenna and multiple-antenna ofdm systems," *Communications Surveys Tutorials, IEEE*, vol. 15, no. 1, pp. 312–335, 2013.

[61] 3GPP, "Evolved universal terrestrial radio access (E-UTRA); x2 general aspects and principles," 3GPP, Technical Specification TS 36.420-V8.0.0, 2007.

[62] ——, "Physical layer procedures," 3GPP, Technical Specification 36.213-V8.6.0, Sep. 2009.

[63] ——, "Technical specification group radio access network; spatial channel model for mimo simulations," 3GPP, Technical Specification TR 25.996-V11.0.0, 2012.

[64] C. Lott, O. Milenkovic, and E. Soljanin, "Hybrid arq: Theory, state of the art and future directions," in *Information Theory for Wireless Networks, 2007 IEEE Information Theory Workshop on*, 2007, pp. 1–5.

[65] P. Wu and N. Jindal, "Performance of hybrid-arq in block-fading channels: A fixed outage probability analysis," *Communications, IEEE Transactions on*, vol. 58, no. 4, pp. 1129–1141, 2010.

[66] E. Uhlemann, L. Rasmussen, A. Grant, and P. Wiberg, "Optimal incremental-redundancy strategy for type-ii hybrid arq," in *Information Theory, 2003. Proceedings. IEEE International Symposium on*, 2003, pp. 448–.

[67] R. Liu, P. Spasojevic, and E. Soljanin, "On the role of puncturing in hybrid arq schemes," in *Information Theory, 2003. Proceedings. IEEE International Symposium on*, 2003, pp. 449–.

[68] N. Gopalakrishnan and S. Gelfand, "Rate selection algorithms for ir hybrid arq," in *Sarnoff Symposium, 2008 IEEE*, 2008, pp. 1–6.

[69] B. Classon, P. Sartori, Y. Blankenship, K. Baum, R. Love, and Y. Sun, "Efficient ofdm-harq system evaluation using a recursive eesm link error prediction," in *Wireless Communications and Networking Conference, 2006. WCNC 2006. IEEE*, vol. 4, april 2006, pp. 1860 –1865.

[70] A. Davydov, G. Morozov, and A. Papathanassiou, "Prediction model for turbo-coded ofdma-systems employing rate matching and harq," in *Vehicular Technology Conference (VTC Spring), 2011 IEEE 73rd*, may 2011, pp. 1 –4.

[71] J.-F. Cheng, "Coding performance of hybrid arq schemes," *Communications, IEEE Transactions on*, vol. 54, no. 6, pp. 1017 –1029, june 2006.

[72] J. C. Ikuno, C. Mehlführer, and M. Rupp, "A novel link error prediction model for OFDM systems with HARQ," in *IEEE International conference on Communications 2011 (ICC)*, Kyoto, Japan, June 2011.

[73] J. Olmos, A. Serra, S. Ruiz, and I. Latif, "On the Use of Mutual Information at Bit Level for Accurate Link Abstraction in LTE with Incremental Redundancy H-ARQ," *COST IC1004 TD(12)05046*, pp. 1–21, 2012.

[74] C. Mehlführer, J. C. Ikuno, M. Simko, S. Schwarz, M. Wrulich, and M. Rupp, "The vienna LTE simulators - enabling reproducibility in wireless communications research," *EURASIP Journal on Advances in Signal Processing*, vol. Vol. 2011, pp. 1–13, 2011.

[75] J. Ellenbcck, "Imtaphy: Lte/lte-advanced system-level simulator," *http://www.lkn.ei.tum.de/personen/jan/imtaphy/index.php*.

[76] G. Piro, L. Grieco, G. Boggia, F. Capozzi, and P. Camarda, "Simulating lte cellular systems: An open-source framework," *Vehicular Technology, IEEE Transactions on*, vol. 60, no. 2, pp. 498–513, 2011.

[77] N. S. 3, "Documentation," *http://www.nsnam.org/ns-3-17/documentation/*.

[78] J. C. Ikuno, "System level modeling and optimization of the LTE downlink," Ph.D. dissertation, Institute of Telecommunications, Vienna University of Technology, 2013.

[79] Ankit Bhamri, Florian Kaltenberger, Raymond Knopp, and Jyri Hämäläinen, "Improving MU-MIMO performance in LTE-(Advanced) by efficiently exploiting feedback resources and through dynamic scheduling," in *WCNC 2013, IEEE Wireless Communications and Networking Conference, April 7-10, 2013, Shanghai, China*, Shanghai, CHINA, 04 2013. [Online]. Available: http://www.eurecom.fr/publication/3917

[80] S. Schwarz, C. Mehlfuhrer, and M. Rupp, "Calculation of the spatial preprocessing and link adaption feedback for 3gpp umts/lte," in *Wireless Advanced (WiAD), 2010 6th Conference on*, 2010, pp. 1–6.

[81] T. Jensen, S. Kant, J. Wehinger, and B. Fleury, "Fast link adaptation for mimo ofdm," *Vehicular Technology, IEEE Transactions on*, vol. 59, no. 8, pp. 3766–3778, 2010.

[82] F. Capozzi, G. Piro, L. Grieco, G. Boggia, and P. Camarda, "Downlink packet scheduling in lte cellular networks: Key design issues and a survey," *Communications Surveys Tutorials, IEEE*, vol. 15, no. 2, pp. 678–700, 2013.